UNIVERSITÉ DU QUÉBEC
EN ABITIBI-TÉMISCAMINGUE

Éléments finis hybrides 3D pour la conduction anisotrope de la chaleur dans un multi-matériaux avec des orientations multiples des tenseurs de conductivité thermique

Par

Zouheir Annasabi

Sous la direction de Fouad Erchiqui

Thèse présentée à l'Université du Québec en Abitibi-Témiscamingue en vue de l'obtention du grade de Philosophae Doctor (3737) en ingénierie

Soutenue le 03 juin 2022

Membres du jury :

François Godard, Ph. D, Université du Québec en Abitibi-Témiscamingue, Président du Jury

Hassan Naji, Ph. D, Université d'Artois en France, Évaluateur externe

Mostapha Tarfaoui, Ph. D, ENSTA-Bretagne en France, Évaluateur externe

Yasar Kocaefe, Ph. D, Université du Québec à Chicoutimi, Évaluateur externe

Québec, Canada

TABLE DES MATIÈRES

LISTE DES TABLEAUX

LISTE DES FIGURES

SYMBOLES ET ABRÉVIATIONS

θ	Transformation de Kirchhoff, W m^{-1}
K	Conductivité thermique, $W.m^{-1}.{}^{o}C^{-1}$
Cp	Chaleur spécifique, $J{\cdot}Kg^{-1}{\cdot}K^{-1}$
ρ	Masse volumique, $kg.m^{-3}$
ρ_w	Masse volumique de l'eau, $kg.m^{-3}$
T	Température, °C
T_m	Température de fusion, °C
T_s	Température à l'état solide, °C
T_l	Température à l'état liquide, °C
T_∞	Température du milieu ambiant, °C
H	Enthalpie volumique, $J.m^{-3}$
h	Coefficient de convection, $W.m^{-2}.K^{-1}$
$\underline{\boldsymbol{\theta}}$	Tenseur intégral de la conductivité thermique anisotrope $W.m^{-1}$
Q	Source de chaleur interne, $W.m^{-3}$
Q_{RF}	Source de chaleur interne RF, $W.m^{-3}$
MC	Teneur en humidité massique, %
GS	Densité SG
L	Chaleur latente de fusion, $J.Kg^{-1}$
L_w	Chaleur latente de fusion de l'eau, $J.Kg^{-1}$
$[\mathbf{k}^{(x,y,z)}]$	Tenseur cartésien de conductivité thermique, $W.m^{-1}.{}^{o}C^{-1}$
$[\mathbf{k}^{(\rho,\phi,z)}]$	Tenseur cylindrique de conductivité thermique, $W.m^{-1}.{}^{o}C^{-1}$
$[\mathbf{k}^{(r,\theta,\phi)}]$	Tenseur sphérique de conductivité thermique, $W.m^{-1}.{}^{o}C^{-1}$
$[\underline{\mathbf{k}}^{(\rho,\phi,z)}]$	Tenseur de conductivité thermique équivalent pour les coordonnées cylindriques, $W.m^{-1}.{}^{o}C^{-1}$
$[\underline{\mathbf{k}}^{(r,\theta,\varphi)}]$	Tenseur de conductivité thermique équivalent pour les coordonnées sphériques, $W.m^{-1}.{}^{o}C^{-1}$

$\left[\mathbf{T}^{(\rho,\phi,\mathbf{z})}\right]$	Matrice de passage d'un repère cylindrique vers un repère cartésien
$\left[\mathbf{T}^{(\mathbf{r},\theta,\phi)}\right]$	Matrice de passage d'un repère sphérique vers un repère cartésien
$\vec{\mathbf{q}}_{(\mathbf{x},\mathbf{y},\mathbf{z})}$	Flux de chaleur cartésien, W.m^{-2}
$\vec{\mathbf{q}}_{(\rho,\phi,\mathbf{z})}$	Flux de chaleur cylindrique, W.m^{-2}
$\vec{\mathbf{q}}_{(\mathbf{r},\theta,\phi)}$	Flux de chaleur sphérique, W.m^{-2}
$\vec{\mathbf{n}}$	Vecteur normal extérieur (n_x, n_y, n_z)
$\vec{\mathbf{r}}$	Vecteur de position, m
$(\mathrm{x},\mathrm{y},\mathrm{z})$	Coordonnées cartésiennes, m
(ρ,ϕ,z)	Coordonnées cylindriques, m
$(\mathrm{r},\theta,\varphi)$	Coordonnées sphériques, m
$\left(\hat{\mathrm{e}}_\mathrm{x},\hat{\mathrm{e}}_\mathrm{y},\hat{\mathrm{e}}_\mathrm{z}\right)$	Système de coordonnées orthonormées global cartésien
$\left(\hat{\mathrm{e}}_\rho,\hat{\mathrm{e}}_\phi,\hat{\mathrm{e}}_\mathrm{z}\right)$	Système de coordonnées orthonormées local cylindrique
$\left(\hat{\mathrm{e}}_\mathrm{r},\hat{\mathrm{e}}_\varphi,\hat{\mathrm{e}}_\theta\right)$	Système de coordonnées orthonormées local sphérique
q	Flux de chaleur incident, W.m^{-2}
a_i, b_i, c_i, a_n, b_n	Coefficients réels
$\mathbf{N}$	Matrice d'interpolation
Ω	Domaine physique
$\partial\Omega$	Frontière du domaine physique Ω
Φ	Fonction de test
RF	Fréquence radio
f	Fréquence, Hz
f_c	Fréquence critique, Hz
τ	Temps de relaxation, s
ε_0	Permittivité du vide, $\boldsymbol{\varepsilon_0 = 8.854\ 10^{12}\mathrm{F.m^{-1}}}$
$\bar{\bar{\boldsymbol{\varepsilon}}}$	Tenseur de permittivité diélectrique, C V^{-1} m^{-1}

$\bar{\bar{\varepsilon}}_r$	Tenseur de permittivité relative, C V^{-1} m^{-1}
$\bar{\bar{\varepsilon}}'$	Partie réelle de la permittivité, C V^{-1} m^{-1}
$\bar{\bar{\varepsilon}}''$	Partie imaginaire de la permittivité, C V^{-1} m^{-1}
μ_0	Perméabilité du vide, $\boldsymbol{\mu_0 = 4\,\pi\,10^{-7} H.m^{-1}}$
$\bar{\bar{\mu}}$	Tenseur de perméabilité magnétique, H·m^{-1}
$\bar{\bar{\mu}}'$	Partie réelle de la perméabilité magnétique, H·m^{-1}
$\bar{\bar{\mu}}''$	Partie imaginaire de la perméabilité magnétique, H·m^{-1}
$\bar{\bar{\mu}}_r$	Tenseur de perméabilité magnétique relative, H·m^{-1}
E	Effusivité thermique, $J.K^{-1}.m^{-2}.s^{-1/2}$
$\vec{P}$, S	Vecteur de Poynting, $W.m^{-2}$
$\mathbf{E}$	Champ électrique, $V.m^{-1}$
$\mathbf{E}^*$	Champ électrique conjugué, $V.m^{-1}$
$\mathbf{H}$	Champ magnétique, $A.m^{-1}$
$\mathbf{H}^*$	Champ magnétique conjugué, $A.m^{-1}$
ω	Fréquence angulaire, $rad.s^{-1}$
$\bar{\bar{I}}$	Tenseur d'identité
γ	Constante de propagation complexe, $\boldsymbol{\gamma = \alpha + j\beta}$
α	Constante d'atténuation
β	Constante de phase
δ	L'angle de perte diélectrique
λ	Longueur d'onde, m.
F_{r-s}	Facteur de forme entre le récepteur et la source

σ	Constante de Stefan-Boltzmann, $\boldsymbol{\sigma = 5.67\ 10^{-8}\ W.m^{-2}.K^{-4}}$
Γ	Surface frontière

DÉDICACE

Je dédie cette thèse : *A mon très cher père Omar Annasabi, que Dieu ait son âme, qui a toujours été pour moi un exemple du père respectueux, honnête, de la personne méticuleuse, je tiens à honorer l'homme qu'il était. Aussi, à ma mère Fatna Annasabi, qui m'a entouré d'amour, d'affection et qui fait tout pour ma réussite, que dieu t'accorde une bonne santé et une vie longue et heureuse.*

REMERCIEMENTS

Je tiens à exprimer mes sentiments de gratitude à mon directeur de recherche, le professeur Fouad Erchiqui de l'Université du Québec en Abitibi-Témiscamingue, pour le suivi de mon projet, sa pédagogie, sa disponibilité, sa qualité de son encadrement et son expertise dans le domaine de transfert de chaleur qui m'ont motivé à progresser dans ce domaine très vaste et novateur

AVANT-PROPOS

Ce projet de recherche représente un continuum pour mon projet de maîtrise, initié par mon directeur de recherche, le professeur Erchiqui, sur la modélisation de transfert de chaleur avec changement de phase dans les solides incompressibles avec application au matériau bois. Cette fois-ci, sous la direction du professeur Erchiqui, le projet est orienté vers la modélisation de transfert de chaleur dans les multi-matériaux anisotropes et non linéaires, avec ou sans changement de phase.

À cet effet, l'équation de la conduction de la chaleur classique pour les solides qui subissent un changement de phase, en termes de l'enthalpie volumique et de la transformée de Kirchhoff, a été redéfinie par une nouvelle formulation utilisant l'enthalpie hybride anisotrope et la transformée de Kirchhoff anisotrope.

L'intérêt de cette nouvelle approche, contrairement aux méthodes numériques existantes, est de pouvoir traiter le transfert de chaleur, avec ou sans changement de phase, dans les milieux formés de plusieurs solides dont les tenseurs de conductivités thermiques sont de natures différentes (sphériques et/ou cylindriques et/ou cartésiens).

Ensuite, on a adapté la nouvelle formulation hybride pour la résolution de la conduction de la chaleur en fonction de la température (au lieu de l'enthalpie et de la transformée de Kirchhoff) pour les solides multi-matériaux et multi-anisotropies.

Les problèmes traités dans ce projet sont de type conduction-convection et conduction-convection-rayonnement. Plusieurs validations ont été réalisées vis-à-vis des résultats issus de la littérature (expérimentaux, analytiques et numériques). De surcroit, le problème de la non linéarité de la conduction de la chaleur, en régime stationnaire, est contourné par le déploiement d'une nouvelle approche, que nous avons initiée, utilisant la méthode de Spline.

Dans l'ensemble, le travail de recherche a fourni 5 articles dans les plus prestigieuses revues:

- ✓ Deux articles dans International Journal of Heat and Mass Transfer (Elsevier, Impact factor: 5.584, Q1, H-Index: 208)
- ✓ Un article dans International Communications in Heat and Mass Transfer (Elsevier, Impact factor : 5.683, Q1, H-index : 101)
- ✓ Un article dans ASME-Heat transfert (ASME, Impact factor : 2.02, Q1, H-index : 126)
- ✓ Un article dans Wood Science and Technology (Springer, Impact factor: 2.58, Q1, H-index: 71).

INTRODUCTION

La conductivité thermique des matériaux anisotropes joue un rôle crucial dans de nombreux domaines de l'ingénierie et de la technologie. Citons par exemple les domaines du refroidissement des batteries Li-ion [1], de la décongélation ou du séchage du bois [2], du traitement par rayonnement des tissus humains [3], du séchage des structures laminées [4], etc. En particulier, l'analyse de la conduction thermique dans des milieux anisotropes hétérogènes, au moyen de l'équation de la conservation de l'énergie, nécessite, d'une part, la connaissance de la nature de l'orientation du tenseur de la conductivité thermique dans l'espace du matériau, et, d'autre part, sa dépendance (ou non) à des variables mesurables telles que la température, la pression, l'humidité, etc. Les caractéristiques du tenseur de conductivité thermique, résultant de considérations mécaniques statistiques [5], sont de nature symétrique [6]. Concernant les méthodes utilisées pour résoudre l'équation de la conduction thermique dans les milieux anisotropes, il existe généralement deux classes : celles basées sur des méthodes analytiques [[7], [8], [9]] et celles basées sur des approximations numériques telles que la méthode des éléments finis [[10], [11]], la méthode des éléments finis de frontières [[12], [13]], la méthode des volumes finis [[14], [15]] et la méthode des différences finies [[16], [17]]. En général, ces méthodes sont résolues dans des systèmes de référence qui respectent les caractéristiques intrinsèques des tenseurs de la conductivité thermique du matériau. Par exemple, la conduction thermique dans le bois, qui possède naturellement une anisotropie cylindrique, doit être modélisée en utilisant l'équation de la conduction thermique en coordonnées cylindriques et non cartésiennes ou sphériques. Cependant, en ce qui concerne la modélisation numérique de la conduction thermique dans un corps solide incompressible multi-matériaux avec des tenseurs de conductivité thermique multi-orientation (cartésiens et/ou cylindriques et/ou sphériques), la littérature ne semble pas avoir suffisamment abordé ce type de problème. En effet, la seule référence détectée qui traite ce type de problème est celle fournie très récemment par Erchiqui et Annasabi [10]. L'approche proposée dans [10], appelée enthalpie spécifique volumétrique

tridimensionnelle hybride basée sur l'analyse par éléments finis, utilise l'équation anisotrope d'énergie en terme d'enthalpie spécifique.

L'autre problème soulevé dans la littérature sur les problèmes thermiques, en régime permanent, est la difficulté de la résolution de l'équation de la conduction thermique par rapport à la transformation de Kirchhoff θ, qui est une fonction mathématique qui représente l'intégrale de la conductivité thermique d'un matériau en fonction de la température. Effectivement, du point de vue de la modélisation numérique, l'efficacité de la transformation de Kirchhoff pour résoudre les problèmes de conduction thermique est généralement limitée aux cas où la conductivité thermique est linéaire [18]. Pour une dépendance fortement non linéaire, la résolution de l'équation de la chaleur est difficile et différentes simplifications de la transformation de Kirchhoff sont souvent nécessaires, notamment l'utilisation de fonctions linéaires, de constantes ou de sous-domaines de température [19]. En fait, l'expression de θ(T) sous forme d'une intégrale est restrictive et entraîne l'inconvénient pratique de la transition inverse de la température à la transformation de Kirchhoff T(θ). Selon Vadasz [19], la transformée de Kirchhoff est un cas particulier de la transformée de Cole-Hopf [20] et sa définition classique avec une intégrale impose des inconvénients pratiques pour la transformation inverse. Par conséquent, certains auteurs comme Vadasz [19] ont suggéré l'utilisation directe de la transformation de Cole-Hopf pour les cas de dépendance exponentielle. Cependant, il existe une classe importante de matériaux dont la dépendance de la conductivité à la température n'est ni polynomiale ni exponentielle. Ces matériaux comprennent le fer, l'aluminium, le cuivre et l'or, dont la conductivité thermique varie avec la température [21]. Par ailleurs, la littérature scientifique traitant de la transformation de Kirchhoff n'aborde pas la convection h, probablement en raison de la difficulté à représenter h et les pertes par convection (h(T-T0)) en termes de θ. Par conséquent, les applications de la transformation de Kirchhoff à la résolution de problèmes de conduction thermique issus d'applications d'ingénierie restent très limitées, tant sur le plan analytique que sur le plan numérique. Un exemple de travaux numériques utilisant θ(T) et son inverse T(θ) trouvé dans la littérature est rapporté par Erchiqui et al. [10] concernant le chauffage anisotrope du bois dans

lequel la dépendance de la conductivité thermique par rapport à la température est linéaire. Parallèlement, un exemple de cas analytique trouvé dans la littérature est rapporté par Al-Khamaiseh et al. [22] à travers une approximation de la perte par convection $h(T-T_\infty)$ par '$-h(T_\infty)$' constante. Cet article propose une méthode permettant de contourner les difficultés inhérentes à la représentation de $\theta(T)$ et de son inverse $T(\theta)$ pour les solides à conductivité fortement non linéaire, avec ou sans convection naturelle, en utilisant une méthode B-Spline [23]. Dans ce contexte, une stratégie basée sur la méthode d'ingénierie inverse proposée dans [24] a été envisagée par Annasabi et Erchiqui [25]. La méthode consiste à identifier le nombre de nœuds et leurs emplacements respectifs dans la courbe $T(\theta)$ en fonction du coût de calcul le plus efficace. Le processus consiste à ajuster la courbe avec des fonctions B-spline pour obtenir l'emplacement des nœuds et à diviser les données en utilisant la méthode de bissection avec une erreur prédéterminée. La même stratégie est également utilisée pour le terme de perte par convection $h\ (T-T_\infty)$. En outre, les nœuds sont optimisés à l'aide de la méthode des moindres carrés non linéaires. L'approche proposée peut être combinée avec une méthode numérique telle que FEM, BEM et FVM pour la résolution non linéaire de l'équation de la chaleur par rapport à la variable.

De surcroît, la modélisation du chauffage diélectrique anisotrope des composites avec changement de phase aussi ne semble pas être élucidée dans la littérature. Effectivement, ce type de problème est très complexe et implique des interactions hautement non linéaires entre les propriétés mécaniques, thermiques et électriques [[26], [27], [2]] . Cela représente un défi de taille pour la simulation numérique, car il faut tenir compte du transfert de chaleur anisotrope et de masse, du changement de phase et des interactions thermomécaniques et électromagnétiques. Généralement, pour ce type de problème, la modélisation de la conduction de la chaleur avec changement de phase nécessite l'une ou l'autre des deux approches rencontrées dans la littérature : i) celle qui exprime l'équation de la conduction anisotrope de la chaleur en terme de la température comme variable dépendante [29-30] et ii) celle qui utilise l'enthalpie de volume [[28], [29]]. Cette dernière approche a l'avantage d'éliminer simultanément la duplication

de l'équation d'énergie pour les phases solide et liquide et d'éviter la présence de la frontière mobile (conditions mathématiques à l'interface eau-glace) [[28], [29]]. Concernant la modélisation de la chaleur dissipée par les ondes électromagnétiques (incluant les micro-ondes), qu'on désignera par Q dans le document, elle nécessite la connaissance du flux de puissance associé à la propagation des ondes électromagnétiques (vecteur de Poynting $\vec{P}$)[30] dans le milieu diélectrique [29]. Cela ne peut être réalisé que par la connaissance du champ électromagnétique induit dans l'espace du matériau, donc par la résolution des équations de Maxwell. Parmi les méthodes numériques déployées pour la résolution des équations de Maxwell on trouve : la méthode des éléments finis [[30], [31]], la méthode de volume fini [32], la méthode des différences finies [33] et la méthode des éléments finis de frontière [34]. Toutefois, lorsqu'il s'agit d'un diélectrique anisotrope, par exemple le matériau bois, les travaux sont trop limités.

Dans ce présent travail, quatre classes de contributions sont réalisées:

- Contribution à la modélisation numérique de la conduction de la chaleur, en régime transitoire, des solides multi-matériaux caractérisés par des tenseurs de conductivité thermique anisotrope et de natures différentes. L'équation de la conduction de la chaleur est exprimée par la variable température.
- Contribution à la modélisation numérique de la conduction de la chaleur, en régime transitoire, des solides multi-matériaux caractérisés par des tenseurs de conductivité thermique anisotrope et de natures différentes, avec ou sans changement de phase. L'équation de la conduction de la chaleur est exprimée par la variable enthalpie volumique.
- Contribution à la modélisation numérique de la conduction de la chaleur, en régime stationnaire, par la transformée de Kirchhoff : i) cas de conduction-convection et ii) cas de conduction-convection-radiation (conditions aux limite).
- Contribution à la modélisation de chauffage diélectrique des biocomposites (matériaux diélectriques) anisotrope et non linéaire avec changement de phase.

Dans le cas de la résolution numérique de l'équation de la conduction en fonction de la température, la méthode implicite des éléments finis est considérée. Pour l'amélioration de l'efficacité et de la précision de la solution numérique, la stratégie prédicteur/correcteur est utilisé [35]. L'approche proposée est validée pour cinq situations :

1. Distribution de la température analytique dans un cylindre anisotrope avec un transfert de chaleur convectif (avec variation circonférentielle).
2. Distribution de la température analytique dans une sphère anisotrope avec un transfert de chaleur convectif (avec variation circonférentielle).
3. Distribution de la température numérique pour une plaque carrée constituée de deux matériaux différents, dont l'un est un matériau isotrope, tandis que le second est orthotrope.
4. Chauffage anisotrope du bois (en tenant compte du changement de phase). À titre, d'application, nous avons considéré le problème de chauffage anisotrope du bois, de l'Amérique du Nord, initialement à l'état gelé, à l'aide des micro-ondes. Ce choix de température négatif est motivé par des considérations climatiques qui caractérisent plusieurs régions de l'Amérique du Nord dont les températures hivernales sont plus basses qu'ailleurs dans le monde. Les propriétés thermo-physiques et diélectriques du bois sont considérées dépendantes de l'humidité, de la température et des trois directions structurelles du bois. Pour l'analyse, nous considérons la fréquence 2,45 GHz et une température initiale de -20^{o}C.
5. Distribution de la température analytique et numérique dans un cylindre creux dont la surface extérieure est soumise à un rayonnement. Trois conductivités thermiques sont considérées : i) constante, ii) linéaire et iii) non linéaire.

CHAPITRE 1

3D HYBRID FINITE ELEMENT ENTHALPY FOR ANISOTROPIC THERMAL CONDUCTION ANALYSIS

Erchiqui[a] F., Annasabi Z. [b]

International Journal of Heat and Mass Transfer, Elsevier. Facteur d'impact : 5.76. Date de soumission le 31 octobre 2018. Accepté le 26 février 2019

[a]: Université du Québec en Abitibi Témiscamingue, école de génie, 455, boulevard de l'Université, Rouyn-Noranda (Québec), Canada J9X 5E4

[b]: Université du Québec en Abitibi-Témiscamingue, école de génie, 455, boulevard de l'Université, Rouyn-Noranda (Québec), Canada J9X 5E4

Rôle de l'étudiant dans cette publication :

Contribution à l'élaboration de modèles mathématiques, de calcul numérique, de l'interprétation des résultats et de la rédaction de l'article.

Abstract: The anisotropic problem of thermal conduction in a solid is generally treated in a reference coordinate system, which adequately describes its thermal conductivity tensor (Cartesian, cylindrical or spherical). For this problem, numerical treatment is difficult, especially if the thermophysical properties are non-linear or if the anisotropic medium undergoes a phase change. In this paper, we propose an approach using a Cartesian reference system to treat the anisotropic thermal conduction of problems for which the solid medium is characterized by a set of tensors of thermal conductivity of different natures (Cartesian and/or cylindrical and/or spherical), with or without phase change. For this purpose, the anisotropic thermal conductivity tensor, with respect to a cylindrical or spherical coordinate system, is transformed by an equivalent tensor into global Cartesian coordinates. The nonlinear heat conduction problem involving phase changes, such as wood freezing, is solved using hybrid three-dimensional volumetric specific enthalpy based on finite-element analysis. The proposed approach is validated by analytical testing for two anisotropic media and with two experimental tests related to the heating of frozen woods. As an application, we have numerically quantified, on the one hand, the minimum time required for the thaw and, on the other hand, the freezing of a log of wood, such as white pine, according to the length of its radius (7.5, 10, 15, 20 and 25 cm). The thermophysical properties are a function of temperature, moisture content and structural orientation.

Résumé : Le problème de la conduction thermique dans un solide anisotrope est généralement traité dans un système de coordonnées de référence qui décrit adéquatement le tenseur de conductivité thermique (cartésien, cylindrique ou sphérique). Pour ce problème, le traitement numérique est difficile, surtout si les propriétés thermophysiques sont non-linéaires ou si le milieu anisotrope subit un changement de phase. Dans cet article, nous proposons une approche utilisant un référentiel cartésien pour traiter la conduction thermique anisotrope de problèmes pour lesquels le milieu solide est caractérisé par un ensemble de tenseurs de conductivité thermique de natures différentes (cartésien et/ou cylindrique et/ou sphérique) avec ou sans changement de phase. Pour cela, le tenseur de conductivité thermique anisotrope, par rapport à un repère cylindrique ou sphérique, est transformé par un tenseur équivalent en coordonnées cartésiennes globales. Le

problème de conduction thermique non linéaire impliquant des changements de phase, tels que la congélation du bois, est résolu en utilisant une enthalpie spécifique volumétrique tridimensionnelle hybride basée sur une analyse par éléments finis. L'approche proposée est validée avec des tests analytiques pour deux milieux anisotropes et avec deux tests expérimentaux liés au chauffage de bois gelés. À titre d'application, nous avons quantifié numériquement, d'une part, le temps minimum requis pour le dégel et, d'autre part, le gel d'une bûche de bois, telle que le pin blanc, en fonction de la longueur de son rayon (7,5, 10, 15, 20 et 25 cm). Les propriétés thermophysiques sont fonction de la température, de la teneur en humidité et de l'orientation structurelle.

1.1 Introduction

The theory of thermal conductivity of anisotropic materials plays an important role in many areas of science and technology. These technical problems include: Li-ion batteries characterized by strong anisotropy of thermal conduction in Li-ion cells [1], the drying and thawing of wood by microwaves (wood is a highly hygroscopic and structurally-thermally anisotropic) [2] , the human tissues [3], the stratified structures [4], etc. In general, we find a lack of documentation to solve problems involving variable heat transfer coefficients on solid bodies (cylindrical, spherical, etc.) and for which the thermal conductivity is of an anisotropic nature. For these anisotropic media, the thermal conductivity must be expressed by a tensor taking into account the variation of the local thermal conductivity with the different directions characterizing the material [5] . From a theoretical point of view, the thermal conductivity tensor represents the general linear thermal conduction relationship between temperature gradients and heat flux in a heterogeneous anisotropic material [5]. This tensor, by the use of statistical mechanics, is symmetrical [6].

Regarding the modeling of the heating of anisotropic media, two classes of methods are generally used for the resolution of the energy conservation equation: one concerns analytical methods and the other numerical methods. Generally, these methods are solved in reference systems that respect the intrinsic characteristics of the tensor components of the thermal conductivity associated with the physical environment. For example, with wood for which the thermal conductivity naturally varies with three directions (longitudinal, circumferential and radial), a cylindrical coordinate system is often used.

Among the problems solved by the analytical methods, one can quote the approach used in [7] to determine, in cylindrical coordinates and in steady state, the distribution of the temperature in an anisotropic cylinder with convective heat transfer and with variable circumference. With an approach similar to that used in [7], the same authors present an analytical method, in spherical coordinates, for thermal conduction in an orthotropic sphere with a circumferentially variable

convection heat transfer [8].However, for the latter problem, it seems that it has never been validated numerically because of the spherical anisotropy that seems to be absent from real problems. With respect to the anisotropic plane structures, let us quote the work realized in [9] which uses an analytical approach, in stationary regime, to solve the problem of heat transfer by conduction in a rectangular thin film of quartz. In this regard, the authors used two variables to convert the anisotropic equations into isotropic equations. In the case of anisotropic monolayers and multilayers, the problem of conduction heat transfer is solved using a linear coordinate transformation that reduces the anisotropic problem to an equivalent isotropic problem [[36]-[37]]. Another example is the one provided in [12] on multilayer spherical fiber reinforced composite laminates and for which the temperature distribution is obtained using the linear boundary conditions and the method of separation of variables.

Concerning numerical methods, there are generally three approaches to study conduction heat transfer in anisotropic media: finite element method (FEM), boundary finite element method (BEM) and finite difference method (FDM). However, the work on heat transfer in anisotropic media is still limited in the scientific literature. Concerning the MEF, let us quote the work done in [2] on the anisotropic heating by microwaves of wood. In this paper, the effect of thermal and dielectric anisotropy on thawing wood is considered. The nonlinear heat conduction problem involving phase changes such as wood freezing is solved using three-dimensional volumetric specific enthalpy based on finite-element analysis. Concerning the BEM method, let us mention the work [[12],[13]] on a transformation approach to numerically treat two-dimensional and even three-dimensional anisotropic problems in field theory. In [9] , an approach based on the finite difference method is presented for the resolution of a 2D thermal conduction problem in an anisotropic medium. The problem is solved for a steady state condition in a rectangular thin film domain.

However, when the medium undergoes a phase change (e.g., solid to liquid), the solving of the numerical solution is more difficult due to the presence of one or more moving boundaries of

the solid-liquid phases. In general, two approaches to this type of problem are used: solving the energy equations for the liquid and solid phases separately, taking into account the moving boundary (solid-liquid interface) [[38],[39]], or solving the energy equation in terms of the enthalpy function [[2],[40]]. Recently, for cases regarding the thawing of frozen anisotropic wood by microwave energy, the nonlinear heat conduction problem is solved using 3D volumetric specific enthalpy based on finite-element analysis [2].

In general, the choice of reference coordinate system, used to study anisotropic problems of thermals conduction of solid, is guided by the natural orientation of the properties of the components in the thermal conductivity tensor of solid media (Cartesian, cylindrical or spherical). For example, the components of the tensor of the thermal conductivity of wood are naturally cylindrical (radial, tangential and longitudinal). In this paper, we propose an approach using a Cartesian reference system to treat anisotropic thermal conduction of problems for which the thermal conductivity tensor is of a cylindrical or spherical nature, with or without a phase change. To this end, we transform the anisotropic thermal conductivity tensor relative to a cylindrical or spherical coordinate system into an equivalent tensor in global Cartesian coordinates. The nonlinear heat conduction problem involving phase changes, such as wood freezing, is solved using hybrid three-dimensional volumetric specific enthalpy based on finite-element analysis. The proposed approach is validated with analytical testing for two anisotropic media (cylinder and spherical with convective transfer with variable circumference) and with two experimental tests related to the heating of frozen woods. In the case of the anisotropic sphere, to our knowledge, this is a first numerical validation study in the literature. As an application, we have numerically quantified, on the one hand, the minimum time required for the thaw and, on the other hand, the freezing of a log of wood, such as white pine, according to the length of its radius (7.5, 10, 15, 20 and 25 cm). In the case of thawing, the log (initial temperature -22 °C) is immersed in water at a constant temperature of 54 ° C. In the case of freezing, the initial log temperature is +22 °C. The thermophysical properties are a function of temperature, moisture content and structural orientation.

1.2 Fourier thermal conduction law

The conductivity tensor characterizes the general linear heat conduction relation between temperature gradients and heat flux in heterogeneous anisotropic material. If we consider the three-dimensional orthogonal coordinate system (x,y,z) as the reference frame and according to Duhamel's generalization of the Fourier thermal conduction law [5] for a linear anisotropic material, we have the following relations:

$$\vec{q}_{(x,y,z)} = \begin{pmatrix} q_x \\ q_y \\ q_z \end{pmatrix} = -\left[k^{(x,y,z)}\right] \begin{pmatrix} \frac{\partial T}{\partial x} \\ \frac{\partial T}{\partial y} \\ \frac{\partial T}{\partial z} \end{pmatrix}, \quad \text{where} \quad \left[k^{(x,y,z)}\right] = \begin{bmatrix} k_{xx} & k_{xy} & k_{xz} \\ k_{yx} & k_{yy} & k_{yz} \\ k_{zx} & k_{zy} & k_{zz} \end{bmatrix} \tag{1}$$

$k_{ij}^{(x,y,z)}$ are the components of the material thermal conductivity tensor, which relates the heat flux vector q_i to the gradient of the temperature field T. The minus sign in (1) assures that the heat flow occurs from a higher to a lower temperature. However, by using nonequilibrium statistical mechanics, Onsager [6] has shown that the conductivity tensor is symmetric:

$$k_{ij}^{(x,y,z)} = k_{ji}^{(x,y,z)} \tag{2}$$

The second law of thermodynamics causes the diametric elements of this tensor to be positive so the following relation must be satisfied [6]:

$$k_{ii}^{(x,y,z)} k_{jj}^{(x,y,z)} > k_{ij}^{(x,y,z)} \quad \text{for} \quad i \neq j \tag{3}$$

Using the Clausius-Duhem inequality, the following inequalities for the conductive coefficients of orthotropic materials are obtained:

$$k_{ii}^{(x,y,z)} \geq 0; \qquad \frac{1}{2}\left(k_{ii}^{(x,y,z)} + k_{jj}^{(x,y,z)} - k_{ji}^{(x,y,z)} k_{ij}^{(x,y,z)}\right) \geq 0 \tag{4}$$

$$\varepsilon_{ijk} k_{1j}^{(x,y,z)} k_{2j}^{(x,y,z)} k_{3j}^{(x,y,z)} \geq 0$$

where k_{ij} represents the symmetric part of tensor :

$$k_{ij}^{(x,y,z)} = k_{ji}^{(x,y,z)} = \frac{k_{ij}^{(x,y,z)} + k_{ji}^{(x,y,z)}}{2} \tag{5}$$

In cases of cylindrical and spherical local coordinate systems, the Fourier thermal conduction law, for a linear anisotropic material, becomes:

$$\vec{q}_{(\rho,\phi,z)} = \begin{pmatrix} q_\rho \\ q_\phi \\ q_z \end{pmatrix} = -\left[k^{(\rho,\phi,z)}\right] \begin{pmatrix} \dfrac{\partial T}{\partial \rho} \\ \dfrac{1}{\rho}\dfrac{\partial T}{\partial \phi} \\ \dfrac{\partial T}{\partial z} \end{pmatrix}, \text{ where } \left[k^{(\rho,\phi,z)}\right] = \begin{bmatrix} k_{\rho\rho} & k_{\rho\phi} & k_{\rho z} \\ k_{\phi\rho} & k_{\phi\phi} & k_{\phi z} \\ k_{z\rho} & k_{z\phi} & k_{zz} \end{bmatrix} \tag{6}$$

$$\vec{q}_{(r,\theta,\phi)} = \begin{pmatrix} q_r \\ q_\theta \\ q_\phi \end{pmatrix} = -\left[k^{(r,\theta,\phi)}\right] \begin{pmatrix} \dfrac{\partial T}{\partial r} \\ \dfrac{1}{r}\dfrac{\partial T}{\partial \theta} \\ \dfrac{1}{r\sin\theta}\dfrac{\partial T}{\partial \phi} \end{pmatrix}, \text{ where } \left[k^{(r,\theta,\phi)}\right] = \begin{bmatrix} k_{rr} & k_{r\theta} & k_{r\phi} \\ k_{\theta r} & k_{\theta\theta} & k_{\theta\phi} \\ k_{\phi r} & k_{\phi\theta} & k_{\phi\phi} \end{bmatrix} \tag{7}$$

$k_{ij}^{(\rho,\phi,z)}$ and $k_{ij}^{(r,\theta,\phi)}$ which are respectively the components of material thermal conductivity tensor in local frames for cylindrical (ρ,ϕ,z) and spherical (r,θ,ϕ) coordinates.

1.3 Hybrid Fourier thermal conduction law

Consider a Cartesian coordinate system in which $(\hat{e}_x,\hat{e}_y,\hat{e}_z)$ designate the set of three-unit vectors carried by the three axes, respectively, (Ox, Oy, Oz), (see **Figure 1**). Thus, every point M of the material space can be located in the global orthonormal coordinate system $(\hat{e}_x,\hat{e}_y,\hat{e}_z)$ by a vector $\vec{r}$ such as (eq. 8):

$$\vec{r}(x,y,z) = x\hat{e}_x + y\hat{e}_y + z\hat{e}_z \tag{8}$$

x, y and z being the Cartesian coordinates of the point M.

In cylindrical coordinates, the point M can be identified by the radius of the cylinder ρ, its dimension z with respect to the reference plane xOy and the angle ϕ (see **Figure 1**) and characterized by a cylindrical local orthonormal coordinate system $(\hat{e}_\rho,\hat{e}_\phi,\hat{e}_z)$.

The relations that connect the Cartesian coordinates (x, y, z) and their derivatives, relative to the cylindrical coordinates (ρ, ϕ, z), are given by the following formulas:

$$x = \rho \cos\phi \quad y = \rho \sin\phi \quad z = z \tag{9.1}$$

$$x_{,\rho} = \cos\phi \quad x_{,\phi} = -\rho \sin\phi \quad x_{,z} = 0 \tag{9.2}$$

$$y_{,\rho} = \sin\phi \quad y_{,\phi} = \rho \cos\phi \quad y_{,z} = 0 \tag{9.3}$$

$$z_{,\rho} = 0 \quad z_{,\phi} = 0 \quad y_{,z} = 1 \tag{9.4}$$

In spherical coordinates, the same point M can be characterized by the radius r (of the sphere to which it belongs), the angle θ (between the direction $\overrightarrow{Oz}$ and the direction $\overrightarrow{OM}$) and the angle φ (between the direction $\overrightarrow{Ox}$ and the direction $\overrightarrow{OM}$), see **Figure 1**: Vector in cylindrical and spherical coordinates. At point M, to which is attached a spherical local orthonormal coordinate system $(\hat{e}_r, \hat{e}_\varphi, \hat{e}_\theta)$, the relations that connect the Cartesian coordinates (x, y, z) and their derivatives, relative to the spherical coordinates (r, θ, φ), are given by the following formulas:

$$x = r \sin\theta \cos\phi \quad y = r \sin\theta \sin\phi \quad z = r \cos\theta \tag{10.1}$$

$$x_{,r} = \sin\theta \cos\phi \quad x_{,\theta} = r \cos\theta \cos\phi \quad x_{,\phi} = -r \sin\theta \sin\phi \tag{10.2}$$

$$y_{,r} = \sin\theta \sin\phi \quad y_{,\theta} = r \cos\theta \sin\phi \quad y_{,\phi} = r \sin\theta \cos\phi \tag{10.3}$$

$$z_{,r} = \cos\theta \quad z_{,\theta} = -r \sin\theta \quad z_{,\phi} = 0 \tag{10.4}$$

The base $(\hat{e}_x, \hat{e}_y, \hat{e}_z)$ is then connected to each of the bases $(\hat{e}_\rho, \hat{e}_\phi, \hat{e}_z)$ and $(\hat{e}_r, \hat{e}_\varphi, \hat{e}_\theta)$ by one or the other matrix expressions:

$$\begin{pmatrix} \hat{e}_\rho \\ \hat{e}_\phi \\ \hat{e}_z \end{pmatrix} = \left[T^{(\rho,\phi,z)}\right] \begin{pmatrix} \hat{e}_x \\ \hat{e}_y \\ \hat{e}_z \end{pmatrix} \quad \text{where} \quad \left[T^{(\rho,\phi,z)}\right] = \begin{bmatrix} \cos(\phi) & \sin(\phi) & 0 \\ -\sin(\phi) & \cos(\phi) & 0 \\ 0 & 0 & 1 \end{bmatrix} \tag{11.1}$$

$$\begin{pmatrix} \hat{e}_r \\ \hat{e}_\theta \\ \hat{e}_\varphi \end{pmatrix} = \left[T^{(r,\theta,\phi)}\right] \begin{pmatrix} \hat{e}_x \\ \hat{e}_y \\ \hat{e}_z \end{pmatrix} \quad \text{where} \quad \left[T^{(r,\theta,\phi)}\right] \tag{11.2}$$

$$= \begin{bmatrix} \sin(\theta)\cos(\varphi) & \sin(\theta)\sin(\varphi) & \cos(\theta) \\ \cos(\theta)\cos(\varphi) & \cos(\theta)\sin(\varphi) & -\sin(\theta) \\ -\sin(\varphi) & \cos(\varphi) & 0 \end{bmatrix}$$

$\left[T^{(\rho,\phi,z)}\right]$ is the matrix of passage from the global Cartesian coordinate system to the local cylindrical coordinate system. $\left[T^{(r,\theta,\phi)}\right]$ is the matrix of passage from the global Cartesian coordinate system to the local spherical coordinate system. Since the basics $(\hat{e}_x, \hat{e}_y, \hat{e}_z)$, $(\hat{e}_\rho, \hat{e}_\phi, \hat{e}_z)$ and $(\hat{e}_r, \hat{e}_\varphi, \hat{e}_\theta)$ are orthonormal, then $\left[T^{(*)}\right]^{-1} = \left[T^{(*)}\right]^t$ where $\left[T^{(*)}\right]^t$ and $\left[T^{(*)}\right]^{-1}$represent respectively the transpose and the inverse of the matrix $\left[T^{(*)}\right]$.

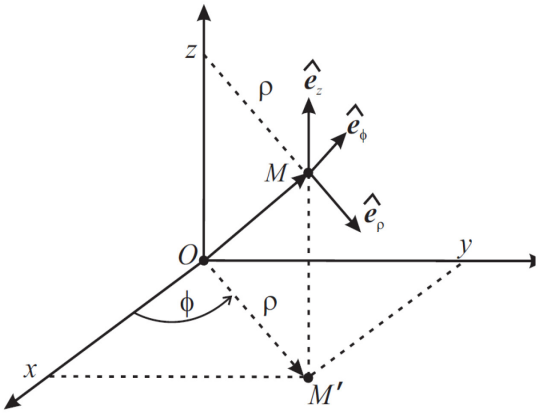

Cylindrical coordinates

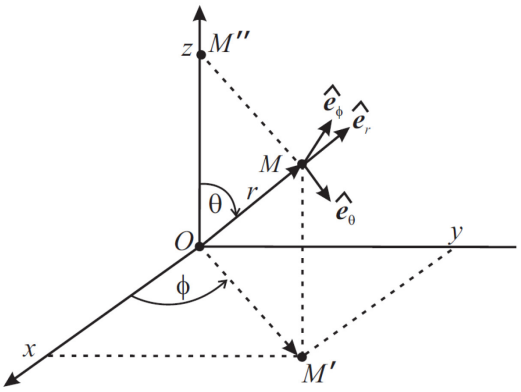

Spherical coordinates

Figure 1: Vector in cylindrical and spherical coordinates

From the formulas (9.2) - (9.4) and the use of the chain derivation rule, the cylindrical coordinate temperature gradient vector (ρ, ϕ, z) can be described by the temperature gradient vector in Cartesian coordinates (x, y, z) by:

$$\begin{pmatrix} \frac{\partial T}{\partial \rho} \\ \frac{1}{\rho}\frac{\partial T}{\partial \phi} \\ \frac{\partial T}{\partial z} \end{pmatrix} = \left[T^{(\rho,\phi,z)}\right]^t \begin{pmatrix} \frac{\partial T}{\partial x} \\ \frac{\partial T}{\partial y} \\ \frac{\partial T}{\partial z} \end{pmatrix} \tag{12.1}$$

In a similar way, using formulas (10.2) - (10.4), the temperature gradient vector in spherical coordinates (r, θ, φ) can be written in Cartesian coordinates (x, y, z) by:

$$\begin{pmatrix} \frac{\partial T}{\partial r} \\ \frac{1}{r}\frac{\partial T}{\partial \theta} \\ \frac{1}{r \sin\theta}\frac{\partial T}{\partial \phi} \end{pmatrix} = \left[T^{(r,\varphi,\theta)}\right]^t \begin{pmatrix} \frac{\partial T}{\partial x} \\ \frac{\partial T}{\partial y} \\ \frac{\partial T}{\partial z} \end{pmatrix} \tag{12.2}$$

Thus, taking into account the relationships (11.1) - (11.2) and (12.1) - (12.2), each of the expressions (6) and (7) of the heat flux, relative to the cylindrical (ρ, ϕ, z) and spherical (r, θ, φ) can be expressed in terms of the temperature gradient in Cartesian coordinates (x, y, z):

$$\vec{q}_{(\rho,\phi,z)} = -\left[\underline{k}^{(\rho,\phi,z)}\right] \vec{\nabla} T \tag{13.1}$$

$$\vec{q}_{(r,\theta,\varphi)} = -\left[\underline{k}^{(r,\theta,\varphi)}\right] \vec{\nabla} T \tag{13.2}$$

with :

$$\vec{\nabla} = \hat{e}_x \frac{\partial}{\partial x} + \hat{e}_y \frac{\partial}{\partial y} + \hat{e}_z \frac{\partial}{\partial z}, \tag{14.1}$$

and

$$\left[\underline{k}^{(\rho,\phi,z)}\right] = \left[T^{(\rho,\phi,z)}\right]^t \left[k^{(\rho,\phi,z)}\right] \left[T^{(\rho,\phi,z)}\right] \tag{14.2}$$

$$\left[\underline{k}^{(r,\theta,\varphi)}\right] = \left[T^{(r,\theta,\varphi)}\right]^t \left[k^{(r,\theta,\varphi)}\right] \left[T^{(r,\theta,\varphi)}\right] \tag{14.3}$$

$\left[\underline{k}^{(\rho,\phi,z)}\right]$ and $\left[\underline{k}^{(r,\theta,\varphi)}\right]$ represent respectively the equivalent tensors of the thermal conductivity relative to the cylindrical and spherical coordinate systems. Consequently, any

anisotropic problem expressed in a cylindrical or spherical coordinate system can be studied in a Cartesian system provided that the tensor of the thermal conductivity, relative to the cylindrical or spherical coordinate system, is replaced by an equivalent tensor in the Cartesian system.

In the case of an anisotropic material relating to a cylindrical system, the six components of the matrix $\left[\underline{k}^{(\rho,\phi,z)}\right]$ are given explicitly, according to the definition (14.2), by the following formulas:

$$\underline{k}_{11}^{(\rho,\phi,z)} = k_{\rho\rho}\cos^2\phi + k_{\phi\phi}\sin^2\phi - k_{\rho\phi}\sin 2\phi \tag{15.1}$$

$$\underline{k}_{12}^{(\rho,\phi,z)} = \underline{k}_{21}^{(\rho,\phi,z)} = \frac{1}{2}\left(k_{\rho\rho} - k_{\phi\phi}\right)\sin 2\phi + k_{\rho\phi}\cos 2\phi \tag{15.2}$$

$$\underline{k}_{13}^{(\rho,\phi,z)} = \underline{k}_{31}^{(\rho,\phi,z)} = \cos\theta\ k_{\rho z} - \sin\phi\, k_{\rho\phi} \tag{15.3}$$

$$\underline{k}_{22}^{(\rho,\phi,z)} = k_{\rho\rho}\sin^2\phi + k_{\phi\phi}\cos^2\phi + k_{\rho\phi}\sin 2\phi \tag{15.4}$$

$$\underline{k}_{23}^{(\rho,\phi,z)} = \underline{k}_{32}^{(\rho,\phi,z)} = \sin\theta\ k_{\rho z} + \cos\phi\, k_{\rho\phi} \tag{15.5}$$

$$\underline{k}_{33}^{(\rho,\phi,z)} = k_{zz} \tag{15.6}$$

In the case of an anisotropic material relating to a spherical system, the six components of the matrix $\left[\underline{k}^{(r,\theta,\varphi)}\right]$ are given explicitly, according to the definition (14.3), by the following formulas:

$$\underline{k}_{11}^{(r,\theta,\varphi)} = \cos^2\varphi\,(k_{rr}\sin^2\theta + k_{\theta\theta}\cos^2\theta + k_{r\theta}\sin 2\theta) + k_{\varphi\varphi}\sin^2\varphi - \sin 2\varphi\,(k_{r\varphi}\sin\theta + k_{\theta\varphi}\cos\theta) \tag{16.1}$$

$$\underline{k}_{12}^{(r,\theta,\varphi)} = \underline{k}_{32}^{(r,\theta,\varphi)} = \frac{1}{2}\sin 2\varphi\left(k_{rr}\sin^2\theta + k_{\theta\theta}\cos^2\theta - k_{\varphi\varphi} + 2k_{r\theta}\sin 2\theta\right) + \cos 2\varphi\left(k_{r\varphi}\sin\theta + k_{\theta\varphi}\cos\theta\right) \tag{16.2}$$

$$\underline{k}_{13}^{(r,\theta,\varphi)} = \underline{k}_{31}^{(r,\theta,\varphi)} = \frac{1}{2}\sin 2\theta\cos\varphi\,(k_{rr} - k_{\theta\theta}) + k_{r\theta}\cos 2\theta\cos\varphi + \sin\varphi\,(k_{\theta\varphi}\sin\theta - k_{r\varphi}\cos\theta) \tag{16.3}$$

$$\underline{k}_{22}^{(r,\theta,\varphi)} = \sin^2\varphi\,(k_{rr}\sin^2\theta + k_{\theta\theta}\cos^2\theta + k_{r\theta}\sin 2\theta) + k_{\varphi\varphi}\cos^2\varphi + \sin 2\varphi\,(k_{r\varphi}\sin\theta + k_{\theta\varphi}\cos\theta) \tag{16.4}$$

$$\underline{k}_{23}^{(r,\theta,\varphi)} = \underline{k}_{32}^{(r,\theta,\varphi)} = \frac{1}{2}\sin 2\theta\sin\varphi\,(k_{rr} - k_{\theta\theta}) + k_{r\theta}\cos 2\theta\,\sin\varphi + \cos\varphi\,(k_{r\varphi}\sin\theta - k_{\theta\varphi}\cos\theta) \tag{16.5}$$

$$\underline{k}_{33}^{(r,\theta,\varphi)} = k_{rr}\cos^2\theta + k_{\theta\theta}\sin^2\theta - 2\,k_{r\theta}\sin\varphi\cos\theta \tag{16.6}$$

In what follows, we consider, for the modeling of the thermal conduction in a cylindrical or spherical anisotropic medium, respectively the expressions (14.2) and (14.3) instead of the formulas used in (6) and (7).

1.4 Enthalpy model for anisotropic media

Heat conduction and phase changes in anisotropic media are naturally described by the energy conservation law in terms of the volumetric enthalpy H(T) [2]. In the case of a Cartesian reference system, this energy equation is given by the following expression [2] :

$$\frac{\partial H(T)}{\partial T} = \left(\frac{\partial}{\partial x_i}\frac{\partial \theta_{ij}(T)}{\partial x_j}\right) + Q(T) \tag{17}$$

where θ_{ij} are components of the anisotropic thermal conductivity integral tensor $\underline{\boldsymbol{\theta}}(T)$. $Q(T)$ is the internal volumetric heat generation. T_m is the fusion temperature. To solve the problem, we introduce the boundary condition into eq. (17) as follows:

$$\left(n_x\frac{\partial \theta_{xx}}{\partial x} + n_y\frac{\partial \theta_{yy}}{\partial y} + n_z\frac{\partial \theta_{zz}}{\partial z}\right) + h(T - T_\infty) - \mathbf{q}\cdot\mathbf{n} = 0 \tag{18}$$

where **q** [W/m^2] is the heat flux, $\vec{n}$ is the outward normal vector (n_x, n_y, n_z) to the surface, h[W/m^2/°C] is the surface heat transfer coefficient and T_∞ is the temperature of the surrounding medium. The term h ($T–T_\infty$) represents the convection heat transfer from the material to the environment. The advantage of using an enthalpy rather than a temperature-based formulation is that it simultaneously eliminates the doubling of the energy equation and the Stefan conditions [41].

Taking into account, on the one hand, the definition of the anisotropic thermal conductivity integral tensor theta presented in [2], and, on the other hand, the notation used to represent the components of the equivalent tensor of the thermal conductivity (presented in section 1.3 above), we have the following expressions for θ_{ij} :

- Thermal conductivity integral relative to the cylindrical coordinates:

$$\theta_{ij}^{(r,\theta,\varphi)}(T \le T_m) = \int_{T_{ref}}^{T} \underline{k}_{ij}^{(r,\theta,\varphi)}(T)\, dT\,, \quad \theta_{ij}^{(r,\theta,\varphi)}(T > T_m) = \int_{T_m}^{T} \underline{k}_{ij}^{(r,\theta,\varphi)}(T)\, dT \tag{18.1}$$

- Thermal conductivity integral relative to the spherical coordinates:

$$\theta_{ij}^{(\rho,\phi,z)}(T \le T_m) = \int_{T_{ref}}^{T} \underline{k}_{ij}^{(\rho,\phi,z)}(T)\, dT\,, \quad \theta_{ij}^{(\rho,\phi,z)}(T > T_m) = \int_{T_m}^{T} \underline{k}_{ij}^{(\rho,\phi,z)}(T)\, dT \tag{18.2}$$

1.5 Implicit time integration scheme

Numerical time approximation schemes are used mainly to obtain the transient response. These numerical integration schemes derive recursion relations that relate H(t) at a moment of time t to H(t+Δt) at another moment of time t+Δt. The solution is then solved step by step starting from the initial conditions at time *t*=0 until the desired duration of the transient response is calculated. The most common numerical schemes for the solution of eq. (17) belong to the weighted Euler difference family of time approximations, as follows [42] :

$$H^{n+\alpha} = (1-\alpha)\, H^{n} + \alpha\, H^{n+1} \tag{19}$$

The parameter α varies in the range [0–1]. The α schemes are unconditionally stable when $\alpha \le 1/2$ and $O(\Delta t)$ are accurate, with the exception of the $O(\Delta t^2)$–convergent Crank–Nicolson scheme ($\alpha = 1/2$). Setting $\alpha = 1$ leads to the backward Euler (fully implicit) scheme, which is only first-order accurate but very stable and hence ideally suited for integration. In the present study, we consistently use the semi-implicit Crank–Nicolson scheme [42]. In this case, eq. (17) becomes:

$$(\mathbf{K}^{*}_{n+1} + \mathbf{G}^{*}_{n+1})\, \mathbf{H}_{n+1} = \mathbf{K}^{*}_{n}.\mathbf{H}_{n} + \mathbf{G}^{*}_{n}.\mathbf{H}^{2}_{n} + \mathbf{R}^{*}_{n,n+1} \tag{20}$$

where $\mathbf{K}^*$, $\mathbf{G}^*$ and $\mathbf{R}^*$ are modified global matrices and $\mathbf{H}_{n+1}$ is the vector of global nodal enthalpies at moment t_{n+1} [2].

1.6 Validation

The dynamic finite-element method outlined in the previous section was implemented in the general-purpose finite-element code *ThermoForm* developed by the principal author, Erchiqui. All computations described below were done on a PC in single precision.

1.6.1 Analytical validation of thermal conduction in an orthotropic cylinder with circumferentially varying convection heat transfer

To validate the enthalpy approach with analytical solution [7], we consider the steady state anisotropic thermal conduction problem of a uniform volumetric heat-generating cylinder Q, of radius R, subjected to circumferentially varying convective heat transfer h on its outer surface. In [7], we find the analytical expressions for the temperature distribution T (r,θ) for the infinite cylinder, and T (r, θ, z) for the finite cylinder. **Figure 2**, extracted from [7], illustrates this problem under two considerations: infinite and finite cylinder. The values of Q and R are respectively 80000 W/m^3 and 0.013 m. **Figure 3** illustrates the variation of h as a function of polar angle θ.

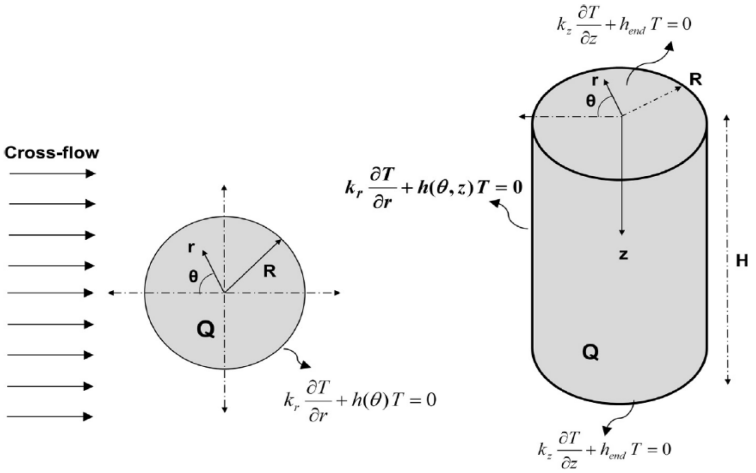

Figure 2: Schematic of the geometry under consideration for infinite and finite cylinder subjected to circumferentially varying convection

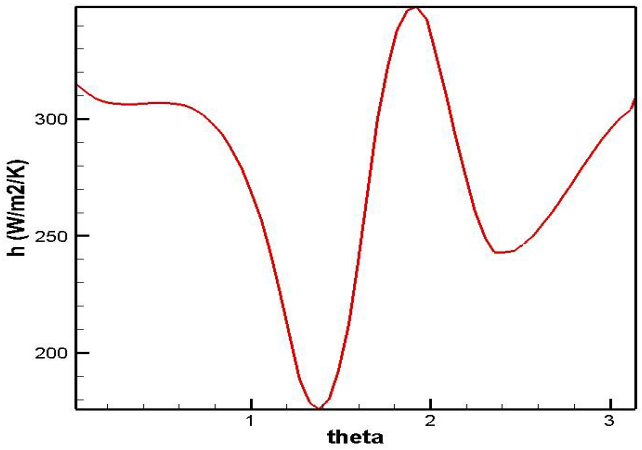

Figure 3: Variation of the exchange coefficient as a function of angle θ (case 3)

The problem of thermal conduction in an orthotropic cylinder, with circumferentially varying convection heat transfer, is governing by bellow energy equation:

$$\frac{k_r}{r}\frac{\partial}{\partial r}\left(r\frac{\partial T}{\partial r}\right)+\frac{k_\theta}{r^2}\frac{\partial^2 T}{\partial \theta^2}+Q=0 \tag{21}$$

subject to the boundary conditions:

$$\frac{\partial T}{\partial r}=0 \ \text{ at } r=0 \tag{22.1}$$

$$k_r\frac{\partial T}{\partial r}+h(\theta).T=0 \ \text{ at } r=R \tag{22.2}$$

$$T(\theta)=T(\theta+2\pi) \tag{22.3}$$

$$\left.\frac{\partial T}{\partial \theta}\right|_{\theta}=\left.\frac{\partial T}{\partial \theta}\right|_{\theta+2\pi} \tag{22.4}$$

Three cases are studied analytically [7]:

- **Case 1**: Cylindrical material is isotropic with constant convective heat transfer coefficient: h = 300 W/m^2 K, $k_r = k_\theta = 30\ W/mK$
- **Case 2**: Cylindrical material is orthotropic with constant convective heat transfer coefficient: h = 300 W/m^2 K, $k_r = 0.2\ W/mK,\ k_\theta = 300\ W/mK$
- **Case 3**: Cylindrical material is orthotropic with circumferentially varying convective heat transfer: h = f(θ) (see Fig.2), $k_r = 0.2\ W/mK,\ k_\theta = 300\ W/mK$

For the finite-element analysis and validation, we consider three types of meshes (see **Figure 4**):

- **Mesh1**: 4-node quadrilateral elements (1009 elements and 980 nodes)
- **Mesh2**: 4-node quadrilateral elements (4264 elements and 4205 nodes).
- **Mesh3**: 8-node hexahedral elements (9800 elements and 11099 nodes).

Since the cylindrical thermal conductivity is orthotropic ($k_{\rho z} = k_{\rho\phi} = k_{z\phi} = 0$), formulas (15.1)-(15.6) are reduced to (to respect the notation given in [7], ϕ is replaced by θ):

$$\underline{k}_{11}^{(\rho,\theta,z)} = k_{\rho\rho}\cos^2\theta + k_{\theta\theta}\sin^2\theta \tag{23.1}$$

$$\underline{k}_{12}^{(\rho,\theta,z)} = \underline{k}_{21}^{(\rho,\theta,z)} = \frac{1}{2}\left(k_{\rho\rho} - k_{\theta\theta}\right)\sin 2\theta \tag{23.2}$$

$$\underline{k}_{13}^{(\rho,\theta,z)} = \underline{k}_{31}^{(\rho,\theta,z)} = \underline{k}_{23}^{(\rho,\theta,z)} = \underline{k}_{32}^{(\rho,\theta,z)} = 0 \tag{23.3}$$

$$\underline{k}_{22}^{(\rho,\theta,z)} = k_{\rho\rho}\sin^2\theta + k_{\theta\theta}\cos^2\theta \tag{23.4}$$

$$\underline{k}_{33}^{(\rho,\theta,z)} = k_{zz} \tag{23.6}$$

For modeling of thermal conduction in an orthotropic cylinder, the thermal conductivities, mentioned above, are used to determine the components, θ_{ij}, of the anisotropic thermal conductivity integral tensor $\underline{\boldsymbol{\theta}}(T)$ (see eq. 7).

Figure 5 illustrates the view of numerical temperature distribution obtained for case 1 by using 2D hybrid enthalpy-finite-element modeling. The following figures show the comparison between the analytical [7] and the numerical solutions obtained by the approach proposed in this paper:

Figure 6 Illustrates a comparison of the analytically computed temperature distribution for the infinite and finite cylinder (at mid-height) [7] with hybrid enthalpy-finite-element modeling results for case 1 (2D) and case 2 (2D and 3D).

Figure 7 Illustrates, in case 3, the analytically and numerically (with mesh1 and mesh2) distribution of the temperature on the surface concerned with the variation of the convection: **Figure-a** shows variation with θ for non-refined and refined mesh and **Figure-b** shows variation in circular domain. For greater precision, a more refined mesh is necessary.

Globally, the results illustrate the excellent agreement between the analytical and numerical solutions. The agreement is very good with an error of less than 0.1%.

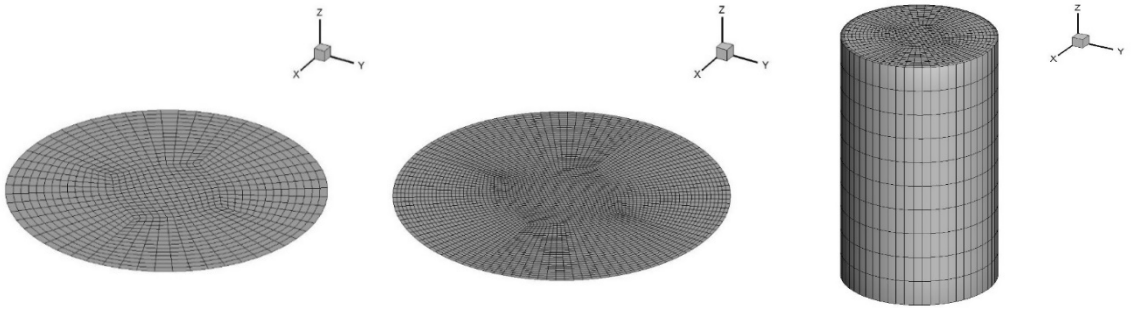

Mesh 1 (2D) *Mesh 2 (2D refined)* *Mesh 3 (3D)*

Figure 4: Circular (2D) and cylindrical (3D) geometry mesh

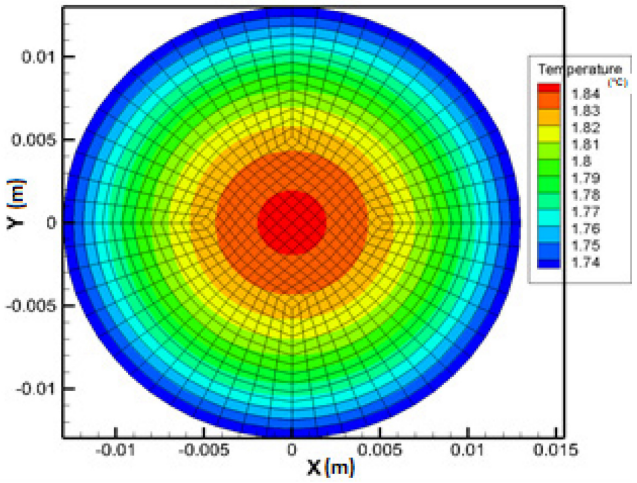

Figure 5: Numerical distribution of temperature (case 1)

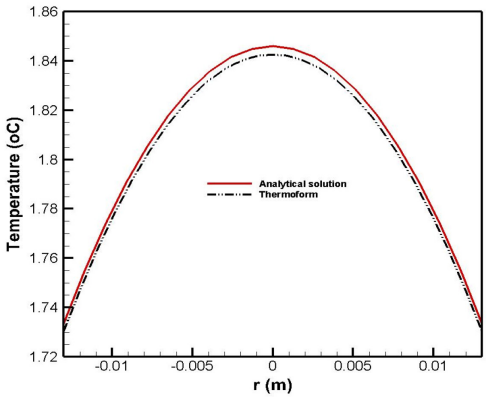

a)Numerical and analytical distribution of temperature for cases 1

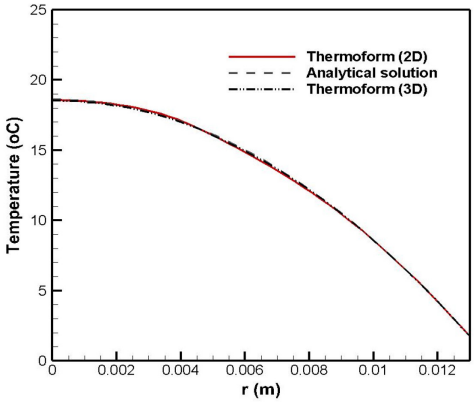

b) *Numerical and analytical distribution of temperature for cases 2*

Figure 6: Numerical and analytical distribution of temperature as a function of radial position

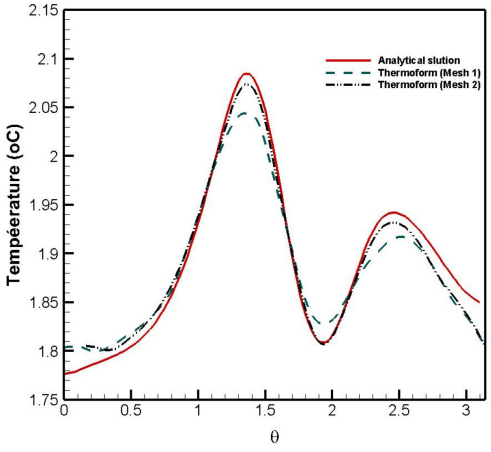

a) Numerical and analytical distribution of temperature as a function of θ for r=R (case 3)

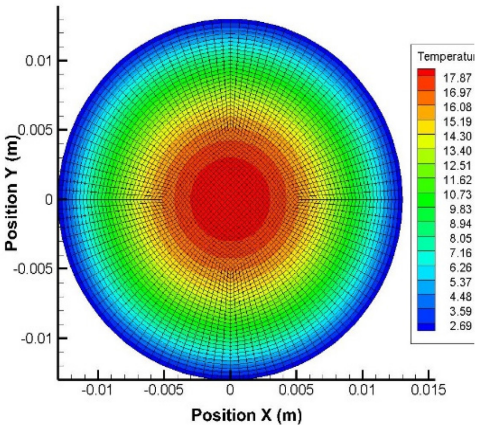

b) Refined mesh for numerical temperature distribution in case 3

Figure 7: Numerical and analytical distribution of temperature as a function of θ (case 3)

1.6.2 Analytical validation of thermal conduction in an orthotropic sphere with circumferentially varying convection heat transfer

To validate the enthalpy approach with analytical solution [8], we consider the spherical steady state anisotropic thermal conduction problem of a uniform volumetric heat-generating Q, of radius R, subjected to circumferentially varying convective heat transfer h on its outer surface. In [8], we find the analytical expressions for the temperature distribution T (r, φ, θ). **Figure 8**, extracted from [8], illustrates this problem. The values of Q and R are respectively 80000 W/m^3

and 0.1 m. The variation of h as a function of φ, illustrated in **Figure 9-a**, is given by: $h = 100\left(1 + \cos^2(\varphi/2)\right)$.

The problem of the spherical steady state anisotropic thermal conduction, with circumferentially varying convection heat transfer, is governing by bellow energy equation:

$$k_r\left(\frac{\partial^2}{\partial r^2} + \frac{2}{r}\frac{\partial T}{\partial r}\right) + \frac{k_\varphi}{r^2(1-\mu^2)}\frac{\partial^2 T}{\partial \varphi^2} + \frac{k_\mu}{r^2}\frac{\partial}{\partial \mu}\left((1-\mu^2)\frac{\partial T}{\partial \mu}\right) + Q = 0 \qquad (24)$$

subject to the boundary conditions:

$$\frac{\partial T}{\partial r} = 0 \ \text{ at } r = 0 \qquad (24.1)$$

$$k_r\frac{\partial T}{\partial r} + h(\varphi,\mu).T = 0 \ \text{ at } r = R \qquad (24.2)$$

$$T(r,\varphi,\mu) = T(r,\varphi+2\pi,\mu) \qquad (24.3)$$

$$\left.\frac{\partial T}{\partial \varphi}\right|_{\varphi} = \left.\frac{\partial T}{\partial \varphi}\right|_{\varphi+2\pi} \qquad (24.5)$$

where $\mu = \cos(\theta)$. $k_r, k_\varphi, \text{and } k_\mu$ are respectively the thermal conductivities in the r, φ and θ directions.

Two cases are studied analytically [8]:

- **Case 1**: Spherical material is isotropic ($k_\rho = k_\theta = k_\varphi = 0.2$ W/mK)
- **Case 2**: Spherical material is orthotropic ($k_\theta = k\varphi = 0.2$ W/mK and k_ρ=0.2, 0.5, 1, 10 W/mK)

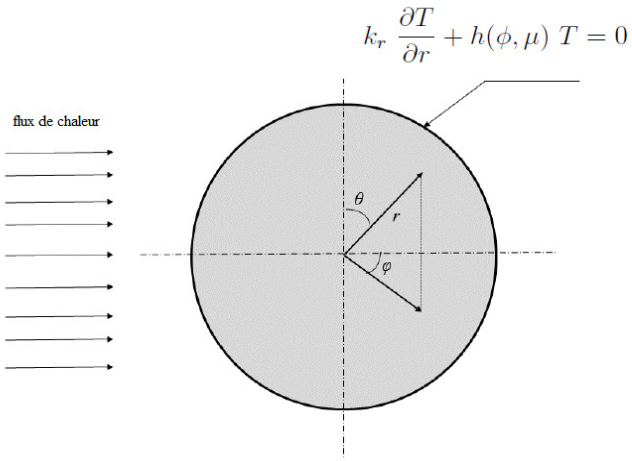

Figure 8: Mathematical description of the heat transfer problem for the spherical domain

Since the spherical thermal conductivity is orthotropic ($k_{r\theta} = k_{r\varphi} = k_{r\varphi} = 0$), formulas (16.1) - (16.6) are reduced to:

$$\underline{k}_{11}^{(r,\theta,\varphi)} = \cos^2\varphi\,(k_{rr}\sin^2\theta + k_{\theta\theta}\cos^2\theta) + k_{\varphi\varphi}\sin^2\varphi \tag{25.1}$$

$$\underline{k}_{12}^{(r,\theta,\varphi)} = \frac{1}{2}\sin 2\varphi\left(k_{rr}\sin^2\theta + k_{\theta\theta}\cos^2\theta - k_{\varphi\varphi}\right) \tag{25.2}$$

$$\underline{k}_{13}^{(r,\theta,\varphi)} = \frac{1}{2}\sin 2\theta\cos\varphi\ (k_{rr} - k_{\theta\theta}) \tag{25.3}$$

$$\underline{k}_{22}^{(r,\theta,\varphi)} = \sin^2\varphi\,(k_{rr}\sin^2\theta + k_{\theta\theta}\cos^2\theta) + k_{\varphi\varphi}\cos^2\varphi \tag{25.4}$$

$$\underline{k}_{23}^{(r,\theta,\varphi)} = \frac{1}{2}\sin 2\theta\sin\varphi\ (k_{rr} - k_{\theta\theta}) \tag{25.5}$$

$$\underline{k}_{33}^{(r,\theta,\varphi)} = k_{rr}\cos^2\theta + k_{\theta\theta}\sin^2\theta \tag{25.6}$$

For modeling of the spherical steady state orthotropic thermal conduction, the components of material thermal conductivity tensor, mentioned above, are used to determine the components, θ_{ij}, of the anisotropic thermal conductivity integral tensor $\underline{\boldsymbol{\theta}}(T)$ (see eq. 7).

For the finite-element analysis and validation, we consider 8-node hexahedral elements (2584 elements and 2401 nodes; see **Figure 9-b**).

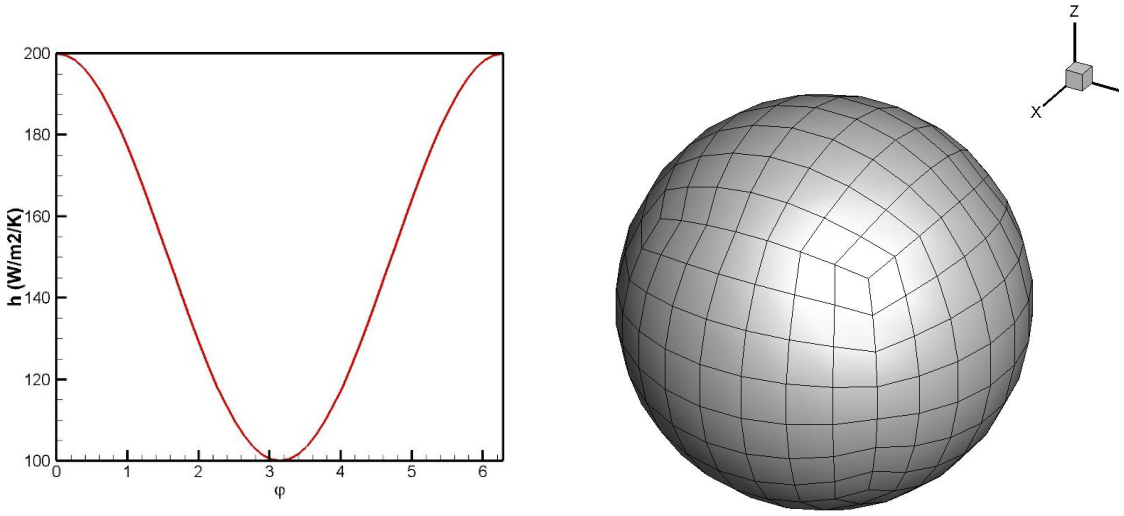

a) Variation of the exchange coefficient as a function of φ

b) Spherical geometry mesh

Figure 9: Variation of the exchange coefficient as a function of φ and Spherical geometry mesh

Figure 10 illustrates the view of numerical temperature distribution (at mid-diameter) obtained by hybrid enthalpy-finite-element modeling for case 1. The **Figure 11** Illustrates a comparison of the analytically computed temperature distribution [8] with *Thermoform* results for case 1 for two test: i) Numerical and analytical distribution of temperature as a function of radial position r and ii) numerical and analytical distribution of temperature as a function of φ for r=R.

The **Figure 12** illustrates, for case 2, the numerical and analytical distribution of temperature versus radial position r for different values of radial conductivity k_r.

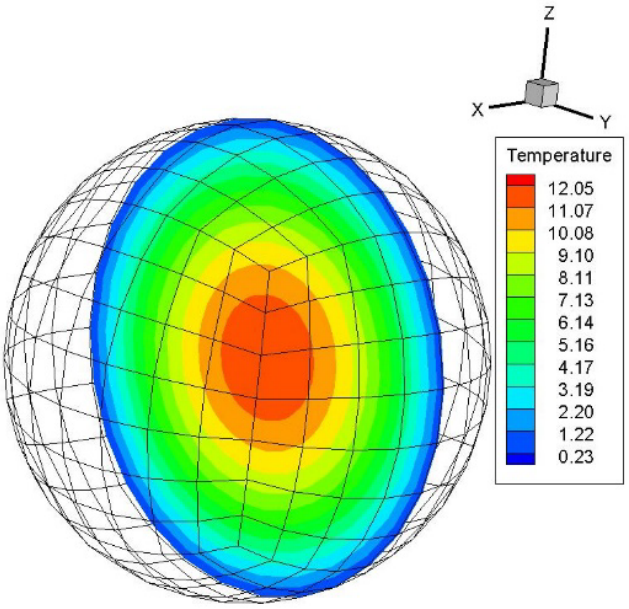

Figure 10: View of temperature distribution

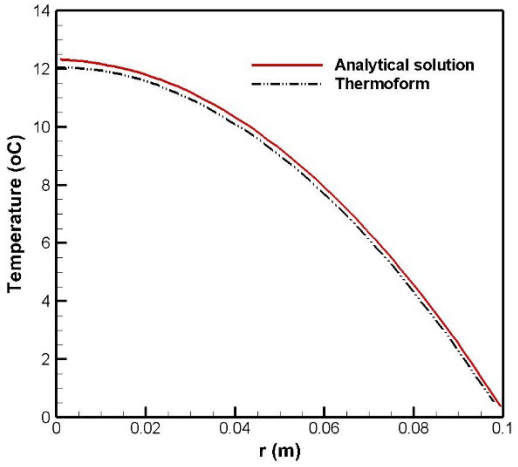

a) Numerical and analytical distribution of temperature as a function of r

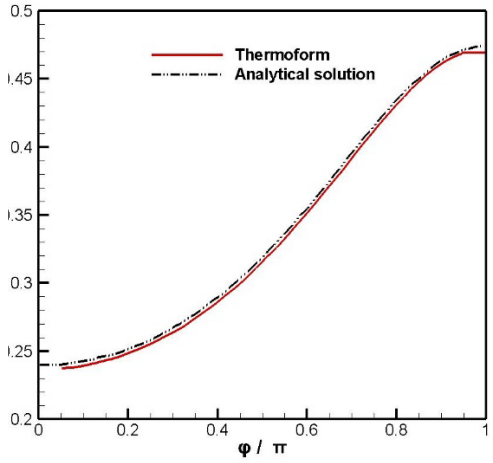

b) Numerical and analytical distribution of temperature as a function of φ for r=R

Figure 11: Numerical and analytical distribution of temperature (case 1)

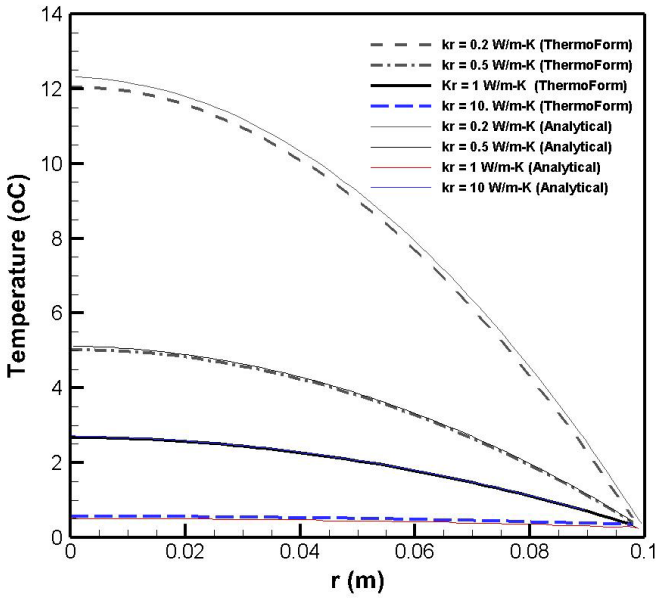

Figure 12: Numerical and analytical distribution of temperature versus r for different values of radial conductivity k_r (case 2)

The results illustrate the excellent agreement between the analytical and numerical solutions. The agreement is very good with an error of less than 0.1%.

1.6.3 Experimental heating validation: transient heating of frozen logs

In this section, firstly, we consider the experimental temperature measurements obtained for transient heating of frozen logs [43], then, those obtained in [11]. For both tests, it involves heating a tree trunk immersed in water at a temperature of 54 °C. In the first case, it is trembling aspen log (radius is 0.3175 m and its initial temperature is -22 °C). In the second test, it is eastern white pine log (the trunk radius is 0.2285 m and its initial temperature is -23 °C). In [43], it is assumed that logs is subjected to radial heating. In [11], it is assumed that logs is subjected to orthotropic heating (radial and longitudinal). For both tests, the heating time is 60 hours. The thermo-physical properties of the wood material are given in [43] and [11] respectively.

For finite element analysis, we consider a quadrilateral mesh (named Mesh1; see **Figure 4**). In **Figure 13**, we presented the history of the temperature obtained numerically (*2D*

hybrid enthalpy-finite-element modeling) and experimentally in the center of the trembling aspen trunk [43]. **Figure 14** illustrates views of the numerical temperature distribution at different times: 900, 1800, 2700, and 3600 minutes.

In **Figure 15**, we presented the temperature against heating time for three different points located 22.9 cm (location 1), 10.2 cm (location 2), and 2.5 cm (location 3) from the surface of an eastern white pine log [43]. The numerical results for the heating of frozen wood showed an excellent agreement with the experimental data, in both cases of tests.

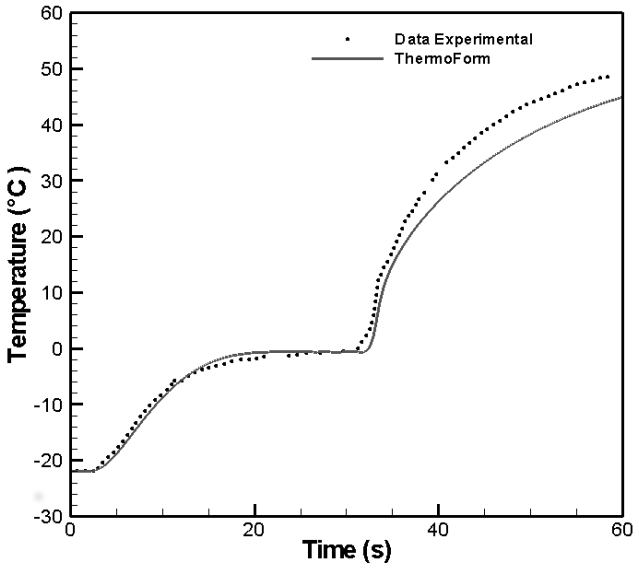

Figure 13: Experimental end numerical temperature vs heating time at the centre of log

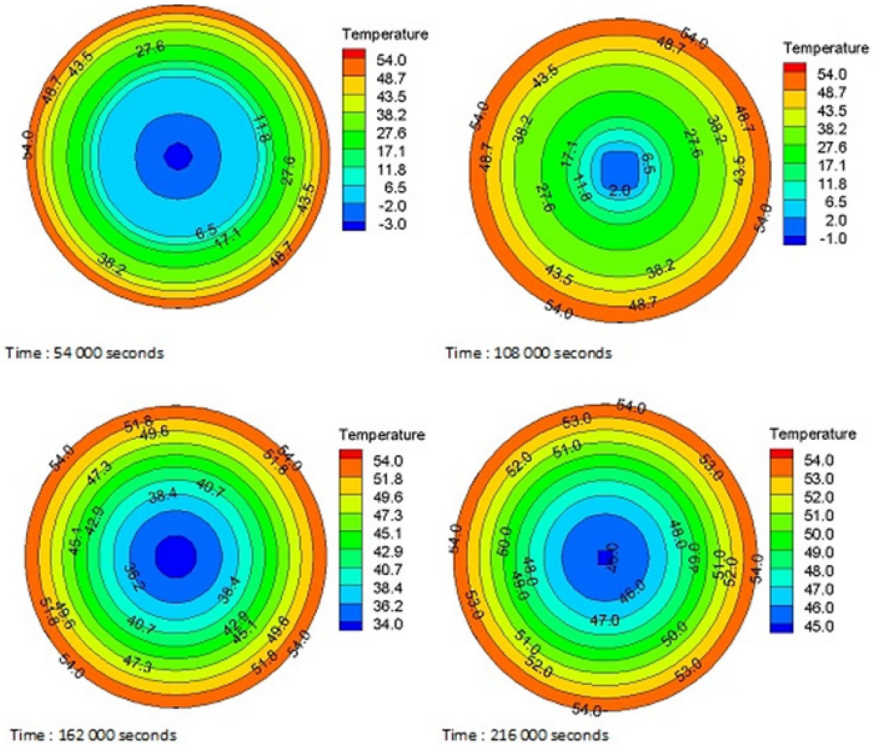

Figure 14: Temperature vs heating time at the centre of log

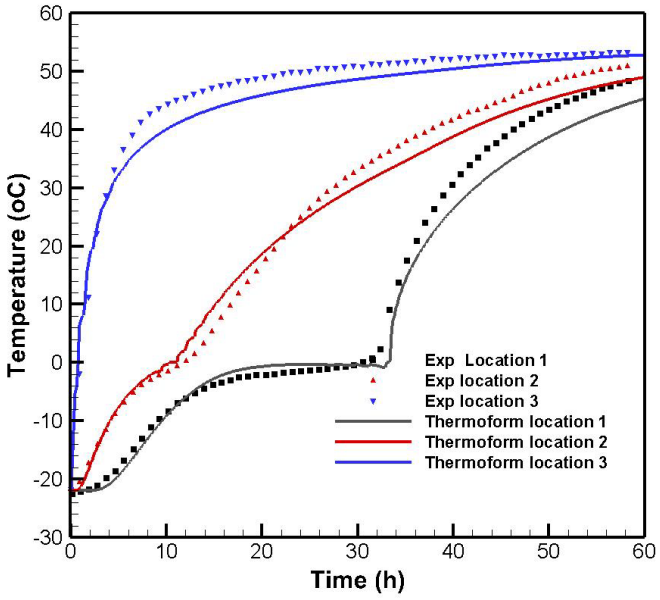

Figure 15: Experimental and numerical temperature vs heating time for three different points located from the surface of an eastern white pine log

1.7 Application: transient heating of frozen lumber

The purpose of this application is to numerically quantify, on the one hand, the minimum time required for the thawing and, on the other hand, the freezing of a log of wood, such as white pine, according to its radius (7.5, 10, 15, 20 and 25 cm). In the case of thawing, the log (initial temperature of -22 °C) is immersed in water at a constant temperature of 54 ° C. The heating time is 60 hours. In the case of freezing, the initial log temperature is +22 °C. For this study, we consider the approach presented in this paper (hybrid volumetric three-dimensional hybrid enthalpy based on finite element analysis).

The frozen log is usually cylindrical orthotropic material and its thermal properties are functions of temperature, moisture content and the structural orientation. The quantification of the thawing of the wood requires knowledge of the heat specific (C_p), through the latent heat of fusion (L), density (ρ) and thermal conductivity for radial (k_r), tangential (k_t) and longitudinal (k_l) directions. According to [38], for several species of wood, the ratio of longitudinal versus radial thermal conductivity is around 1.75 and 2.2, while the tangential thermal conductivity is usually slightly smaller (0.9 to 0.95 times) than the radial conductivity. However, in this work, we will retain the values of the thermal conductivity, in the longitudinal and radial directions (k_l= 2.5k_r), provided in reference [43]. Generally, the density, specific heat capacity and radial conductivity (k_R) are calculated as functions of temperature, moisture content MC (expressed in % of the dry mass of wood) and specific gravity (SG). For the calculation of thermophysical variables (ρ, C_p, k_r) and latent heat enthalpy we will use the following formulas, provided by [43]:

Tableau 1 : Thermophysical properties of logwood

Density	$\rho = \rho_w GS(1 + MC)$	(26)
Latent heat enthalpy	$L = \frac{L_w(MC - 30)}{MC + 100}$	(27)
Specific Heat	$T < T_f, \quad C_p = 2280 + 16.6 * T$ $T_f < T, \quad C_p = 2000 + 8.71 * MC + 4.98 * T$	(28)
Radial thermal conductivity	$T < T_f, \quad k_r = (0.096 + 0.0033 * MC - 0.0008 * T) * (0.105 + 2.03 * GS)$ $T_f < T, \quad k_r = (0.138 + 0.0019 * MC + 0.00022 * T) * (0.105 + 2.03 * GS)$	(29)

ρ_w and L_w are respectively the density and the latent heat of water fusion (334 10^3 J/kg). For trembling aspen log, the moisture content MC and specific gravity SG are fixed at 97% and 0.32 respectively [11].

For the numerical modeling, the cylindrical log is meshed with hexahedra comprising eight nodes (Mesh3; see Fig 3).

Figure 16 shows the temperature plotted against heating time for five different lengths of radius (7.5, 10, 15, 20 and 25 cm) of the eastern white pine log. According to **Figure 16** and for each case studied, we notice that during the frozen phase of the log, characterized by the presence of water in the ice form (negative temperatures), the temperature evolves more slowly than that observed in the phase after freezing (characterized by the presence of liquid water in the log). This remark is explained by two factors:

- Thermal conductivity. As a matter of fact, the thermal conductivity of wood is lower in the frozen phase than the liquid phase; see (eq. 29). In addition, since the thermal conductivities along the longitudinal and tangential directions are closely proportional to the radial conductivity, the same remark remains.
- The latent energy accumulation time in the frozen wood material. As a matter of fact, at the beginning of latent energy accumulation, the wood material is at a

melting temperature of 0 °C, which remains constant along this phase. Then, the temperature of the material increases more easily because of the thermal conductivity associated with the liquid phase.

In addition, we note that reaching the stationary regime depends largely on the radius of the log. In the case of the 7.5 cm, 10 cm and 15 cm, the stationary regimes are reached, respectively, for heating times of around 14h, 25h and 50 h. For the radius of 20 cm and 25 cm, the temperatures reached are respectively 51.1 °C and 39.6 °C, which is different from the temperature characterizing the stationary regime, which is 54 °C. Concerning the minimum heating times necessary for the thawing of the logs, they are also function of the radius of logs. It is minimal for the radius of 7.5cm (3.53 hours) and maximal for the radius of 25cm (39.2 hours).

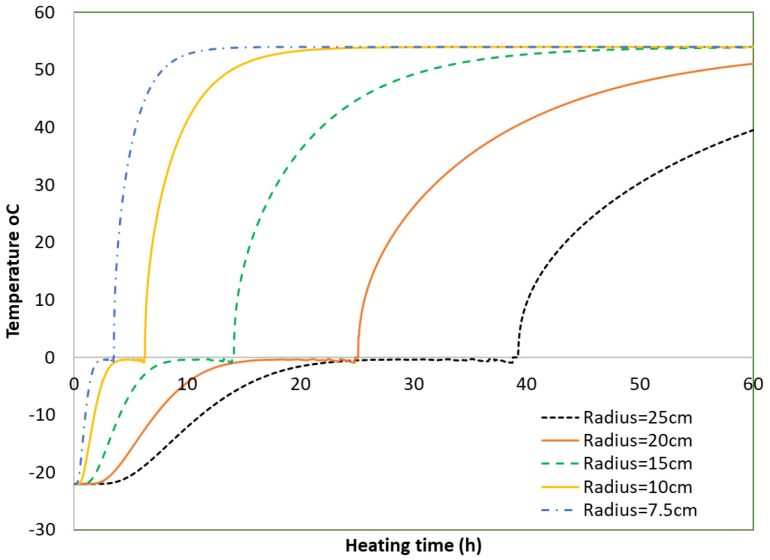

Figure 16: Temperature vs heating time at the centre of various radius of log

Figure 17 illustrates the minimum heating times required to thaw eastern white pine logs, for an initial temperature of -22 °C, as a function of radius of the log. In addition, in the same figure, we presented the correlation curve between the thawing time and the radius of the log. The correlation, with an almost perfect coefficient (R = 1), allows the mathematical description of eastern

white pine logs thaw time according to the radius, by a quadratic function in R, according to the following function:

$$T(R) \approx 0.062R^2 \quad (27)$$

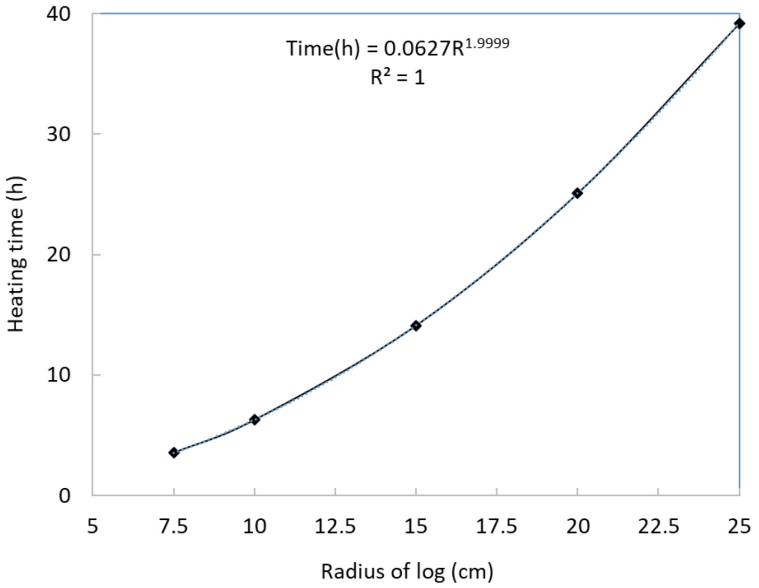

Figure 17: Relation between heating time (h) and radius of log (cm)

Figure 18 shows the temperature plotted against freezing time for the five different lengths of radius (7.5, 10, 15, 20 and 25 cm) of the eastern white pine log. According to this figure and for each case studied, the temperature decreases with time and the radius of the log. In **Figure 19**, we presented the correlation curve between the freezing time and the radius of the log. The correlation, with an almost perfect coefficient (R = 1), allows the mathematical description of eastern white pine logs freezing time according to the radius, by a quadratic function in R, according to the following function:

$$T(R) \approx 0.1175R^2 \quad (28)$$

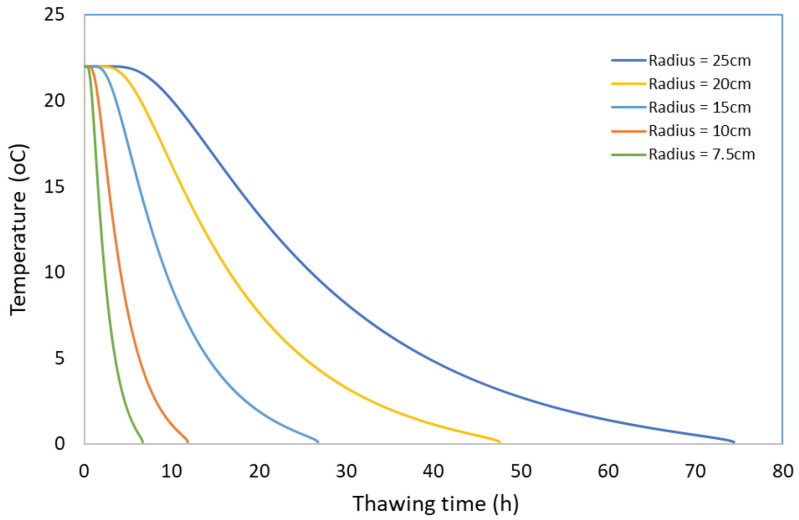

Figure 18: Temperature vs thawing time at the centre of various radius of log

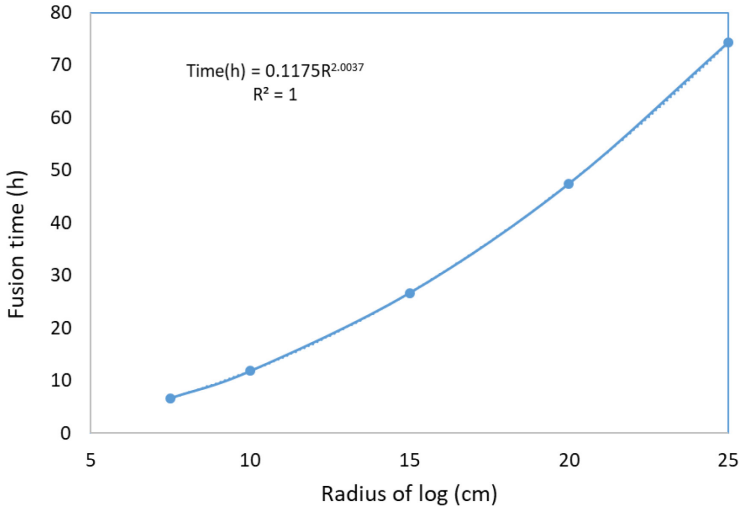

Figure 19: Relation between fustion time (h) and radius of log (cm)

In the light of the above results, the following remarks can be made on thawing or freezing logs:

- During the frozen phase of the log, the temperature evolves more slowly than that observed in the phase after freezing.
- Thawing time depends on the latent enthalpy and the conductivity of the wood.
- Thawing time is proportional to the square of the radius of the log.
- Freezing time is proportional to the square of the radius of the log.

This example of a numerical application on thawing or freezing of wood shows the advantage of using Cartesian finite element hybrid enthalpy to solve anisotropic thermal conduction problems. For the thawing of frozen logs, the general case will be treated in a future work using microwave energy.

1.8 Conclusion

This paper addresses the numerical heat conduction problem involving phase changes in anisotropic cylindrical and spherical media involving phase changes. For this, we have proposed a hybrid volumetric specific enthalpy based on finite-element analysis, involving Cartesian coordinates. To this purpose, we transformed the anisotropic thermal conductivity tensor relative to a cylindrical or spherical coordinate system into an equivalent tensor in global Cartesian coordinates. The numerical method is validated with the analytical testing of two anisotropic media (cylinder and spherical with convective transfer with variable circumference) and with two experimental tests associated with the heating of frozen woods. In the case of the anisotropic sphere, to our knowledge, this is a first numerical validation study in the literature. Finally, as an application, we have numerically quantified the minimum time required for the thawing of a wood log, such as eastern white pine, according to its radius (7.5, 10, 15, 20 and 25 cm). The thermophysical properties are a function of temperature, moisture content and structural orientation.

CHAPITRE 2

ROBUST KIRCHHOFF TRANSFORMATION USING B-SPLINE FOR FINITE ELEMENT ANALYSIS OF THE NON-LINEAR HEAT CONDUCTION

Annasabi Z. [a], Erchiqui F. [b]

International Communications in Heat and Mass Transfer, Elsevier. Facteur d'impact : 5.61. Publié le 28 octobre 2020

[a]: Université du Québec en Abitibi Témiscamingue, école de génie, 455, boulevard de l'Université, Rouyn-Noranda (Québec), Canada J9X 5E4

[b]: Université du Québec en Abitibi-Témiscamingue, école de génie, 455, boulevard de l'Université, Rouyn-Noranda (Québec), Canada J9X 5E4

Rôle de l'étudiant dans cette publication :

Contribution à l'élaboration de modèles mathématiques, de calcul numérique, de l'interprétation des résultats et de la rédaction de l'article.

Abstract: For non-linear problems, the solution of the heat equation in terms of the Kirchhoff transformation, $\theta(T)$, is very limited. This restriction is due to the practical disadvantage of the inverse temperature shift from the Kirchhoff transform $\theta(T)$. In order to get around the difficulties associated with the representation of $\theta(T)$ and its inverse $\theta(T)$ for solids with strongly non-linear conductivities, a strategy based on a reverse engineering method is considered. It consists in identifying the number of knots and their respective locations on the curve $\theta(T)$ at the most efficient computational cost. In order to obtain the location of the knots, the curve is fitted by B-spline functions and the data is partitioned by an application of the bisectional method with a predetermined error. These knots are further optimized using the non-linear least squares method. The proposed approach can be combined with a numerical method such as the FEM, BEM, and FVM to provide the non-linear solution of the heat equation in terms of θ. However, in this work we have limited ourselves to the FEM. The validation of the proposed approach is achieved through several cases ranging from constant to strongly non-linear thermal conductivities with or without convection. As an application, the 3D finite element method is applied to determine the non-linear temperature distribution in a copper block with an imposed temperature.

Résumé: Pour les problèmes non linéaires, la solution de l'équation de la chaleur en fonction de la transformation de Kirchhoff $\theta(T)$ est limitée. Cette limitation est due à la difficulté à trouver la fonction inverse de la transformée de Kirchhoff $T(\theta)$. Afin de contourner la difficulté liée à la représentation de $\theta(T)$ et de son inverse $T(\theta)$, pour les solides à conductivité thermique fortement non linéaire, une stratégie basée sur une méthode de rétro-ingénierie est envisagée. Elle consiste à identifier le nombre de nœuds et leurs emplacements respectifs sur la courbe $\theta(T)$ tout en minimisant le coût de calcul. Afin d'obtenir la localisation des nœuds, la courbe est approximée par des fonctions B-Spline et les données sont partitionnées par une application de la méthode de bissection avec une erreur prédéterminée. Ces nœuds sont encore optimisés à l'aide de la méthode des moindres carrés non linéaires. L'approche proposée peut être combinée avec une méthode numérique telle que FEM, BEM et FVM pour avoir la solution non linéaire de l'équation de la chaleur. Dans ce travail, la validation de l'approche proposée est réalisée par la méthode des

éléments finis FEM, pour plusieurs cas allant de conductivité thermique constante à fortement non linéaires avec ou sans convection. Comme application, la méthode des éléments finis 3D est appliquée pour déterminer la distribution de température non linéaire dans un bloc de cuivre avec une température imposée.

2.1 Introduction

The Kirchhoff transformation is a mathematical function that represents the integral of the thermal conductivity of a material in terms of the temperature. This function, noted $\theta(T)$, was introduced by Kirchhoff in 1894 to solve the problems of non-linear thermal conduction with temperature-dependent properties [44]. From the physical point of view, the choice to use the Kirchhoff transformation $\theta(T)$, generally in combination with the volume enthalpy H(T), is consistent with the first principle of thermodynamics especially for solids undergoing a phase change [45]. However, from the point of view of numerical modelling, the efficiency of the Kirchhoff transformation in solving non-linear heat conduction problems is generally limited to cases where the thermal conductivity is linear [[10],[18]]. For a strongly non-linear dependence, the solution of the heat equation is difficult and different simplifications of the Kirchhoff transformation are often needed, including the use of linear functions, constants, or temperature subdomains [19]. In fact an expression of $\theta(T)$ in terms of an integral is restrictive and causes the practical disadvantage of the inverse transition from the temperature to the Kirchhoff transform $T(\theta)$. According to Vadasz [19], the Kirchhoff transform is a particular case of the Cole-Hopf transform [20] and its classical definition with an integral imposes practical drawbacks for the inverse transformation. Consequently, some authors like Vadasz [19] have suggested the direct use of the Cole-Hopf transformation for the cases of exponential dependence. However, there is an important class of materials whose conductivity dependence on temperature is neither polynomial nor exponential. These materials include iron, aluminum, copper and gold, whose thermal conductivity varies with temperature [21]. Furthermore, the scientific literature treating the Kirchhoff transformation does not address h-convection, probably due to the difficulty to represent h and the convection losses (h(T-T0)) in terms of θ. As a result, the applications of Kirchhoff's transformation to the solution of heat conduction problems deriving from engineering applications remain very limited both analytically and numerically. An example of numerical works using $\theta(T)$ and its inverse $T(\theta)$ found in literature is reported by Erchiqui and al. [10] concerning anisotropic heating of wood in which the dependence of thermal conductivity on temperature is linear. Meanwhile, an example of analytical case found in literature is reported by Al-Khamaiseh and al. [22], an approximation of the

convection loss h (T-T_0) by h(θ-T_0), while T is approximated by θ and h is kept constant. This paper proposes a method to get around the difficulties inherent to the representation of θ(T) and its inverse T(θ) for solids with highly non-linear conductivities both with or without natural convection using a B-Spline method [23]. In this regard, a strategy based on a the reverse engineering method proposed in [24] is considered. The method consists in identifying the number of knots and their respective locations in the T(θ) curve based on the most efficient computational cost. The process consists in fitting the curve with B-spline functions to obtain the location of the knots and dividing the data using the bisection method with a predetermined error. The same strategy is also used for the convection loss term h ((T)-T_0). Furthermore, the knots are optimized using the non-linear least squares method. The proposed approach can be combined with a numerical method such as FEM, BEM, and FVM for the non-linear solution of the heat equation with respect to the variable θ.

The developed approach, in association with FEM, is further validated for the following cases:

- Materials with both a constant thermal conductivity and an imposed temperature;
- Materials with both a linear thermal conductivity and an imposed temperature;
- Materials with both a strongly nonlinear thermal conductivity and an imposed temperature;
- Materials with a constant thermal conductivity subjected to natural convection;
- Materials with a linear thermal conductivity subjected to natural convection;
- Materials with strongly nonlinear thermal conductivity subjected to natural convection.

The proposed approach was put into application through the finite element determination of the temperature distribution induced in a 3D copper block, which successively shows an imposed temperature on the upper surface, a lower adiabatic surface and convectional loss on the four sides.

2.2 The heat conduction equation

The steady state equation of energy for an anisotropic material in a region Ω bounded by a surface $\partial\Omega$ ($=\partial\Omega^1 \cup \partial\Omega^2$) is defined by Eq. (1) in a Euclidean space R^3, where T [°C] is the temperature, k [W/m/K] is the thermal conductivity of the material and Q is the source term [W/m^3].

$$\boldsymbol{\nabla}.(\mathrm{k(T)}\,\boldsymbol{\nabla}\mathrm{T(x,y,z)}) = \mathrm{Q}\,; \qquad (\mathrm{x,y,z}) \in \Omega \tag{1}$$

Eq. (1) is subjected to the following boundary condition:

$$\mathrm{T} = \varphi(\mathrm{x,y,z}); \qquad (\mathrm{x,y,z}) \in \partial\Omega^1 \tag{2}$$

$$\mathrm{k}\,\boldsymbol{\nabla}\mathrm{T}\cdot\mathbf{n} = \mathrm{h}(\mathrm{T}_\infty - \mathrm{T}) + \mathrm{q_n}; \qquad (\mathrm{x,y,z}) \in \partial\Omega^2 \tag{3}$$

where q [W/m^2] is the incident heat flux, **n** is the outward normal (n_x, n_y, n_z) to the surface, h [$W/m^2/°C$] is the heat transfer coefficient and T_∞ [°C] is the temperature of the surrounding medium. The Kirchhoff transform of the thermal conductivity, which also shows its variation with temperature, is defined by Elliot et al. [46] as shown in Eq. (4), where T_{ref} is a reference temperature.

$$\theta(\mathrm{T}) = \int_{\mathrm{T_{ref}}}^{\mathrm{T}} \mathrm{k}\,(\mathrm{T})\mathrm{dT}\,; \qquad \forall\ \mathrm{T(x,y,z)} \tag{4}$$

The gradient of the Kirchhoff transform can be rewritten using the Leibniz rule [47], to yield Eq. (5).

$$\boldsymbol{\nabla}\,\theta = \mathrm{k(T)}.\boldsymbol{\nabla}\,\mathrm{T} \tag{5}$$

An application of the $\boldsymbol{\nabla}$ operator on Eq. (5) yields Eq. (6) which follows:

$$\boldsymbol{\nabla}\,.\,(\mathrm{k(T)}\,\boldsymbol{\nabla}\,\mathrm{T}) = \nabla^2\,\theta \tag{6}$$

An insertion of Eq. (6) into Eq. (1) gives an expression of the heat equation in terms of θ as shown in Eq. (7).

$$\nabla^2\,\theta(\mathrm{T}) - \mathrm{Q} \;=\; 0 \tag{7}$$

The boundary conditions associated with Eq. (7) is expressed in terms of θ based on Eq. (3) as follows:

$$\frac{\partial\theta(\mathrm{x,y.z})}{\partial\mathrm{n}} = \boldsymbol{\nabla}\theta.\mathbf{n} = \mathrm{k}\boldsymbol{\nabla}\mathrm{T}\cdot\mathbf{n} = \mathrm{q_n} + \mathrm{h}(\mathrm{T}_\infty - \mathrm{T})\,; \qquad (\mathrm{x,y,z}) \in \partial\Omega^2 \tag{8}$$

In the contrary of Eq. (1) which expresses the heat equation in terms of temperature T, it can be seen from Eq. (7) that the advantage of expressing the heat equation in terms of θ lies in its linear form. However, in the cases where the thermal conductivity is dependent on temperature, the inverse integral function associated with the representation with respect to the temperature is quite challenging. In order to tackle this challenge, it is therefore necessary to apply the appropriate algorithms. It is in this context that the following sections are oriented. Firstly, the finite element approach that was used to solve the heat equation in terms of θ is described. Secondly, we describe the B-spline approach to determine the function $T(\theta)$ (inverse of $\theta(T)$) and its association with the finite element method to solve the heat conduction equation are described.

2.3 Finite Element Analysis

The spatial discretization of the boundary value problem associated with the heat conduction equation (eq. 7) is done using the Galerkin form of the method of weighted residuals [47]. In this regard, the domain Ω is subdivided by a finite number of finite elements. The variation of the θ-field in each element is approximated by the form given by Eq, (9):

$$\theta^{e}(x_i) = \sum_{n=1}^{N_e} N_e^n(x_i)\, \theta_e^n \tag{9}$$

Where N_e^n denotes the elementary interpolation function associated with the node n and θ_e^n the corresponding nodal-θ in the element. In order to develop the formulation of a Galerkin weighted residual valid throughout the Ω domain, the variations of the local functions associated with the node n and θ_e^n the corresponding nodal-θ given in Eq. (9) must be extended as shown by Eq. (10), which is written in matrix form as Eq. (11):

$$\theta(x_i) = \sum_{n=1}^{N} N^n(x_i)\, \theta^{e} \tag{10}$$

$$\theta(x_i) = \mathbf{N}^{T} \cdot \boldsymbol{\theta} \tag{11}$$

Where N is a vector of the interpolation functions defined on Ω, $\boldsymbol{\theta}$ is a Kirchhoff transform vector of nodal unknown points, superscript T denotes a vector transpose and N (see eq.10) is the

number of nodal points in the domain Ω. The substitution of Eq. (11) in the differential equation Eq. (7) leads to a set of residual equations which are designated by R:

$$\frac{\partial}{\partial x_i}\left(\frac{\partial\left(\mathbf{N^T}\cdot\boldsymbol{\theta}\right)}{\partial x_j}\right)-Q\left(\mathbf{N^T}\cdot\boldsymbol{\theta}\right)=R \tag{12}$$

However, it is worth noting that the Galerkin approach ensures the orthogonality of the residual vectors with respect to the interpolation functions. In other words:

$$R=0=\langle\mathbf{N},\mathbf{R}\rangle=\int_{\Omega}\mathbf{N}\cdot\ \mathbf{R}\,\mathbf{d\Omega} \tag{13}$$

By substituting the expression of R, given by Eq. (12), into Eq. (13), we then obtain Eq. (14).

$$\int_{\Omega}\mathbf{N}\left[\frac{\partial}{\partial x_i}\left(\frac{\partial\left(\mathbf{N^T}\cdot\boldsymbol{\theta}\right)}{\partial x_j}\right)-Q\left(\mathbf{N^T}\cdot\boldsymbol{\theta}\right)\right]d\Omega=0 \tag{14}$$

The integral equation above can be reformulated in a more practical form by reducing the order of derivation by one and introducing the boundary conditions of Eq. (8). This is achieved by applying the divergence theorem to equation (14), which gives Eq. (15):

$$\int_{\Omega}\frac{\partial\mathbf{N}}{\partial x_i}\left(\frac{\partial\mathbf{N^T}}{\partial x_j}\boldsymbol{\theta}\right)d\Omega=\int_{\Omega}\mathbf{N}Q\,d\Omega+\int_{\partial\Omega}\mathbf{N}\left(q_n+\ h(T_\infty-T\ )\right)d\Gamma \tag{15}$$

According to the integral equation Eq. (15), the quality of the algebraic solution is closely related to the quality of the representation of the temperature T and the product of the heat transfer coefficient with temperature, hT, in terms of θ. Finally, by placing the nodal unknowns outside the integrals, we obtained the algebraic form of Eq. (15):

$$\mathbf{K}\cdot\boldsymbol{\theta}=\mathbf{F_Q}+\mathbf{F_h} \tag{16}$$

where:

$$\mathbf{K}=\int_{\Omega}\frac{\partial\mathbf{N}}{\partial x_i}\left(\frac{\partial\mathbf{N^T}}{\partial x_j}\right)d\Omega \tag{16.1}$$

$$\mathbf{F_Q}=\int_{\Omega}\mathbf{N}Q(\theta)\,d\Omega \tag{16.2}$$

$$\mathbf{F_h} = \int_{\partial\Omega} \mathbf{N}\ \left(q_n + h(T_\infty - T)\right) d\Gamma \tag{16.3}$$

Equations (16.1)-(16.3) shows that during the numerical application of the Galerkin method, it is essential to represent each integral by an appropriate local approximation followed by an application of the standard process of assembling the global matrix **K** and the global vector **F** from their integral elementary contributions.

2.4 Expression of θ(T) and T(θ)

This work assumes that each function k(T), θ(T) and T(θ) can be represented by a function defined piecewise. Under these conditions, each of the functions can be defined by multiple sub-functions over a finite number of sub-domains (sub-intervals) of the main function. For the analysis, each function is assumed to be representable by a piecewise polynomial function. Consequently, each sub-function will be described by a polynomial on each sub-domain, but possibly a different polynomial on each sub-function.

Consider the case where the conductivity k(T) can be described by a continuous function over the interval [T_{min}, T_{max}] as follow:

$$k(T) = \sum_{ni=0}^{di} a_{ni} T^{ni}, \quad \text{for } T \in [T_i, T_{i+1}];\ T_{min} = T_0 < T_1 \ldots < T_n = T_{max} \tag{17}$$

Under its conditions, the new expression of the Kirchhoff transform of the Eq.(4) is given by Eq. (18):

$$\theta(T) = \sum_{ni=0}^{di+1} b_{ni} T^{i}\ ,\ \text{for } T \in [T_i, T_{i+1}] \tag{18}$$

The coefficients a_{ni} and b_{ni} ensure, respectively, the continuity of the functions k(T) and θ(T) in the interval [T_{min},T_{max}].

Similarly, taking into account Eq. (18), the temperature T is rewritten with respect to θ as shown in Eq. (19):

$$T(\theta) = \sum_{nj=0}^{dj} c_{nj} \theta^{nj}; \quad \text{for } \theta \in [\theta_i, \theta_{i+1}] \tag{19}$$

The coefficients c_{nj} ensure the continuity of the functions $\theta(T)$ over the interval $[T_{min},T_{max}]$. From the above equation, the elementary matrix expression of the temperature T, as a function of θ, in each element Ω^e of the domain Ω is:

$$\{T\}^e = \{c_0\} + [c_1].\{\theta\}^e + [c_2].\{\theta^2\}^e + \cdots [c_{dj}].\{\theta^{dj}\}^e, \qquad \text{for } \theta \in [\theta_i, \theta_{i+1}] \tag{20}$$

Taking into account the expression of Eq. (20), the algebraic equation Eq. (16) becomes:

$$(\mathbf{K} + \mathbf{C}) \cdot \boldsymbol{\theta} = \mathbf{F} \tag{21}$$

where:

$$\mathbf{C} = \int_{\Omega} h\,\mathbf{N} \cdot \left(\mathbf{C}_1 \cdot \boldsymbol{\theta}^1 + \mathbf{C}_2 \cdot \boldsymbol{\theta}^2 + \cdots + \mathbf{C}_{dj} \cdot \boldsymbol{\theta}^{dj-1}\right) \cdot \mathbf{N}^T \, d\Omega \tag{21.1}$$

$$\mathbf{F} = \int_{\partial\Omega} \mathbf{N}\ (q_n + hT_\infty)\, d\Gamma + \int_{\Omega} \mathbf{N}\, Q\, d\Gamma - \int_{\partial\Omega} h\,\mathbf{N} \cdot \mathbf{C}_0 \cdot \mathbf{N}^T \, d\Gamma \tag{21.2}$$

The matrix **K** is given by Eq.(16.1). In solving the algebraic system Eq. (21), it is essential to express the temperature as a function of θ and this according to the representation (16). For this purpose, the B-spline method is thus used as described in the paragraph below.

Strategy for the determination of T(θ)

The inverse of Eq. (4) is very tricky. In fact, finding the temperature according to θ is not easy, especially when the thermal conductivity is of degree 2 and higher. To get around this problem, a number of m points (T_i, θ_i) are constructed to describe the curve θ(T); followed by a temperature interpolation using B-splines functions from these data. The B-splines method of interpolation is chosen because it allows more local control of the curve, besides keeping the continuity of the function and its derivative.

A B-spline curve associated with n + 1 control points P_0, P_1,…. P_n is defined as shown in Eq. (22) [24]:

$$\overrightarrow{OM} = \sum_{i=0}^{n} B_{(i,k)} \overrightarrow{OP_i} \tag{22}$$

Where, $B_{(i,k)}$ are polynomial functions of degree k whose influence is localized to a number of elementary sub-domains of the curve θ(T). Thus, depending on the variation of the conductivity

as a function of temperature, the appropriate polynomial degree can be selected for each sector of the curve θ(T).

The choice of the distribution and number of control points plays an important role in the optimization of the calculation time and also in the final expression of the temperature according to θ. The smaller the number n, the more optimal the distribution of the control points. In this case, the expression of T as a function of θ is less elaborate (fewer polynomial segments). To improve the quality of the representation of T(θ), there are several strategies in the literature to solve this optimization problem [24]. In this case, the algorithm and the choice of control points is initialized by two points (T_{min} and T_{max}). Then, the position of the control points which minimizes the coefficient of determination of the curve T(θ) is located in each iteration. The loop stops when the desired accuracy is reached.

2.5 Validation

The dynamic finite-element method outlined in the previous section was implemented in *ThermoForm*, a general-purpose finite-element code. All computations were performed on a PC in a single precision.

The approach proposed in this document has been compared and validated with several cases obtained by the ANSYS software using the classical equation of the thermal conduction in terms of temperature. The cases concerned by the validation are:

- Materials with both a constant thermal conductivity and an imposed temperature;
- Materials with a linear thermal conductivity and an imposed temperature;
- Materials with both a strongly non-linear thermal conductivity and an imposed temperature;
- Materials with a constant thermal conductivity subjected to natural convection
- Materials with a linear thermal conductivity subjected to natural convection;
- Materials with strongly non-linear thermal conductivity subjected to natural convection.

2.5.1. Case 1: A material with both a constant thermal conductivity and an imposed temperature

This first case concerns a hollow disc with an internal radius of 0.25 m and an external radius of 1 m, subjected to an external temperature of 1 °C and an internal temperature of 40 °C. The thermal conductivity is constant 10 W/m/K. The finite-element analysis is done by considering a quadrilateral mesh with 1444 elements and 1520 nodes.

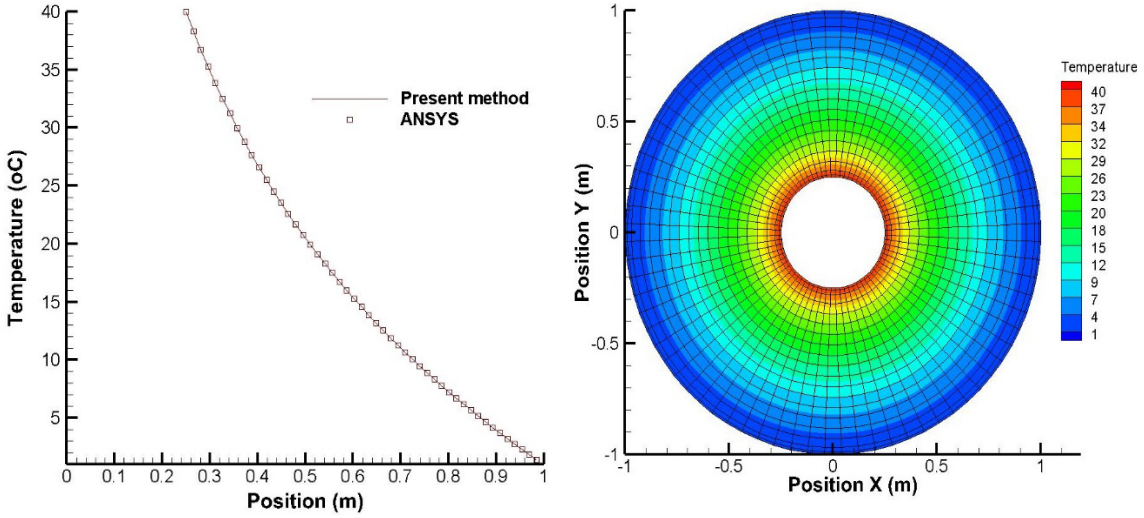

a. Comparison of temperature distribution: our method vs ANSYS

b. View of temperature distribution by present method

Figure 20: Comparative temperature distribution obtained by both the present method and ANSYS

Figure 20-a shows the comparison between the results of the temperature distribution obtained by the present method based on the Kirchhoff transformation θ and those derived from the ANSYS software based on the expression of the classical heat conduction equation in terms of the temperature T. Moreover, **Figure 20-b** gives a view of the temperature distribution in the study domain derived from the proposed method. It illustrates an excellent agreement between the two numerical solutions.

2.5.2. Case 2: A material with both a linear thermal conductivity and an imposed temperature

Unlike the first validation case where the thermal conductivity is constant, this second case considers a linear dependence of the conductivity with temperature. The application is made of an aluminum alloy. The physical domain considered for the analysis is similar in every aspect

(including the mesh size) to the one used in the first validation case. Similarly, the temperatures imposed are 40 °C for the inner circular boundary and 1 °C for the outer boundary. The conductivity is given by Eq. (20) that follows.

$$k(T) = 144 + 0.21\,T \quad , T \text{ in } ^{o}C \text{ and } k \text{ in W/m/K.} \tag{20}$$

Figure 21-a shows a comparison between the results of the temperature distribution obtained by both the proposed method and the ANSYS software, using of the classical heat conduction equation in terms of the variable temperature. The temperature distributions illustrate an excellent agreement between the two numerical solutions. **Figure 21-b** shows the view of the temperature distribution obtained by the present method.

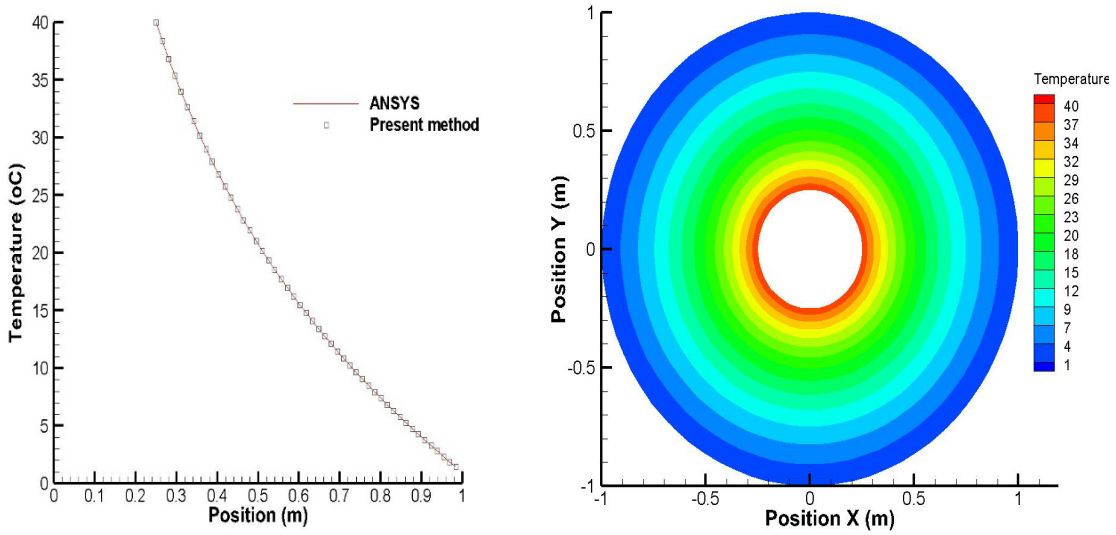

a. Comparison of temperature distribution: present method vs ANSYS *b. View of temperature distribution by present method*

Figure 21: Temperature distribution obtained by our method and ANSYS

2.5.3. Case 3: A material with both a strongly non-linear thermal conductivity and an imposed temperature

Contrary to the two previous validation cases, the third considers copper which thermal conductivity is strongly non-linear in the region of 0 and 70 K as shown in **Figure 22**. The physical domain used for the analysis is similar to that of the first validation case: That is a hollow disc with an internal radius of 0.25 m, an external radius of 1 m as well as the same mesh size. An imposed

temperature of 1 K was considered on the inner region of the disc, while 40 K, 60 K and 70 K were the three temperature cases on its outer border.

For the first case, where the imposed temperature is 40 K, a correlation factor of 0.999928 for the B-spline method was used. The convergence to the inverse function $T(\theta)$ which required three iterations, gave three third-degree polynomial sub-curves as shown in **Figure 23**. **Figure 24-a** shows a comparison between the results of the temperature distribution obtained by both the proposed method and the ANSYS software, using the classical heat conduction equation expressed in terms of the temperature T. It illustrates an excellent agreement between the two numerical solutions. **Figure 24-b** shows the view of the temperature distribution in the study domain based on the proposed method.

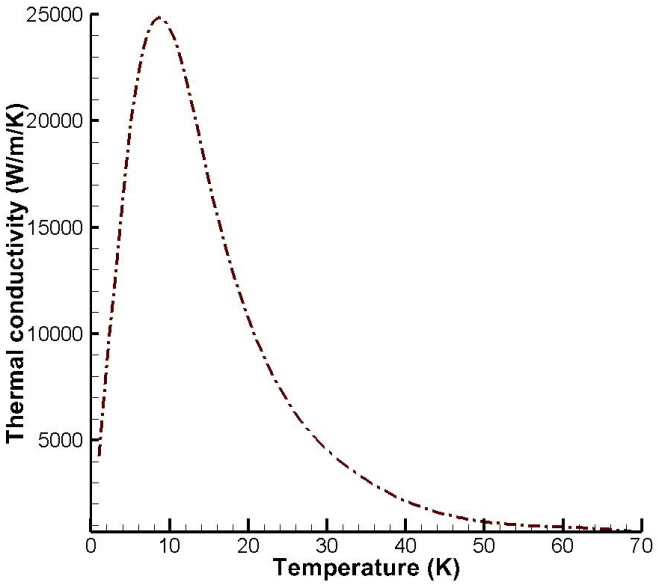

Figure 22: Variations of the thermal conductivity of copper with temperature in the non-linear region

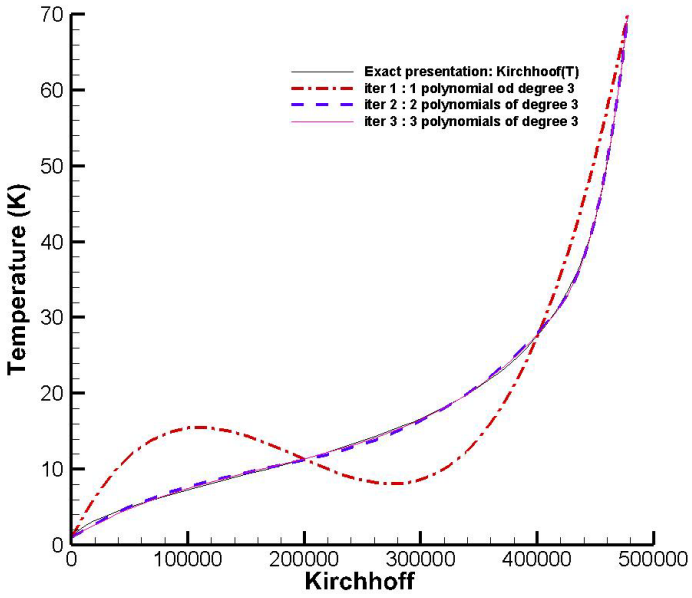

Figure 23: Convergence of iterations for the calculation of the inverse function T (θ)

In the two remaining cases where the imposed temperatures are 60 K and 70 K, the operation of finding the inverse of T(θ) was limited to a correlation of 0.999. The comparison between the results obtained from the two methods is shown in **Figure 25-a** and **Figure 25-b**, respectively, for the imposed temperatures of 60K and 70K. The temperature distributions illustrate an excellent agreement between the two numerical solutions.

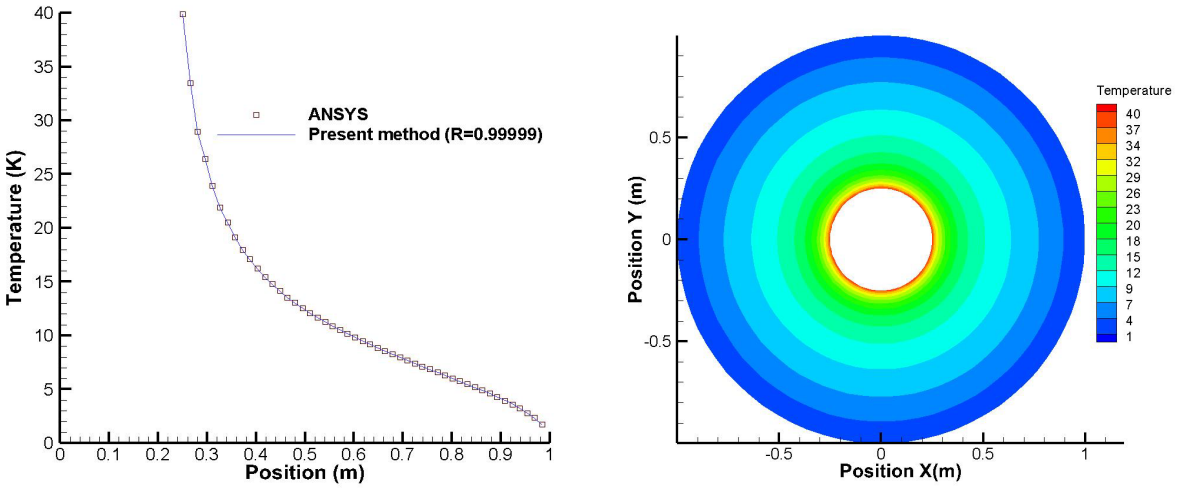

a. Comparison of the temperature distribution: the proposed method vs ANSYS

b. View of the temperature distribution by the proposed method

Figure 24: Temperature distribution derived from both the proposed method and ANSYS (T= 40 °C)

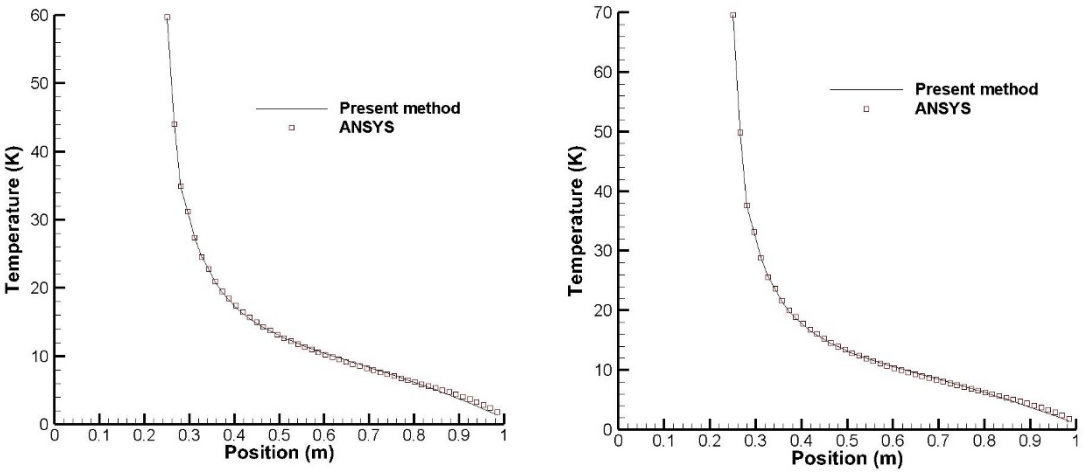

a. *Comparison of the temperature distribution: Imposed temperature 60* K

b. Comparison of the temperature distribution: Imposed temperature 70 K

Figure 25: Temperature distribution obtained derived from both the proposed method and ANSYS (T= 60 °C)

2.5.4. Case 4: A material with a constant thermal conductivity subjected to the natural convection

This case takes into consideration the natural convection problem. The physical domain use in the analysis is similar to that of the first validation case and bears the same mesh size. The heat transfer coefficient considered is 450 [W/m^2/K]. The ambient temperatures in the outer and inner part of the circular annular domain are respectively 1 and 40 °C. The temperature distributions illustrate an excellent agreement between the solutions derived from the two numerical approaches as shown in **Figure 26-a**. **Figure 26-b** shows the view of the temperature distribution in the field of study obtained by the proposed method.

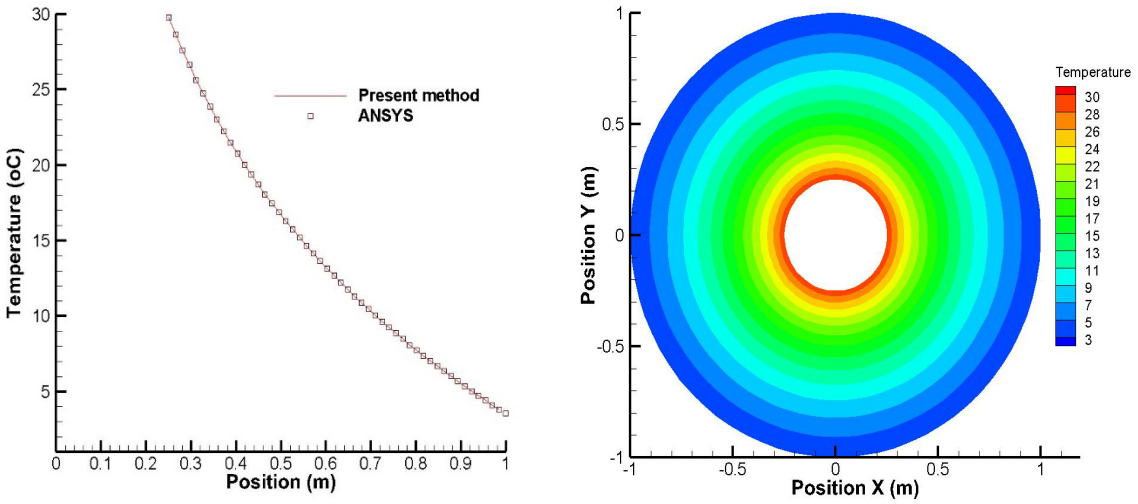

a. *Comparison of temperature from the two methods*

b. *View of temperature distribution derived from the proposed by present m*ethod

Figure 26 :Comparison between the temperature distributions derived from the proposed method and ANSYS

2.5.5. Case 5: A material with a linear thermal conductivity subjected to the natural convection

This case considers the natural convection of a material made of aluminum alloy. The physical domain used for the analysis is similar to that of the first validation case and uses the same mesh size. The heat transfer coefficient considered is 450 [W/m^2/K]. The ambient temperatures in the outer and inner parts of the circular annular domain are 1^{o}C and 40^{o}C respectively. The temperature distributions illustrate an excellent agreement between the solutions derived from the two numerical approaches as shown in **Figure 27-a**. **Figure 27-b** shows the temperature distribution in the field of study obtained by the proposed method.

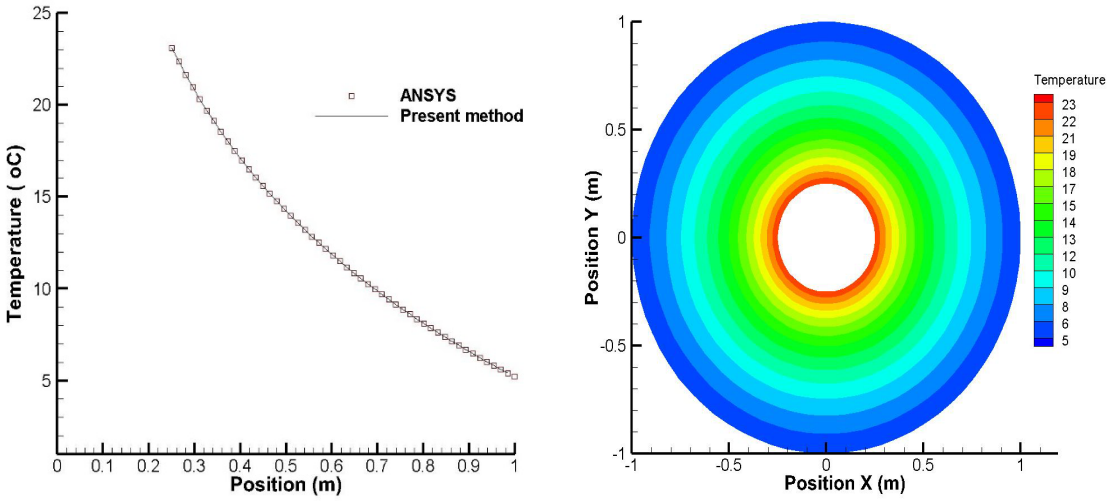

a. Comparison of temperature distribution from the two approaches *b. View of temperature distribution derived from the proposed method*

Figure 27: Comparison between the temperature distributions derived from both the proposed method and ANSYS

2.5.6. Case 6: A material with a strongly non-linear thermal conductivity subjected to the natural convection

The final validation case deals with the natural convection of copper in the region where its thermal conductivity is strongly non-linear between 0 and 70 K. The physical domain considered in the analysis is similar to that of the first validation case and uses the same mesh size. The heat transfer coefficient of copper is 450 [$W/m^2/K$]. The ambient temperatures in the outer and inner parts of the circular annular domain are 1 K and 70 K respectively. It is observed in **Figure 28-a** that the temperature distributions obtained by both the proposed method and ANSYS Software are in an excellent agreement. **Figure 28-b** further gives a view of the temperature distribution in the field of study obtained by the proposed method

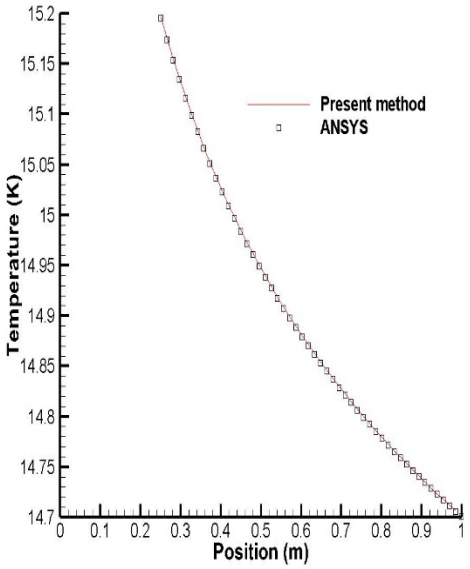

a.Comparison between the temperature distribution from both the proposed method and ANSYS

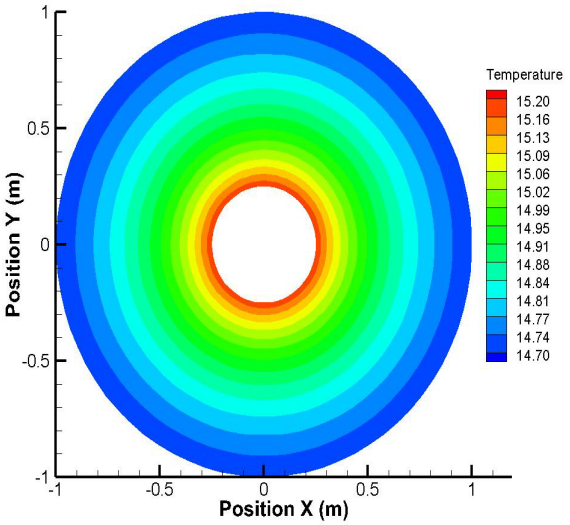

b. A view of the temperature distribution based on the proposed method

Figure 28: Comparison of the temperature distribution obtained by both the proposed method and ANSYS

In the light of the numerical validations of the method proposed for the solution of the heat conduction equation based on the Kirchhoff transform, and applied by *ThermoForm*, the following remarks can be made on the performance of this method:

Tableau 2 : Numerical performance of the proposed method

	Imposed temperature without convection		Imposed temperature with convection	
	ANSYS (*Full Newton Raphson*)	ThermoForm	ANSYS (*Full Newton-Raphson*)	ThermoForm (*Picard method*)
Aluminum alloy	2 iterations	0 iteration	2 iterations	2 iterations
Copper	18 iterations	0 iteration	3 iterations	5 iterations

Remarks: The iterations appearing in the case of the imposed temperature with natural convection is due to the non-linear nature of the problem since the inverse of the convective term h (T-T∞) must be found. It is also necessary to underline that the full Newton Raphson method requires a high computing time.

2.6 Application

Two cases of application by the finite element method are considered: i) The first case concerns the temperature distribution induced in a 3D copper block with the following conditions: temperature imposed on the upper surface, convection loss on the four lateral surfaces of the block (h=450 [W/m2/°C]) and the lower surface is adiabatic and ii) The second case, two-dimensional, is based on a hypothetical non-linear conductivity whose shape is similar to the hump of a camel, which we have called *camel conductivity* as shown in **Figure 29**.

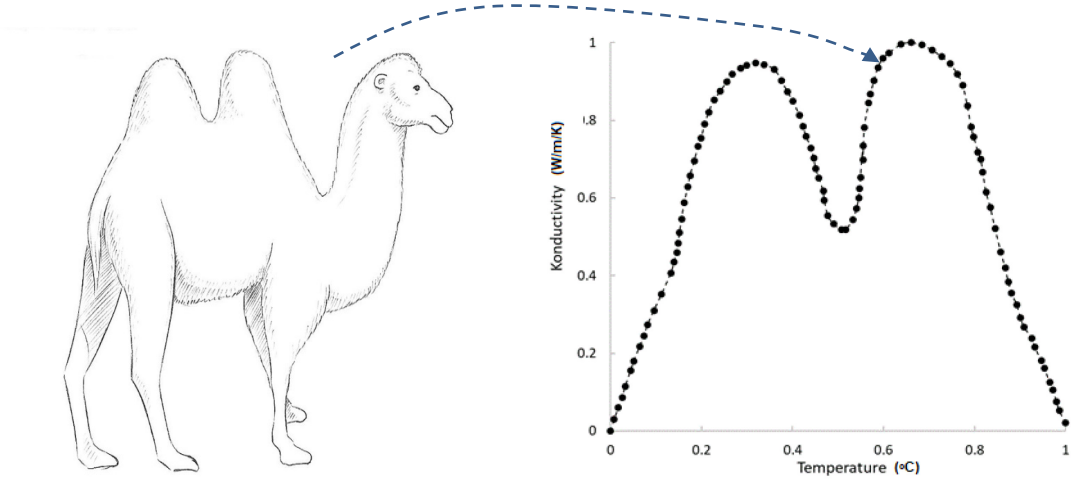

Figure 29: Hypothetical non-linear conductivity: Camel Conductivity

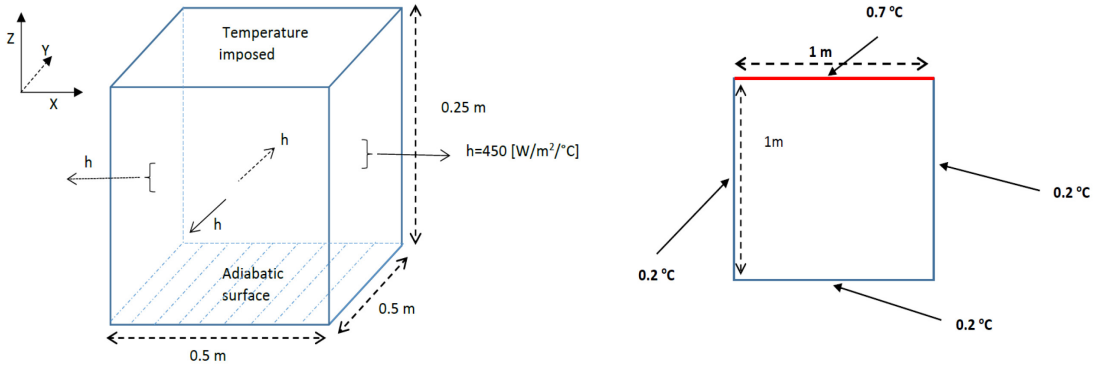

a) 3D copper block *b) 2D Camel conductivity*

Figure 30: Geometrical and thermal boundary conditions characteristics

The geometrical characteristics as well as the thermal boundary conditions for these two examples are given in **Figure 30-a** and **Figure 30-b** respectively.

2.6.1. Case 1: Temperature distribution in a 3D copper block

In this case of 3D-FEM modeling application, the cooper block is meshed with hexahedrons comprising eight nodes (2744 elements and 3375 nodes). The thermal non-linear conductivity of cooper is illustrated in **Figure 22**.

Figure 31, **Figure 32** and **Figure 33** illustrate the central lines temperature distribution in the cooper block in x, y and z direction respectively. It can be seen that the temperature distribution patterns are identical between **Figure 31** and **Figure 32**. This is due to the boundary conditions which are similar on the side surfaces. These Figures show that the temperature is higher in the central regions (46.42 ^{o}C) in comparison to its edges (44.90 ^{o}C). However, the shape of the temperature distribution in the central direction Z is different from that of the x and y directions as shown in **Figure 33**.

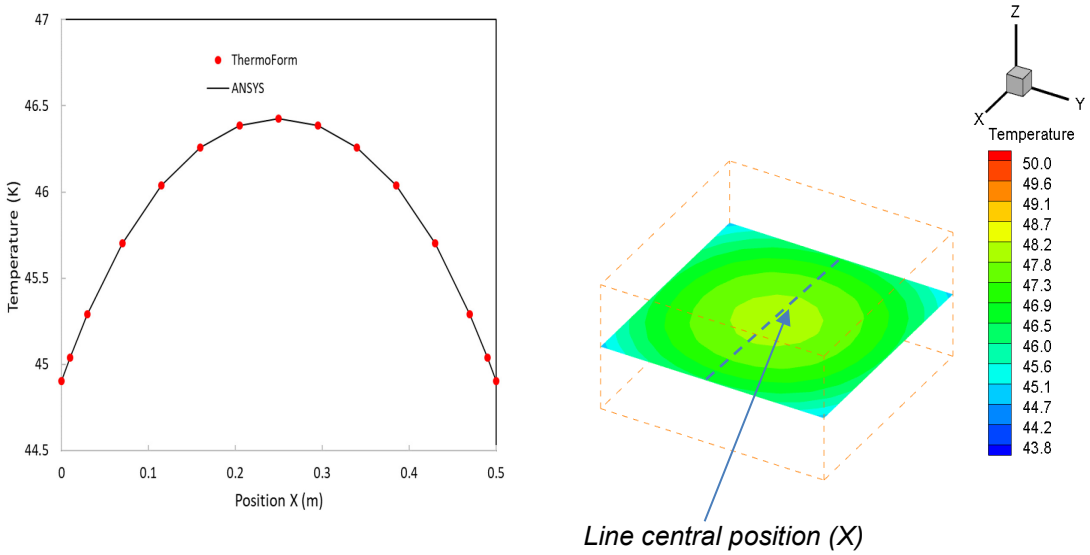

Figure 31: Temperature distribution in central line in X direction

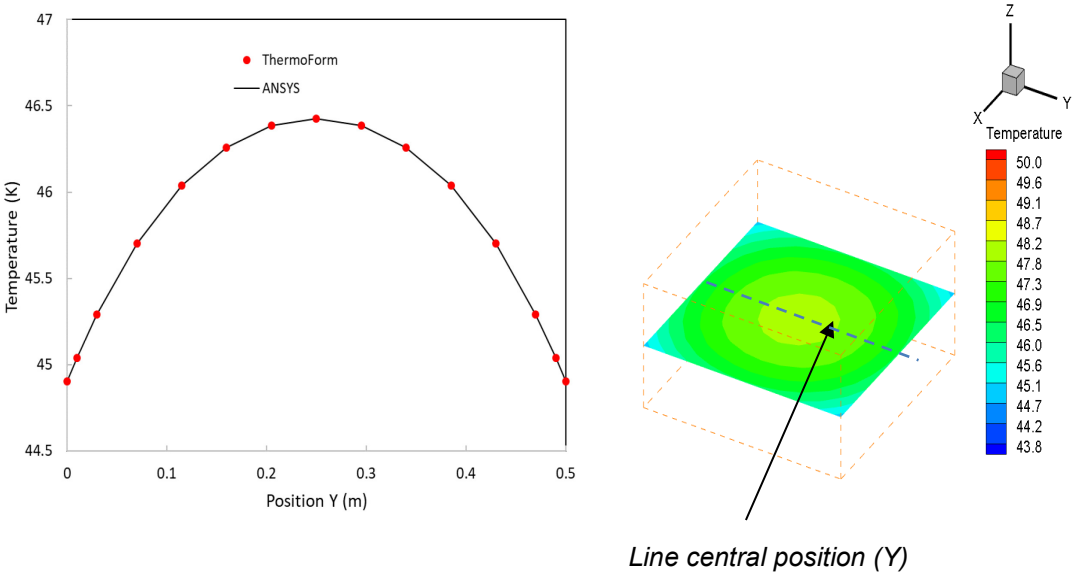

Figure 32: Temperature distribution in central line in Y direction

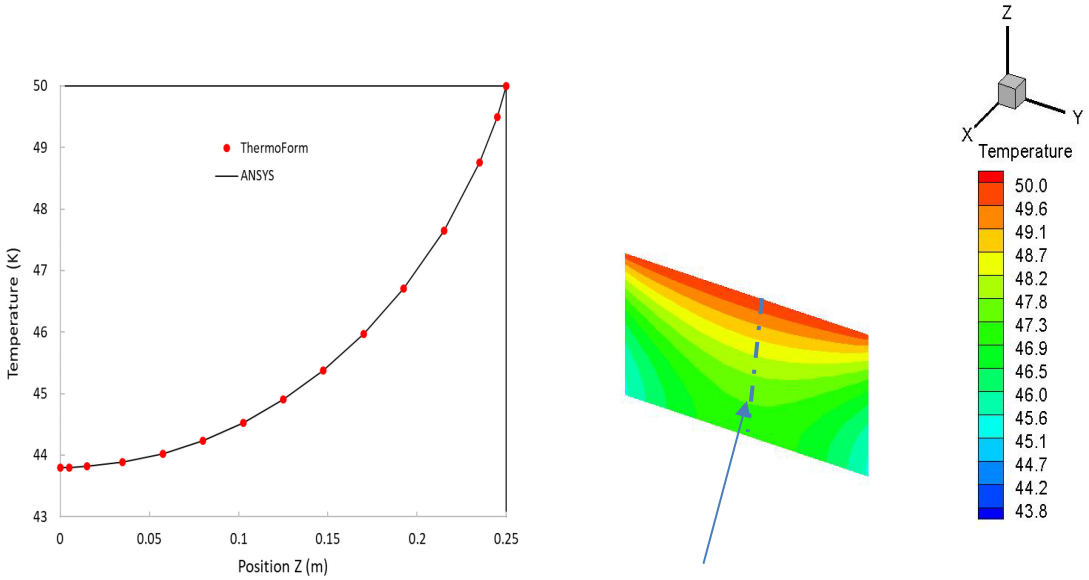

Figure 33: Temperature distribution in central line in Z direction

Figure 34-a and **Figure 34-b** represent different views of the temperature distribution on the outer surface of the copper block.

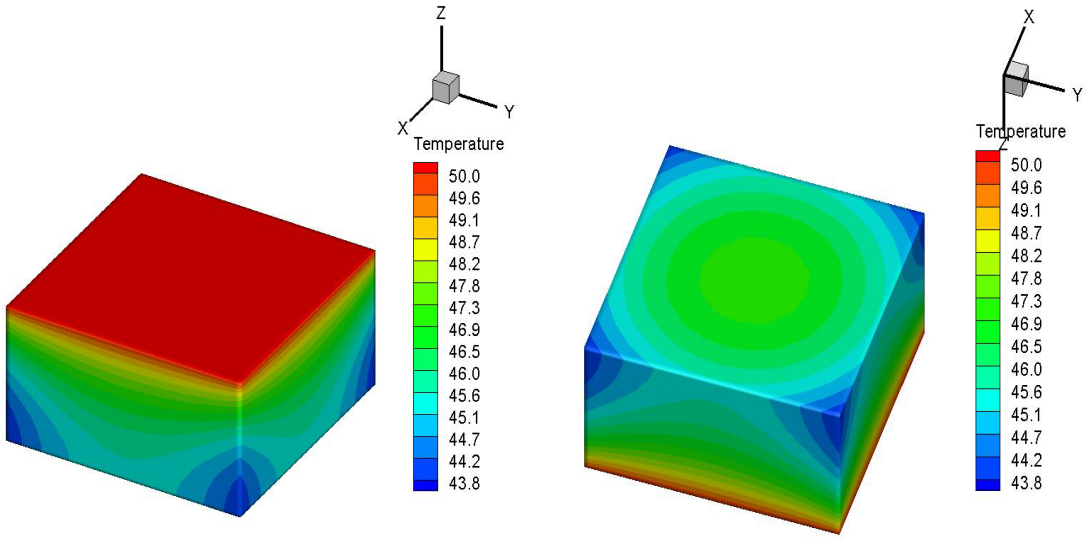

a. Temperature distribution (view 1) *b. Temperature distribution (view 2)*

Figure 34: Views of temperature distribution

2.6.2. Case 2: Temperature distribution in a hypothetical Camel-type 2D block

This application considers a 1 m x 1m unitary plate subjected to a uniform temperature. For the finite-element analysis, we consider a quadrilateral mesh with 361 elements and 400

nodes (See **Figure 30-b**). The upper side is maintained at a temperature of 0.7 °C and 0.2 °C on the other sides (See **Figure 30-b**). The thermal conductivity curve was approximated by fourth order splines and the results obtained in iterations 1, 3 and 30 are presented in **Figure 35-a.** Moreover, **Figure 35-b** shows the exact inverse function T(θ) obtained by fitting with B-spline. An excellent reproduction of the inverse function by the b-spline can be seen from the latter figure. **Figure 36-a** and **Figure 36-b** illustrate the central temperature distribution in the domain in the x and y direction respectively. **Figure 37** represents the views of the temperature distribution on the domain.

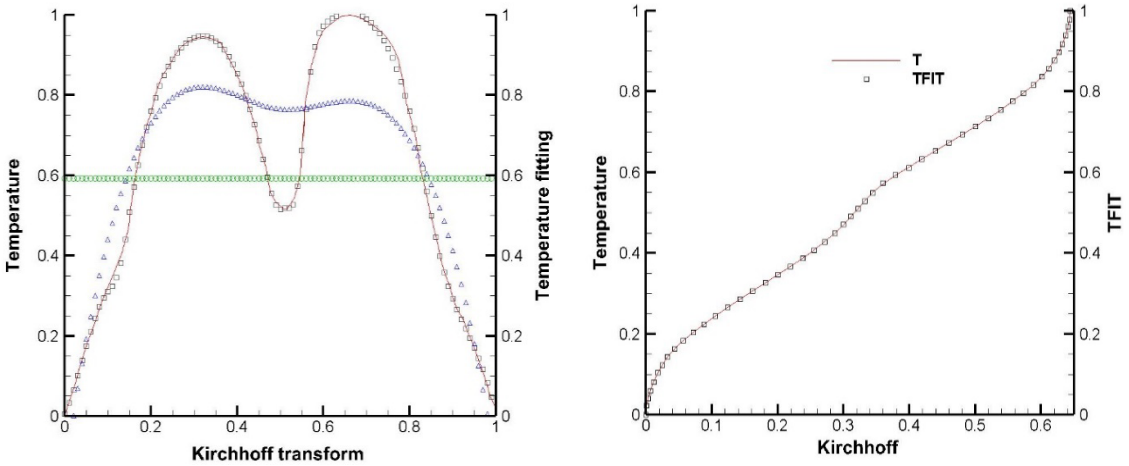

a. Approximated by fourth order splines of Camel Conductivity function

b. Exact inverse function T(θ) and that obtained by fitting with spline B

Figure 35: Approximation of Camel Conductivity and its inverse

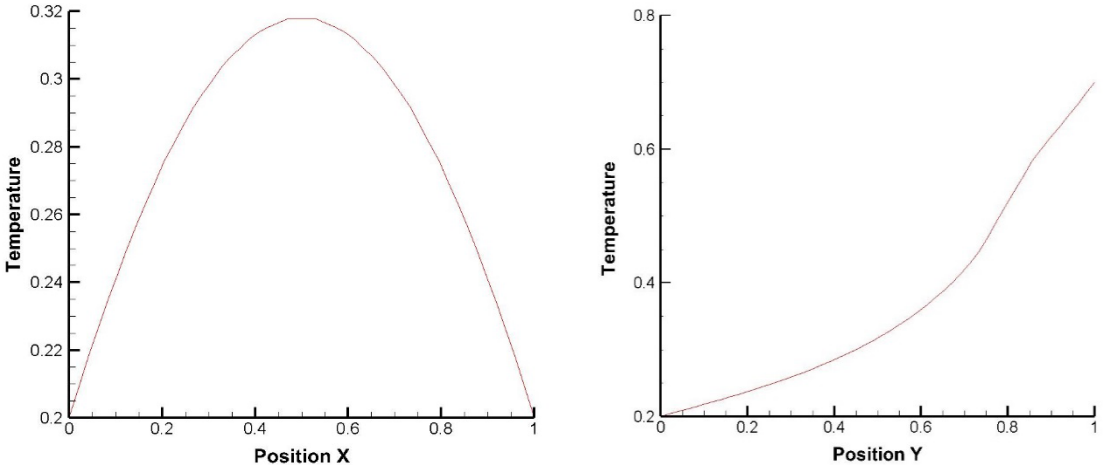

a. Central X-Direction *b. Central X-Direction*

Figure 36: Temperature distribution

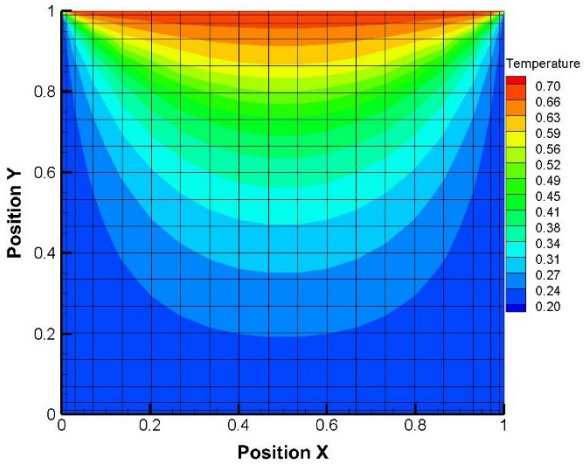

Figure 37: A view of the temperature distribution in the (x, y) plan

With regard to the last two examples (3D Copper block and *camel conductivity problem*), the following remarks can be noted on the performance of the proposed method:

Tableau 3 : Numerical performance of the proposed method

	Imposed temperature without convection		Imposed temperature with convection	
	ANSYS (*Full Newton Raphson*)	ThermoForm	ANSYS (*Full Newton-Raphson*)	ThermoForm (*Picard method*)
3D Copper block conductivity (2D)	-	-	4 iterations	3 iterations

In the light of the new proposed method to solve the energy equation in terms of the Kirchhoff transform, and owing to the quality of the results obtained, the following remarks can be formulated:

- In order to characterize the Kirchhoff transform and its inverse for non-linear thermal conduction analysis, the B-Spline method can be coupled to other numerical approaches in the example of the boundary finite element, the finite volume and the finite difference methods.
- If the boundary conditions are of the imposed temperatures type, the numerical solution requires no iteration, independently of the form of the function of thermal conductivity with respect to temperature (linear or not linear).
- The B-Spline method can be used to characterize the volume enthalpy of non-linear materials either with or without phase change.
- The B-Spline method can be coupled with the energy equation for the transient analysis of strongly non-linear materials in terms of both the volume enthalpy and Kirchhoff transformation. This operation can either be carried on with or without phase change.
- The B-Spline method can be used in combination with the energy equation for the representation of the inverse of the non-linear temperature boundary conditions that can be imposed on a material, in terms of the Kirchhoff transformation (and volume enthalpy).
- The proposed B-Spline method can easily be incorporated into other numerical methods: boundary finite element method, finite volume method, finite difference method, etc. And this, for problems with or without phase change.

The potential of the proposed approach is high and could be used for more general problems in the field of heat transfer such as the heating of non-linear materials by infrared radiation and electromagnetic waves, which will be addressed in future work.

2.7 Conclusion

This paper addresses the new method of solving the non-linear heat conduction equation using Kirchhoff transformation, $\theta(T)$, based on finite-element analysis.

In order to tackle the challenges associated with representation of θ (T) and its inverse T(θ), for solids with strongly non-linear conductivities, a strategy based on a reverse engineering method is considered. It is achieved by applying the B-spline method to the curve. The proposed approach can be combined with a numerical method to solve the non-linear heat equation in terms of θ. In the case where the boundary conditions are of the type of temperatures imposed, the proposed method does not require any numerical iteration and this independently of the thermal conductivity function with respect to temperature (linear or non-linear). However, this work has focused on the finite element method. The approach is validated on several cases of thermal conductivity (from constant to non-linear) either with convection or not. Through its application, the proposed method has used the 3D finite element method to determine the temperature distribution in a copper block and proposed a new numerical analysis test whose thermal conductivity, with respect to temperature, has the shape of a camel hump.

CHAPITRE 3

INVESTIGATION OF THE RADIOFREQUENCY HEATING OF ANISOTROPIC DIELECTRIC MATERIALS WITH A PHASE CHANGE: APPLICATION TO FROZEN DOUGLAS-FIR AND WHITE OAK WOODS

F. Erchiqui [a], Z. Annasabi [b], M. Diagne [c]

Wood Science and Technology, Springer. Facteur d'impact : 2.58. Publié le 28 octobre 2021

[a]: Université du Québec en Abitibi-Témiscamingue, école de génie, 455, boulevard de l'Université, Rouyn-Noranda (Québec), Canada J9X 5E4

[b]: Université du Québec en Abitibi-Témiscamingue, école de génie, 455, boulevard de l'Université, Rouyn-Noranda (Québec), Canada J9X 5E4

[c]: Université du Québec en Abitibi-Témiscamingue, école de génie, 455, boulevard de l'Université, Rouyn-Noranda (Québec), Canada J9X 5E4

Rôle de l'étudiant dans cette publication :

Contribution à l'élaboration de modèles mathématiques, de calcul numérique, de l'interprétation des résultats et de la rédaction de l'article.

Abstract: Dielectric heating is a promising process for the uniform sterilization of food products as well as for the drying of products. However, radio frequency heating of wood-based materials (they are highly anisotropic materials with temperature, moisture and structural orientation dependent properties) does not seem to be elucidated in the literature. It is within this framework that this study is carried out and concerns the modeling of anisotropic dielectric heating by radio frequency (RF) and its application to the thawing of frozen wood. The non-linear heat conduction problem involving phase changes is formulated in terms of volume enthalpy. For the numerical resolution of the thermal conduction equation, the finite element method is considered. Thermophysical and dielectric properties are expressed as a function of temperature, moisture content (MC) and structural orientation. The numerical approach is further validated by a combination of the analytical, numerical and experimental analyses. Finally, the effect of RF on the thawing of the Douglas-fir (*Pseudotsuga menziesii*) and the White oak (Quercus alba), which are two North American wood species, was studied based on an initial temperature of -20 ^{o}C and a frequency of 50 MHz. In this regard, two MC of 65% and 90% are considered. For the two species of the studied wood, it is observed that the RF induce a uniform temperature profile.

Résumé: Le chauffage diélectrique est un procédé prometteur pour la stérilisation uniforme des produits alimentaires ainsi que pour le séchage des produits. Cependant, le chauffage par micro-ondes des matériaux à base de bois (un matériau hautement anisotrope avec des propriétés dépendantes de la température, de l'humidité et de l'orientation structurelle) ne semble pas être élucidé dans la littérature. C'est dans ce cadre que cette étude est réalisée et concerne la modélisation du chauffage diélectrique anisotrope par radiofréquence (RF) et son application au dégel du bois gelé. Le problème de conduction thermique non linéaire impliquant des changements de phase est formulé en termes d'enthalpie volumique. Pour la résolution numérique de l'équation de conduction thermique, la méthode des éléments finis est considérée. Les propriétés thermophysiques et diélectriques sont exprimées en fonction de la température, de la teneur en humidité (MC) et de l'orientation structurelle. L'approche numérique est validée par une combinaison d'analyses analytiques, numériques et expérimentales. Enfin, l'effet des RF sur le

dégel du douglas (*Pseudotsuga menziesii*) et du chêne blanc (Quercus alba), qui sont deux essences de bois nord-américaines, a été étudié avec une température initiale de -20 ^{o}C et une fréquence de 50 MHz. À cet égard, deux MC de 65 % et 90 % sont considérés. Pour les deux essences de bois étudiées, on observe que les RF induisent un profil de température uniforme.

3.1 Introduction

Nowadays, radio frequencies (RF) are used in various applications, particularly in both civilian and military communication as well as the healthcare sector for both tumor treatment and emergency services. The frequency of its electromagnetic waves ranges from 3 to 300 MHz. Their interactions with the dielectric media can be described by their dielectric properties. The two main interactions of interest are: i) the absorption resulting from the partial storage of the wave energy in the dielectric material and ii) the partial dissipation of the energy absorbed by the dielectric material in the form of heat [48]. The ability of a dielectric material to absorb and store energy is generally described by the complex dielectric constant which is a second order tensor [48]. However, the degradation of the energy contained in the electric field of the wave, in the form of heat, requires the presence of polar molecules. In general, there are four cases of polarization of dielectric materials listed below [49] :

- Interfacial polarization: it occurs only in non-homogeneous media and it comes from the accumulation of free charges at the interface of two media of different permittivities.
- Electron polarization: it is related to the displacement of individual electrons in an atom in response to external fields.
- Atomic polarization: it is related to the displacement of the atomic nucleus with respect to the group of atomic electrons.
- Molecular polarization: it is related to the displacement of individual atoms in a molecule.

All these polarization mechanisms can occur in any dielectric material. However, it occurs with time, without necessarily following a variable electric field. This shift between the polarization vector and the electric field is the fundamental condition for the dissipation of the electrical energy as heat in a dielectric material. Indeed, under the effect of an incident electric field, polar molecules tend to align themselves with the field with a certain delay with respect to the external electric field (generally harmonic). The response time of this shift depends not only on the intermolecular forces,

but also on the inertial forces opposing the electric field. The time needed to overcome these forces is also known as the relaxation time. Consequently, the first response of dielectrics is polarization, followed by dielectric relaxation. At frequencies below relaxation, the time for the electric field to change direction is long enough for the dipoles to be able to follow it and they remain in phase with the field. In this case, losses do not appear in the material. The same is true if the frequencies are very high; the field changes too quickly and the dipoles cannot follow the reversal of polarity. Under these conditions, no energy is lost in the medium. However, there is an intermediate frequency between these two extremes where there is a delay or a temporal phase shift between the dipole moment and the electric field resulting in an energy dissipation inside the material [50]. This lost energy is responsible for the temperature evolution in the dielectric and they reach a maximum value at the frequency f_c, linked to the relaxation time by $\tau=1/(2\pi f_c)$. The electrical energy is then converted into the thermal energy with a power proportional to the square of the distribution of the electric field in the dielectric [48].

In the case of RF, interfacial and dipolar polarization are generally most associated to the mechanisms of thermal activation through charge carrier migration and general molecular motion within the material [50]. However, the energy transported or converted into heat by RF is considered too low to either cause a breakdown of the chemical bonds of the materials or cause an electron extraction from them [51]. Consequently, RF are considered non-ionizing radiations which can be used in many telecommunication and health engineering applications.

When dealing with wood, which is a composite material characterized by anisotropy in the longitudinal, radial and transverse directions, the dielectric properties are expressed as a function of the following two second order tensors [[48], [26]]: i) the dielectric permittivity tensor $\bar{\bar{\boldsymbol{\varepsilon}}}$ associated with the electrical component of the wave and ii) the magnetic permeability tensor $\bar{\bar{\boldsymbol{\mu}}}$ associated with the magnetic component of the wave. The real parts of the tensors $\bar{\bar{\boldsymbol{\varepsilon}}}$ and $\bar{\bar{\boldsymbol{\mu}}}$, which are referred to as $\bar{\bar{\boldsymbol{\varepsilon}}}'$ and $\bar{\bar{\boldsymbol{\mu}}}'$ respectively, express the phase shift of the electromagnetic wave (deceleration that can be characterized by a refractive index tensor **n)** for wood, and the imaginary parts $\bar{\bar{\boldsymbol{\varepsilon}}}''$ and $\bar{\bar{\boldsymbol{\mu}}}''$

respectively referring to the loss factors through the dissipation of the energy of the electromagnetic wave. Usually, the dielectric permittivity $\bar{\bar{\varepsilon}}$ and the magnetic permeability $\bar{\bar{\mu}}$ are normalized with respect to those of the vacuum $\varepsilon_0(= 8.854\ 10^{12}\ F/m)$ and $\mu_0(= 4\ \pi\ 10^{-7}\ H/m)$. In this regard, the dielectric and magnetic permittivities of wood relative to vacuum are often referred to as $\bar{\bar{\varepsilon}}_r$ and $\bar{\bar{\mu}}_r$, respectively. The values of the permittivity (or permeability) of a material are closer to unity whenever its dielectric (or magnetic) properties are close to those of vacuum. This means that the higher the $\bar{\bar{\varepsilon}}'_r$ ($\bar{\bar{\mu}}'_r$), the more the material tends to reflect RF. Similarly, the higher the $\bar{\bar{\varepsilon}}''_r$ ($\bar{\bar{\mu}}''_r$), the more the material could dissipate the energy contained in the RF. In the case of wood, the dielectric tensor $\bar{\bar{\varepsilon}}_r$varies considerably with many parameters such as the type (characterized by the specific gravity (SG), frequency, density, moisture content (MC), temperature and structural orientations of its fibers (longitudinal, radial, and transverse) [[48], [43]]. However, it is generally accepted that at a given set of temperature (T), frequency (f) and the MC, the dielectric properties of wood do not significantly change with the electric field vector [52].

The current literature on the dielectric heating of wood mostly deals with the use of microwaves [[28], [2],[48]]. The anisotropic heating of wood using RF does not seem to be elucidated both with respect to the experimental stage and the mathematical modelling. In addition, there is a lack of studies supporting the efficiency of the RF heating, as well as many uncertainties still to be clarified. In this regard, the ability of this technique to penetrate the structure of wood or to be used for a phytosanitary treatment for the eradication of pathogens present in wood and wood products has not yet been validated. Moreover, a proper expression of the penetration of RF radiation into wood is a complex process due to the multitude of parameters it entails. Some of the most in view are the frequency, temperature, moisture content, structural orientation and dielectric properties. Other concerns are related to the industrial application of this technique. In fact, the proper speed at which the dissipated heat generated by RF radiation moves through the wooden material (characterized by thermal diffusivity (α)) and the speed at which wood absorbs thermal energy (characterized by thermal effusivity (E)) are not clearly expounded in the literature. It is rather directly related to the non-linear and the anisotropic thermo-physical properties of the

wooden material including the specific heat C_p, the density ρ and the thermal conductivity tensor $\overline{\overline{\boldsymbol{k}}}$ [48]. In the case of frozen wood, the knowledge of the latent energy (L) is essential as it implicitly characterizes the energy supplied by the RF for the melting of frozen water present in the wooden structure. Moreover, all its properties are a function of the moisture content, temperature and its structural orientation. Finally, the frequencies arrayed in the RF domain belong to the set authorized by the International Telecommunication Union (ITU) for the prevention of the interferences with other equipments and installations.

In the wood industry, the main issue evolves around reducing the heat time treatment of wood products, thus the justification of the general use of microwaves instead of RF. This choice is motivated by economic considerations based on the duration of the heat treatment process, which is shorter for microwaves as they are more energetic than RF. Consequently, there is a wide range of microwave equipment operating at the frequency of 915 MHz for industrial applications and 2.45GHz for domestic ovens. In fact, the depths of the microwave penetration are influenced by the choice of these frequencies. However, it has been reported that the major disadvantage of microwave heating is the presence of hot and cold heat spots in the wooden structure, indicating a heterogeneous temperature distribution [2]. Such phenomenon had been dealt with through an incorporation of the rotary systems into the microwave ovens where they act by reducing the temperature differences induced in the material. This paper deals with an investigation of the use of the RF as an alternate approach to tackle the disadvantages of an application of the microwaves in the wood industry. This choice is motivated by previous works carried out by Erchiqui et al. [2], showing that the distribution of the power dissipated by RF in wooden materials is uniform across the thickness of the analyzed samples for all practical purposes. In fact, such findings deserve a thorough investigation for a qualitative and quantitative characterization of the temperature distribution induced by RF in the wood samples subjected to it. Within the defined framework, this paper focuses specifically on the modeling of the dielectric heating of frozen wood samples by RF.

The modeling of the RF heating of anisotropic dielectric materials with phase change is a complex process involving non-linear interactions between mechanical, thermal and electrical properties [[2], [31], [53]]. This represents a major challenge for numerical simulation because heat and mass transfer, phase change, as well as thermo-mechanical and electromagnetic interactions must be taken into consideration. Two approaches are often found in the literature for the modeling of heat conduction in materials with phase change. The first one expresses the anisotropic heat conduction equation in terms of temperature as a dependent variable [[10],[48],[54], [41]], while the second one uses volume enthalpy [[2], [48]]. The latter approach has the advantage of simultaneously eliminating the duplication of the energy equation for the solid and liquid phases and avoiding the presence of the moving boundary which is the mathematical condition at the water-ice interface [48]. The modeling of the heat dissipated by electromagnetic waves including RF and microwaves referred to as Q requires the knowledge of the power flux associated with the propagation of the electromagnetic waves (Poynting vector $\vec{P}$) in the dielectric medium [2]. This can only be achieved by the knowledge of the electromagnetic field induced in the space of the material, thus by the resolution of Maxwell's equations. The common numerical methods applied in the literature to solve the Maxwell equations are the finite element method [[55], [2]], the finite volume method [56], the finite difference method [57] and the boundary finite element method [58]. However, in the case of an anisotropic dielectric material such as wood, the published works are limited and usually only deal with microwave heating.

This work is concerned with the finite element investigation of the RF heating of two North American frozen wood species which are by nature anisotropic. These species include the Douglas-fir (*Pseudotsuga menziesii*) and the White oak (*Quercus alba*). A radiofrequency of 50 MHz and an initial temperature of -20 ℃ were considered for analytical purposes. The choice of the negative initial temperature is supported by the specific North American climatic considerations, where winter temperatures are reputedly amongst the lowest of the world. The thermo-physical and dielectric properties of both wood species are considered dependent on moisture, temperature and the three structural orientations of the wood fibers.

3.2 Enthalpy model

The heat conduction analysis of anisotropic incompressible solids with phase change is naturally described by the enthalpy term H(T) [2] which, in the case of a three-dimensional Cartesian coordinate system is given by equation (1) [10]:

$$\frac{\partial \mathrm{H}}{\partial \mathrm{t}} = \left(\frac{\partial}{\partial \mathrm{x_i}} \frac{\partial \theta_{\mathrm{ij}}}{\partial \mathrm{x_j}}\right) + \mathrm{Q_{RF}}\,; \quad \mathrm{i,j} = 1,2,3 \tag{1}$$

Where θ_{ij} are the components of the Kirchhoff transformation tensor $\boldsymbol{\theta}$, and Q_{RF} is the internal heat source. The θ_{ij} components are related to the temperature-dependent thermal conductivity tensor $\bar{\bar{\mathbf{k}}}$ by equation (1.1) [10] :

$$\theta_{\mathrm{ij}}(\mathrm{T} \le \mathrm{T_m}) = \int_{\mathrm{T_{ref}}}^{\mathrm{T}} \mathrm{k_{ij}^s}\,(\mathrm{T})\,\mathrm{dT}\,, \qquad \theta_{\mathrm{ij}}(\mathrm{T} > \mathrm{T_m}) = \int_{\mathrm{T_m}}^{\mathrm{T}} \mathrm{k_{ij}^l}\,(\mathrm{T})\,\mathrm{dT} \tag{1.1}$$

Where T_m [°C] and T_{ref} [°C] are the material's melting temperature and the reference temperature, respectively. In the case where the phase change occurs at melting temperature, which is assumed to be constant, the enthalpy H(T) is expressed by equations (1.2) and (1.3) [10]:

$$\mathrm{H}(\mathrm{T} \le \mathrm{T_m}) = \int_{\mathrm{T_{ref}}}^{\mathrm{T}} \rho^{\mathrm{s}}(\mathrm{T}) \mathrm{C_p^s}(\mathrm{T}) \mathrm{dT} \tag{1.2}$$

$$\mathrm{H}(\mathrm{T} > \mathrm{T_m}) = \int_{\mathrm{T_{ref}}}^{\mathrm{T_m}} \rho^{\mathrm{s}}(\mathrm{T}) \mathrm{C_p^s}(\mathrm{T}) \mathrm{dT} + \rho(\mathrm{T}) \mathrm{L} + \int_{\mathrm{T_m}}^{\mathrm{T}} \rho^{\mathrm{f}}(\mathrm{T}).\, \mathrm{C_p^f}(\mathrm{T}) \mathrm{dT} \tag{1.3}$$

L is the latent heat of water fusion [kJ/kg]. The exponent's "*s*" and "*l*" appearing on the density ρ^*[kg/m^3], the specific heat C_p^* [J/kg/^{o}C] and the components of conductivity tensor k_{ij}^* [W/m/^{o}C] of the material refer to the solid and liquid state, respectively. The term ρ represents the density at the solid-liquid interface of the material.

The internal volumetric heat generation of RF energy Q_{RF} is related to the instantaneous Poynting vector $\mathbf{S}$ by equation (2) that follows [2]:

$$\mathrm{Q_{RF}}(\mathrm{T}) = -\mathrm{Re}(\boldsymbol{\nabla} \cdot \mathbf{S}) \tag{2}$$

The boundary conditions associated to equation (1) is:

$$\left(n_x \frac{\partial \theta_x}{\partial x} + n_y \frac{\partial \theta_y}{\partial y} + n_z \frac{\partial \theta_z}{\partial z}\right) + h(T - T_\infty) - \mathbf{q} \cdot \mathbf{n} = 0 \quad (3)$$

where **q** [W/m^2] is the incident radiative heat flux, **n** is the outward normal vector to the material surface, h [W/m^2/°C] is the heat transfer coefficient and T_∞ is the temperature of the surrounding fluid.

3.3 Implicit time integration scheme

A variety of the numerical schemes are available for the numerical analysis of transient responses to problems associated with heat conduction. The most common belonging to the weighted Euler difference family of time approximations [42] that are considered in this paper following equation (4):

$$H^{n+\alpha} = (1 - \alpha)\, H^n + \alpha\, H^{n+1}, \text{ with : } \alpha = \frac{t - t_n}{\Delta t} \quad (4)$$

The parameter α varies in the range [0–1]. The α schemes are unconditionally stable when $\alpha \leq 1/2$ and $O(\Delta t)$ are accurate, except for the $O(\Delta t^2)$ – convergent Crank–Nicolson scheme ($\alpha = 1/2$). In this work, the semi-implicit Crank-Nicolson scheme [42] is considered. Consequently, equation (1) is transformed into equation (5):

$$(\mathbf{K}^*_{n+1} + \mathbf{G}^*_{n+1})\, \mathbf{H}_{n+1} = \mathbf{K}^*_n . \mathbf{H}_n + \mathbf{G}^*_n . \mathbf{H}^2_n + \mathbf{R}^*_{n,n+1} \quad (5)$$

K*, **G*** and **R*** are modified global matrices and $\mathbf{H_{n+1}}$ is the vector of global nodal enthalpies at moment t_{n+1} [2].

3.4 Poynting's theorem and RF-wave energy

The Poynting vector **S** given in equation (6) is the result of the vector product of the field's electric and magnetic components of the electromagnetic wave [59]:

$$\mathbf{S} = \frac{\mathbf{1}}{\mathbf{2}} \mathbf{E} \times \mathbf{H}^* \quad (6)$$

Where E and H* are the electric field (V.m^{-1}) and the conjugate magnetic field intensity (A.m^{-1}), respectively. In general, such problem deals with the steady-state harmonic time-varying fields. It is thus convenient to represent each field vector as a complex phasor by an application of

a Fourier transformation. An assumption of a monochromatic wave leads to the expression of E by equation (7):

$$\mathbf{E}(\mathbf{r},\mathrm{t}) = \mathrm{e}^{-\mathrm{j}\omega\mathrm{t}}\bar{\mathbf{E}}(\mathbf{r}) \tag{7}$$

where $\bar{\mathbf{E}}$ is a complex vector and a function of **r** (m) and ω (radian.s^{-1}) is the angular frequency of the incident radiation. The other field vectors can be written using the same notation as in equation (7).

A combination of the definition of equation (6) and Maxwell's equations [28] results in an expression of $\boldsymbol{\nabla}\cdot\mathbf{S}$ using equations (8), (8.1) and (8.2):

$$\boldsymbol{\nabla}\cdot\mathbf{S} = -\mathrm{j}\frac{\omega}{2}([\varepsilon_0(\bar{\mathbf{E}}\cdot\bar{\bar{\boldsymbol{\varepsilon}}}\cdot\bar{\mathbf{E}}^*)] + [\mu_0(\bar{\mathbf{H}}\cdot\bar{\bar{\boldsymbol{\mu}}}\cdot\bar{\mathbf{H}}^*)]) \tag{8}$$

with:

$$Re(\boldsymbol{\nabla}\cdot\mathbf{S}) = -\frac{\omega}{2}\left(\varepsilon_0(\bar{\mathbf{E}}\cdot Im(\bar{\bar{\boldsymbol{\varepsilon}}})\cdot\bar{\mathbf{E}}^*) + \mu_0(\bar{\mathbf{H}}\cdot Im(\bar{\bar{\boldsymbol{\mu}}})\cdot\bar{\mathbf{H}}^*)\right) \tag{8.1}$$

$$Im(\boldsymbol{\nabla}\cdot\mathbf{S}) = -2\omega\left(\frac{1}{4}\varepsilon_0(\bar{\mathbf{E}}\cdot Re(\bar{\bar{\boldsymbol{\varepsilon}}})\cdot\bar{\mathbf{E}}^*) + \frac{1}{4}\mu_0(\bar{\mathbf{H}}\cdot Re(\bar{\bar{\boldsymbol{\mu}}})\cdot\bar{\mathbf{H}}^*)\right) \tag{8.2}$$

The imaginary ($Im(\boldsymbol{\nabla}\cdot\mathbf{S})$) and real $Re(\boldsymbol{\nabla}\cdot\mathbf{S})$ parts of the complex $\boldsymbol{\nabla}\cdot\mathbf{S}$ represent, respectively, the net reactive power stored and the net power dissipated by the RF per unit volume in the anisotropic dielectric material [[48], [54]] :

$$\mathrm{Q_{RF}} = \frac{\omega}{2}\left(\varepsilon_0(\bar{\mathbf{E}}\cdot\mathrm{Im}(\bar{\bar{\boldsymbol{\varepsilon}}})\cdot\bar{\mathbf{E}}^*) + \mu_0(\bar{\mathbf{H}}\cdot\mathrm{Im}(\bar{\bar{\boldsymbol{\mu}}})\cdot\bar{\mathbf{H}}^*)\right) \tag{9}$$

In wood systems, the magnetic permeability tensor $\bar{\bar{\boldsymbol{\mu}}}$ is closely approximated by the real tensor $\boldsymbol{\mu_0}\bar{\bar{\boldsymbol{I}}}$; ($\bar{\bar{\boldsymbol{I}}}$ is the identity tensor) [60]. This assumption is made in this paper resulting into an expression of the power dissipated by RF (per unit volume) as equation (10):

$$\mathrm{Q_{RF}} = \frac{\omega}{2}\varepsilon_0(\mathbf{E}\cdot\mathrm{Im}(\bar{\bar{\boldsymbol{\varepsilon}}})\cdot\mathbf{E}) \tag{10}$$

It is clear from equation (10) that the calculation of the power dissipated by RF at any moment requires the knowledge of the electric field at any point of the dielectric material. This

requires the resolution of Maxwell's equations with respect to an anisotropic dielectric medium subjected to the RF. If the RF are normal to the three main directions of the wood sample (longitudinal, radial and tangential), the power dissipated per unit volume can be further simplified [2]. The last consideration is made in this work. Assuming the electro-neutrality of wood $\nabla(\nabla \cdot \mathbf{E}) = 0$, the expression of the Helmholtz's equation of wave propagation is deduced from the Maxwell's equation for each principal direction [28]:

$$\nabla^2 \bar{\mathbf{E}} - \gamma^2 \bar{\mathbf{E}} = 0 \qquad (11)$$

where γ is the constant complex propagation $\gamma = \alpha + j\beta$,while β and α are respectively the attenuation and the phase constants. These parameters are related to the dielectric properties of the material and the radiation frequency. These in turn are a function of temperature (T), moisture content (MC), frequency (f) and the structural direction (L, R, T) of the wood according to the following formulae:

$$\alpha_{\mathrm{d}}(\mathrm{T},\mathrm{MC},\mathrm{f}) = \frac{\omega}{\mathrm{c}} \sqrt{\frac{\varepsilon''_{\mathrm{d}}(\mathrm{T},\mathrm{MC},\mathrm{f})}{2}} \sqrt{1 + \tan^2 \delta\big((\mathrm{T},\mathrm{MC},\mathrm{f})\big)} + 1;\ \text{(d: L, R or T)} \qquad (12.1)$$

$$\beta_{\mathrm{d}}(\mathrm{T},\mathrm{MC},\mathrm{f}) = \frac{\omega}{\mathrm{c}} \sqrt{\frac{\varepsilon''_{\mathrm{d}}(\mathrm{T},\mathrm{MC},\mathrm{f})}{2}} \sqrt{1 + \tan^2 \delta\big((\mathrm{T},\mathrm{MC},\mathrm{f})\big)} - 1;\ \text{(d: L, R or T)} \qquad (12.2)$$

$\mathrm{c} = \mathbf{1}/\sqrt{\mu_0 \varepsilon_0}$ is the speed of the light. The term δ (=$\mathrm{tg}^{-1}(\varepsilon''_d/\varepsilon'_d)$) is the dielectric loss angle. The attenuation constant, β, controls the rate at which the incident field intensity decays in the dielectric material. $1/(2\beta)$ is known as the penetration depth. The phase constant, α, represents the change of phase of the radiation propagation and is related to its wavelength by the expression $\lambda = 2\pi/\alpha$.

3.4.1 Uniform plane wave propagation and power dissipation

In this paper, it is assumed that each component of the electric field $\mathbf{E} = (\mathbf{E_x}, \mathbf{E_{y,}}, \mathbf{E_z})$ is a uniform plane RF. In the same manner, each wave component is assumed to be normally incident to the opposite faces of the sample (see **Figure 38**). These electric components are given by equations (13.1), (13.2) and (13.3):

x direction: longitudinal direction L

$$\mathbf{E_x} = \mathrm{E_x(z)}\mathbf{a_x} \tag{13.1}$$

y direction: radial direction R

$$\mathbf{E_y} = \mathrm{E_y(x)}\ \mathbf{a_y} \tag{13.2}$$

z direction: tangential direction T

$$\mathbf{E_z} = \mathrm{E_z(y)}\ \mathbf{a_z} \tag{13.3}$$

where x is a component of the electric field (E_x), which is a function of the parameter z, y is a component of the electric field (E_y), which is a function of the parameter x, and z is a component of the electric field (E_z), which is a function of the parameter y, as represented in **Figure 38**.

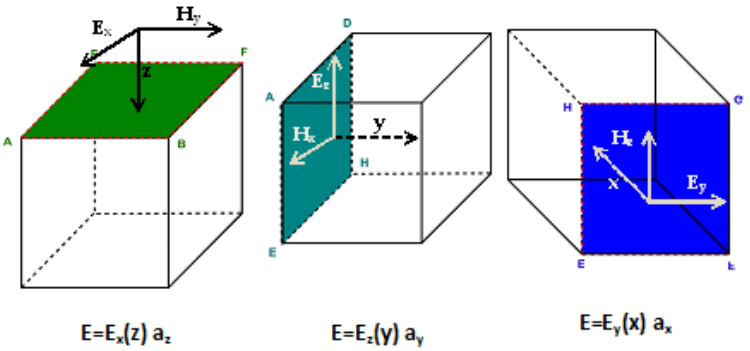

Figure 38: Schematic representation of the wood sample exposed to plane RF from the three principal faces.

The unit vectors $\boldsymbol{a}_z, \boldsymbol{a}_y$ and $\boldsymbol{a}_x$ are respectively the normal to the surfaces (AEFB), (ADHE) and (HCTE) of the wood sample.

3.4.2 Expressions of the power dissipation

According to equations (11) and (13.1) - (13.3), the exact expressions of the absorbed powers in each principal direction of the wood sample are given respectively by the expressions of equations (14.1) – (14.3) [28]:

Longitudinal direction:

$$\mathrm{Q_{RF}^x} = 2\mathrm{I_0^x}\beta^x \left[\frac{\mathrm{e}^{-2\beta^x \mathrm{x}} + (\overline{\mathrm{R}}_{23}^{\mathrm{x}})^2 \mathrm{e}^{-4\beta^x \mathrm{L_x}} \mathrm{e}^{2\beta^x \mathrm{x}} + 2\overline{\mathrm{R}}_{23}^{\mathrm{x}} \mathrm{e}^{-2\beta^x \mathrm{L_x}} \cos(2\alpha^x(\mathrm{x} - \mathrm{L_x}) - \theta_{23}^{\mathrm{x}})}{1 + (\overline{\mathrm{R}}_{12}^{\mathrm{x}})^2 (\overline{\mathrm{R}}_{23}^{\mathrm{x}})^2 \mathrm{e}^{-4\beta^x \mathrm{L_x}} - 2\overline{\mathrm{R}}_{12}^{\mathrm{x}} \overline{\mathrm{R}}_{23}^{\mathrm{x}} \cos(\theta_{12}^{\mathrm{x}} + \theta_{23}^{\mathrm{x}} + 2\alpha^x \mathrm{L_x}) \mathrm{e}^{-2\beta^x \mathrm{L_x}}}\right] \tag{14.1}$$

Radial direction:

$$Q_{RF}^{y} = 2I_0^y \beta^y \left[\frac{e^{-2\beta^y y} + \left(\overline{R}_{23}^{y}\right)^2 e^{-4\beta^y} e^{2\beta^y y} + 2\overline{R}_{23}^{y} e^{-2\beta^y L_y} \cos\left(2\alpha^y \left(y - L_y\right) - \theta_{23}^{y}\right)}{1 + \left(\overline{R}_{12}^{y}\right)^2 \left(\overline{R}_{23}^{y}\right)^2 e^{-4\beta^y L_y} - 2\overline{R}_{12}^{y} \overline{R}_{23}^{y} \cos\left(\theta_{12}^{y} + \theta_{23}^{y} + 2\alpha^y L_y\right) e^{-2\beta^y L_y}} \right] \quad (14.2)$$

Tangential direction:

$$Q_{RF}^{z} = 2I_0^z \beta^z \left[\frac{e^{-2\beta^z z} + (\overline{R}_{23}^{z})^2 e^{-4\beta^z L_z} e^{2\beta^z z} + 2\overline{R}_{23}^{z} e^{-2\beta^z L_z} \cos(2\alpha^z (z - L_z) - \theta_{23}^{z})}{1 + (\overline{R}_{12}^{z})^2 (\overline{R}_{23}^{z})^2 e^{-4\beta^z L_z} - 2\overline{R}_{12}^{z} \overline{R}_{23}^{z} \cos(\theta_{12}^{z} + \theta_{23}^{z} + 2\alpha^z L_z) e^{-2\beta^z L_z}} \right] \quad (14.3)$$

The superscripts x, y and z are respectively associated with the longitudinal, radial and tangential directions. θ_{ij} is the phase angle for the reflection coefficient at the interface between layers i and j; while $\overline{R}_{ij}$ is the absolute value of the complex reflection coefficient. Finally, L_x, L_y and L_z are respectively the length of the wood sample in the x, y and z directions.

3.5 Numerical validation of enthalpy model

The dynamic finite element method outlined in the previous section was implemented in *ThermoForm*, a general-purpose code developed by Erchiqui, the principal author. All computations were performed on a PC with a single precision.

The numerical approach, based on the volumetric enthalpy, was validated for the following situations:

- The microwave dielectric heating of a beef sample. The parameters validated include the power dissipation as well as the temperature distribution within the material [28].
- The thawing of a wood trunk, immersed in hot water, for which the simulated and the experimental results were compared [10].
- An anisotropic cooling by convection of a cylindrical solid ion battery subjected to a spherical rotation [54]. The interested readers can consult the given references for further information [[2], [10], [60]].

3.6 The radiofrequency heating of an anisotropic wood sample

3.6.1 Preliminary considerations

The dielectric and the thermo-physical properties of wood products, which are cylindrical and anisotropic in nature, are conditioned by the orientation of the rings on the tree trunk. Consequently, the x, y and z directions associated with the Cartesian coordinate system do not represent the longitudinal (L), radial (R) and tangential (T) directions as defined by the anatomical structure of the wood sample. However, for the orientation θ shown in **Figure 39**, there is a transition relationship from a cylindrical to a Cartesian coordinate system as shown by equations (15.1) and (15.2) [10]:

$$k_x = -k_R \sin\theta + k_T \cos\theta, \quad k_y = -k_R \cos\theta + k_T \sin\theta, \quad k_z = k_L \tag{15.1}$$

$$\varepsilon_x = -\varepsilon_R \sin\theta + \varepsilon_T \sin\theta, \ \varepsilon_y = -\varepsilon_R \cos\theta + \varepsilon_T \sin\theta, \quad \varepsilon_z = \varepsilon_L \tag{15.2}$$

where (k_L, k_R, k_T) and $(\varepsilon_L, \varepsilon_R, \varepsilon_T)$ are respectively the thermal conductivities and the complex dielectric permittivity of the wood samples in the principal directions L, R, and T. An angular position close to zero is considered for the heat transfer analysis. These conditions imply that $k_z = k_T$, $k_y = k_R$ and $k_x = k_L$.

According to the literature [48], most of the wood species have a the longitudinal (k_L) and radial (k_R) thermal conductivity of about 1.75 and 2.2 respectively, while the tangential (k_T) thermal conductivity varies between 0.9 and 0.95 of the radial term. Consequently, the values considered in this work are given by equation (16):

$$k_L = 1.8\, k_R \ \text{ and } \ k_T = 0.9\, k_R \tag{16}$$

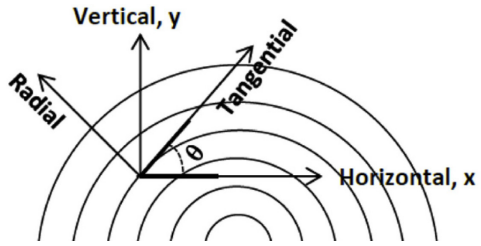

Figure 39: Cross-section of the wood sample showing an illustration of the (x, y, T, R) directions as well as the angle θ.

3.6.2 Modelling considerations

This section focuses on an application of the enthalpy-based finite element method for the description of the thaw time of the Douglas-fir (*Pseudotsuga menziesii*) and the White oak (*Quercus alba*), two North American wood species following their exposure to the RF. The Douglas-fir is a medium-density softwood, while the White oak is a moderately high-density ring porous hardwood. The studied wood sample had a parallelepiped geometry with equal sides length Lx = Ly = Lz = 5 cm. The RF intensity and frequency are 1 W/cm^2 and 50 MHz respectively. The six faces of the wood samples were all exposed to the same intensity (1 W/cm^2). The initial temperature of the sample is -20^{o}C and the maximum heating time is set at 1800 s. The density (rho), specific heat capacity (C_p) and radial conductivity (k_R) were expressed as a function of the moisture content, the temperature (T) and the specific gravity (SG) which in turn is expressed as a percentage of the dry mass of wood and calculated by the formulae found in the literature [43]. In this regard, two MC of 65% and 90% are considered and the specific gravities are 0.48 and 0.68 for respectively the Douglas-fir and the White oak species. Moreover, the data for the thermo-physical properties of the Douglas-fir and the White oak expressed as a function of temperature are given in **Tables** (4) and (5) respectively for the two moisture MC considered. Consequently, the anisotropic dielectric properties at the frequency of 50 MHz and the data extracted from [61] and expressed as a function of temperature and MC are given in **Figure 40** and **Figure 41** for the Douglas-fir and **Figure 42** and **Figure 43** for the White Oak. For numerical modelling, the regression polynomials associated with the data were used as shown in **Figure 40**-**43**. The wood geometry was meshed with identical hexahedra comprising eight nodes (2744 elements and 3375 nodes).

Tableau 4 : The thermo-physical properties of the Douglas-fir

Douglas-fir (SG = 0.48)	
MC = 65%	
Density $[Kg/m^3]$	$\rho = 792$
Latent heat $[KJ/m^3]$	$L = 0.70848\ x\ 10^8$
Specific heat $[J/Kg°C]$	
$T < 0°C$	$T > 0°C$
$C_p = 2280 + 16.6 \times T(°C)$	$C_p = 2566.15 + 4.98 \times T(°C)$
Thermal conductivity $[W/m°C]$	
$T < 0°C$	$T > 0°C$
$k_L = 0.6703 - 0.00172706 \times T(°C)$	$k_L = 0.564526 + 0.00201848 \times T(°C)$
$k_R = 0.301635 - 0.00077718 \times T(°C)$	$k_R = 0.2540367 + 0.0090832 \times T(°C)$
$k_T = 0.33515 - 0.00086352 \times T(°C)$	$k_T = 0.282263 + 0.00100924 \times T(°C)$
MC = 90%	
Density $[Kg/m^3]$	$\rho = 912.0$
Latent heat $[KJ/m^3]$	$L = 1.05\ x\ 10^8$
Specific heat $[J/Kg°C]$	
$T < 0°C$	$T > 0°C$
$C_p = 2280 + 16.6 \times T(°C)$	$C_p = 2783.9 + 4.98 \times T(°C)$
Thermal conductivity $[W/m°C]$	
$T < 0°C$	$T > 0°C$
$k_L = 0.8484 - 0.00172704 \times T(°C)$	$k_L = 0.667069 + 0.00261214 \times T(°C)$
$k_R = 0.38178 - 0.00077717 \times T(°C)$	$k_R = 0.30018105 + 0.00117546 \times T(°C)$
$k_T = 0.42420 - 0.0008635 \times T(°C)$	$k_T = 0.3335345 + 0.00130607 \times T(°C)$

Tableau 5 : The thermo-physical properties of the White oak

White oak (SG = 0.68)	
MC = 65%	
Density $[Kg/m^3]$	$\rho = 1122$
Latent heat $[KJ/m^3]$	$L = 0.70848\ x\ 10^8$
Specific heat $[J/Kg°C]$	
$T < 0°C$	$T > 0°C$
$C_p = 2280 + 16.6 \times T(°C)$	$C_p = 2566.15 + 4.98 \times T(°C)$
Thermal conductivity $[W/m°C]$	
$T < 0°C$	$T > 0°C$

$k_L = 0.9224334 - 0.00237664 \times T(℃)$	$k_L = 0.7768642 + 0.0027777 \times T(℃)$
$k_R = 0.41509503 - 0.00106949 \times T(℃)$	$k_R = 0.34958889 + 0.00124997 \times T(℃)$
$k_T = 0.4612167 - 0.00118832 \times T(℃)$	$k_T = 0.3884321 + 0.00138885 \times T(℃)$
MC = 90%	
Density $[Kg/m^3]$	$\rho = 1292.0$
Latent heat $[KJ/m^3]$	$L = 1.05 \times 10^8$
Specific heat [J/Kg℃]	
$T < 0℃$	$T > 0℃$
$C_p = 2280 + 16.6 \times T(℃)$	$C_p = 2783.9 + 4.98 \times T(℃)$
Thermal conductivity [W/m℃]	
$T < 0℃$	$T > 0℃$
$k_L = 1.1675244 - 0.00213898 \times T(℃)$	$k_L = 0.9179772 + 0.00359466 \times T(℃)$
$k_R = 0.52538598 - 0.00106949 \times T(℃)$	$k_R = 0.41308974 + 0.0016176 \times T(℃)$
$k_T = 0.5837622 - 0.00118832 \times T(℃)$	$k_T = 0.4589886 + 0.00179733 \times T(℃)$

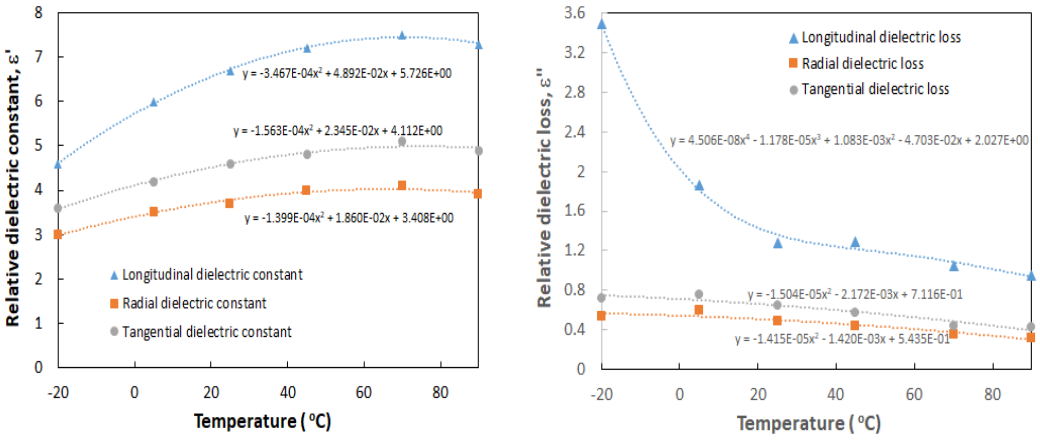

Figure 40: The dielectric properties of the Douglas-fir wood samples at a frequency of 50 MHz and 65% MC.

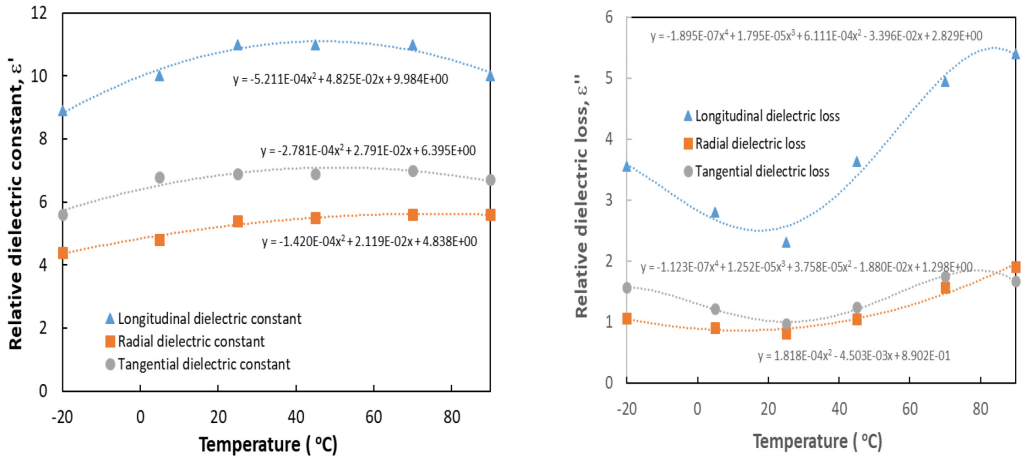

Figure 41: The dielectric properties of Douglas-fir wood samples at a frequency of 50 MHz and 90% MC.

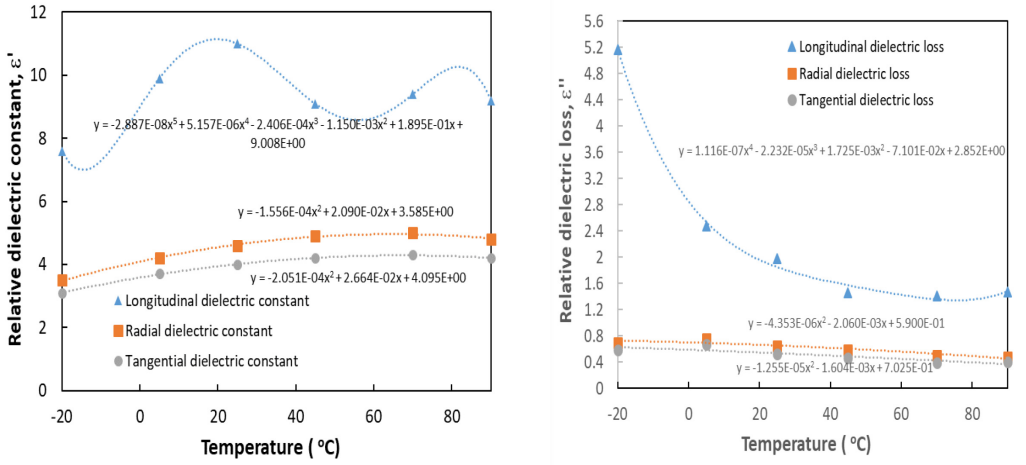

Figure 42: The dielectric properties of the White oak wood samples at a frequency of 50 MHz and 65% MC.

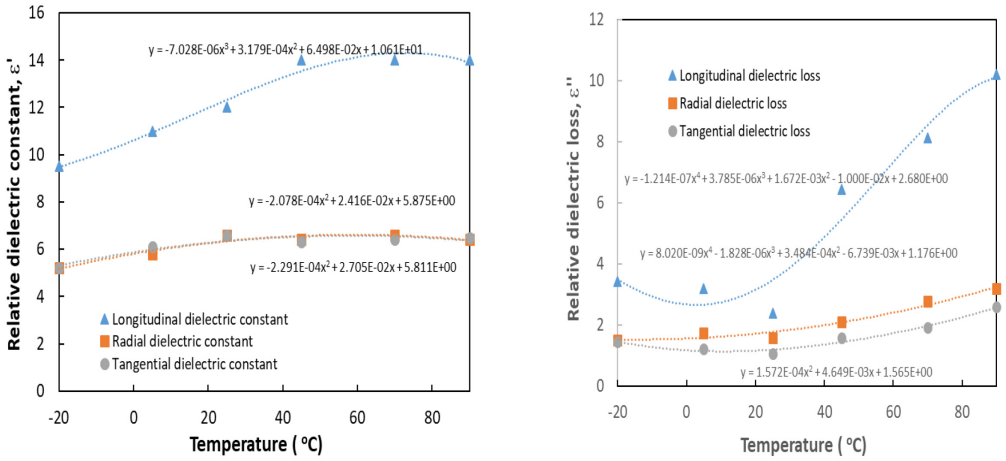

Figure 43: The dielectric properties of the White oak wood samples at a frequency of 50 MHz and 90% MC.

3.7 Results and discussions

Figure 44 shows the variations of the temperature at the center of both wood samples species as a function of the heating time for both 65 % and 90 % moisture content. **Figure 45** further shows a comparison between the temperature variations of two wood species with time at fixed MC of 65 % and 90 % respectively.

The observed behavior is similar for all the investigated species and parameters. They consist in three phases made of an increase from -20℃ to 0℃ where there is a plateau followed by another increase. It can be noted that the first phase is related to the presence of water in the form of ice due to the negative temperature. The observed figures show that the wood samples' temperature evolves faster in the first phase as compared to the phase after the freezing state. The explanation for such observation can be found in the variations of the thermal conductivity, the latent energy and the specific gravity which are three associated parameters.

In fact, **Tables (4)** and **(5)** have shown that the thermal conductivity of wood is closely related to its physical state; it appears that it is lower in the frozen state as compared to the unfrozen one which is characterized by the presence of water in the liquid state.

Moreover, the time required by the RF for changing the absorbed wood water from the solid (near negative zero) to the liquid state (near positive zero) is important and it increases with the wood sample's MC. In fact, at the beginning of the latent energy accumulation, the wood sample temperature is 0℃ and remains constant throughout this phase. However, once this latent energy is exceeded, the wood temperature increases more easily due to the large thermal conductivity associated with the liquid phase of water, as compared to that of its solid phase.

Finally, at a constant MC, the time required for heating the wood sample from -20℃ to 0℃ depends on its SG and is found to be shorter for low SG such as those of the lightwood. The same observation applies to the liquid state where the slope of the variations of the temperature with time is higher for the Douglas-fir in comparison to the White oak.

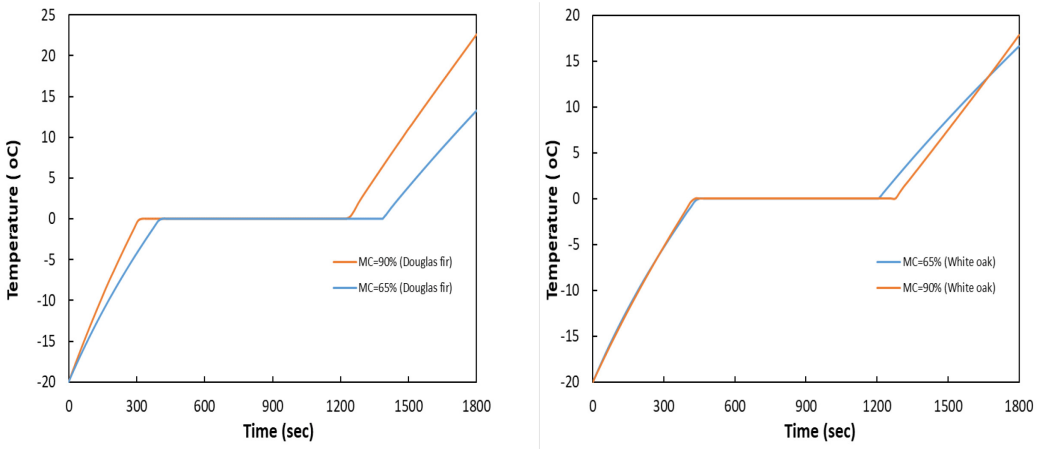

Figure 44: Variations of the temperature at the center of the Douglas-fir and the White oak wood samples with the heating time for both 65 % and 90 % MC.

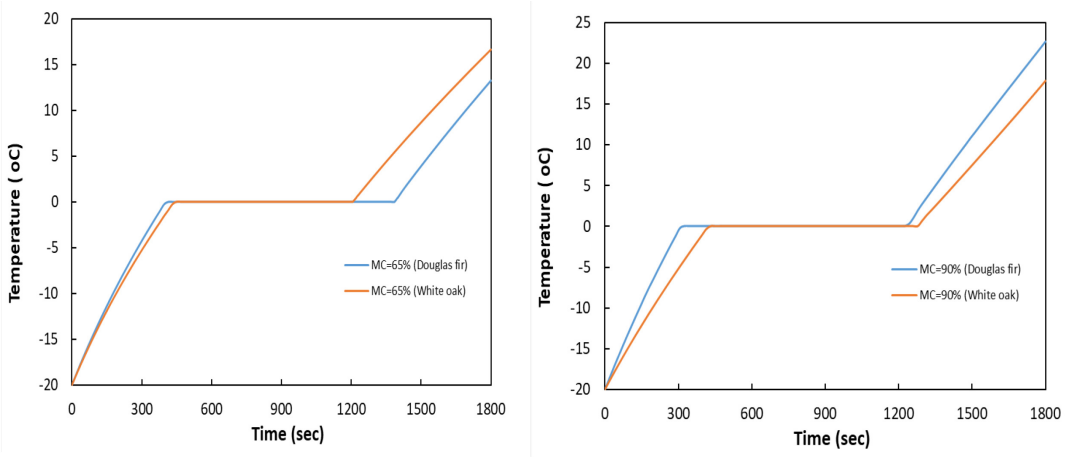

Figure 45: Comparative temperature variations at the center of the Douglas-fir and White oak wood samples with the heating time at fixed MC of 65% and 90% respectively.

Figure 46 and **Figure 47** show the variations of the temperature profile of the Douglas-fir wood samples, across their XY, YZ and ZX half-planes of symmetry. These profiles were induced by the RF for the heating cycles ending at 300 and 1800 s for 65% and 90% MC, respectively. Moreover, **Figure 48** and **Figure 49** show different views of the temperature distribution at 300 s for 65% and 90% MC, respectively. In the same manner, **Figure 50** and **Figure 51** show various views of the temperature distribution at 1800 s for 65% and 90% MC, respectively.

These results show that the temperature field induced by RF in the Douglas-fir wood samples is almost constant for the two investigated MC. Moreover, these observations show no temperature gradient as no temperature point was present. Finally, the observed maximum variation does not exceed 0.12%.

In the same manner as for the Douglas-fir wood samples, **Figure 52** and **Figure 53** show the temperature profiles induced by the RF at 300 and 1800 s on the XY, YZ and ZX half-planes of symmetry of the White oak-wood samples for 65% and 90% MC, respectively. Finally, **Figure 54**, **Figure 55**, **Figure 56** and **Figure 57** show different views of the temperature profile of the White oak wood samples, measured at 300 and 1800 s, for 65% and 90 % MC, respectively. Similar remarks to those of the Douglas-fir can be made for the White oak wood samples. In fact, the

induced temperature field is uniform. This RF-induced characteristic of temperature uniformity within wood samples does not seem to be achievable by microwaves. Indeed, according to the work done in [2] for the thawing of several Canadian wood samples (same size as the one used in this work), the microwave-induced temperature field is very heterogeneous with variations of up to 20% between minimum and maximum values. Consequently, the following important points can be made from the general observations on dielectric heating frozen wood:

- The RF heating induces a nearly uniform temperature distribution in wooden materials.
- The heating time by RF is longer, as compared to the heating by microwave.
- The microwave heating induces a very significant temperature gradient.
- The heating time and the quality of the temperature distribution in the frozen or unfrozen wood sample requires a trade off for the choice of an intermediate frequency between RF and microwave.
- A comparative study on the wood heating or thawing time would be desirable between the infrared and RF radiation.

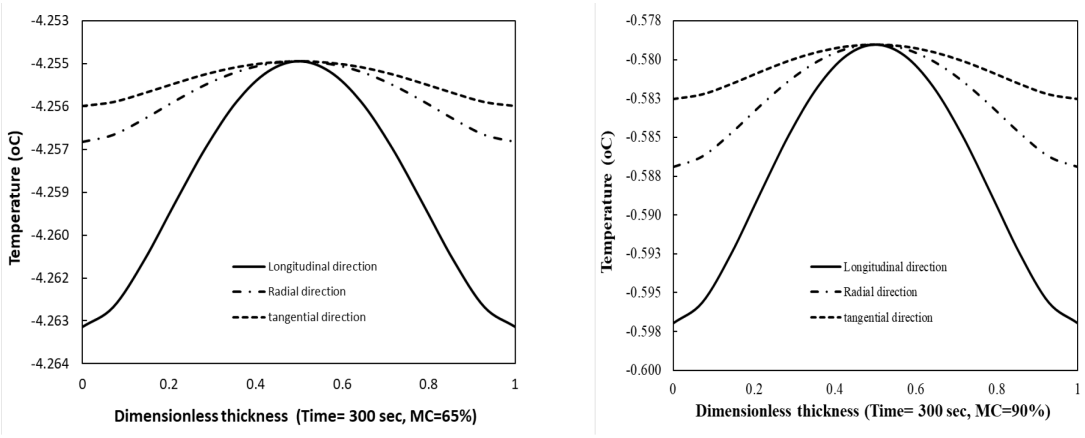

a) *MC = 65%* b) *MC = 905%*

Figure 46: Temperature distribution in the principal directions (L, R, T) at time 300 s for raw Douglas-fir wood samples exposed at RF parameters: I0 =1.0 W/cm2, frequency = 50 MHz: a) MC = 65% and b) MC = 90%.

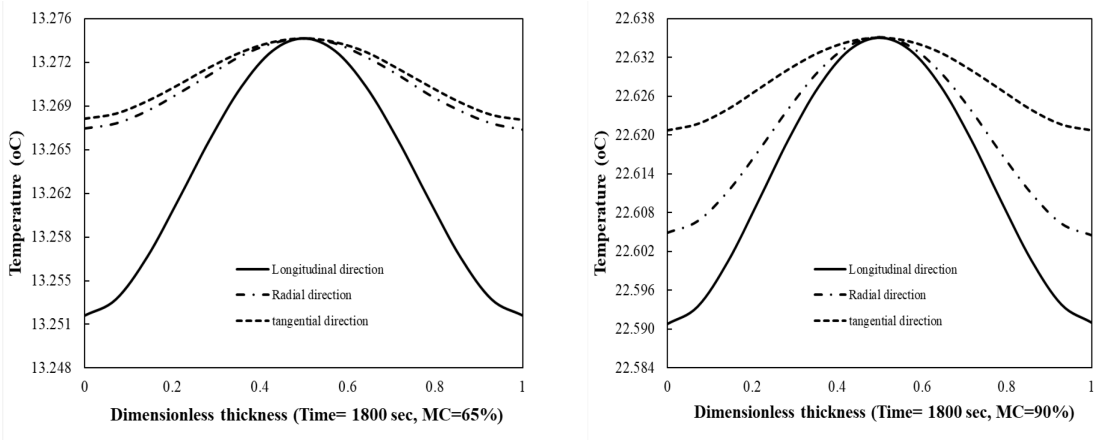

a) MC = 65% *b) MC = 90%*

Figure 47: Temperature distribution in the principal directions (L, R, T) at time 1800 s for raw Douglas-fir wood samples exposed at RF parameters: I0 =1.0 W/cm2, frequency = 50 MHz: a) MC = 65% and b) MC = 90%.

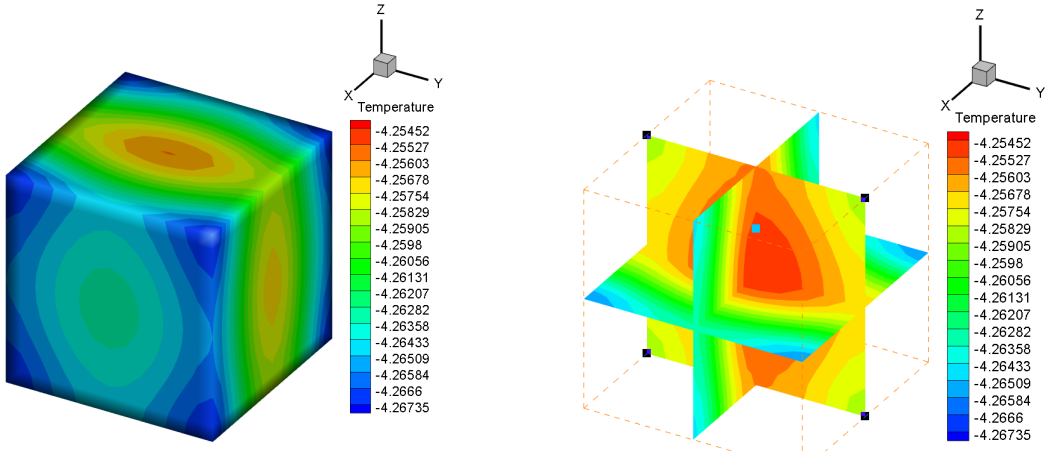

Figure 48: Temperature distribution view at the final heating time (300 s) for raw Douglas-fir wood samples exposed at RF parameters: I0 =1.0 W/cm2, frequency= 50 MHz and MC= 65%

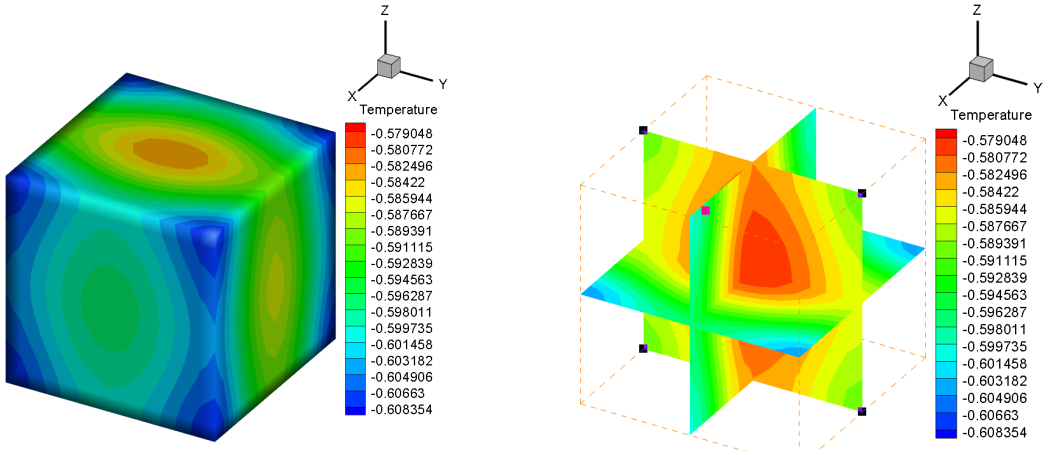

Figure 49: Temperature distribution view at the final heating time (300 s) for raw Douglas-fir wood samples exposed at RF parameters: I0 =1.0 W/cm2, frequency = 50 MHz and MC = 90%.

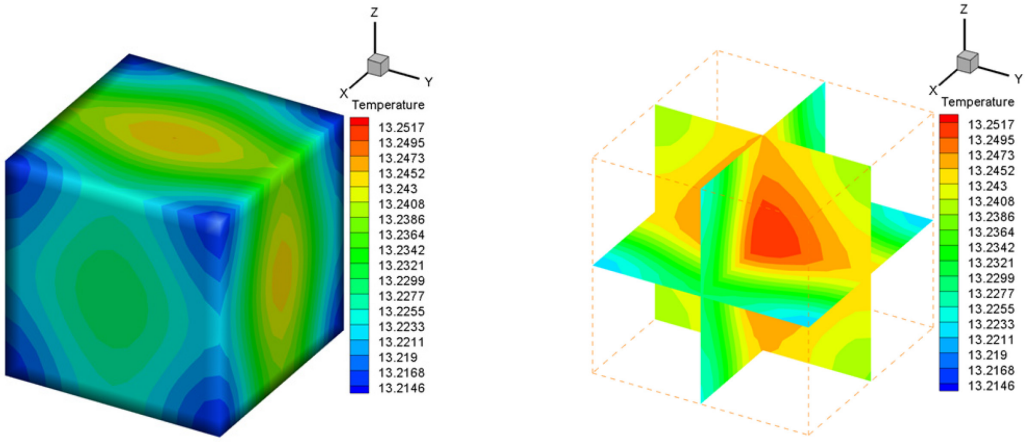

Figure 50: Temperature distribution view at the final heating time (1800 s) for raw Douglas-fir wood samples exposed at RF parameters: I0 = 1.0 W/cm2, frequency = 50 MHz and MC = 65%.

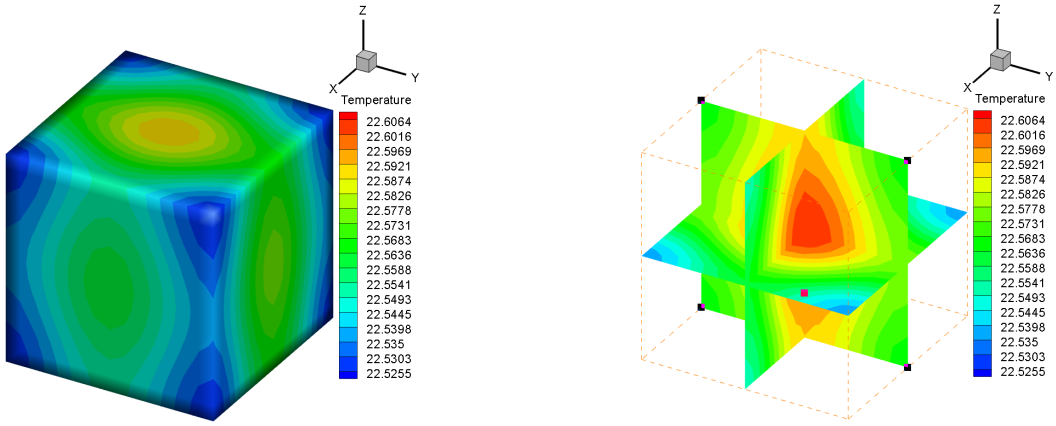

Figure 51: Temperature distribution view at the final heating time (1800 s) for raw Douglas-fir wood samples exposed at RF parameters: I0 = 1.0 W/cm2, frequency = 50 MHz and MC = 90 %.

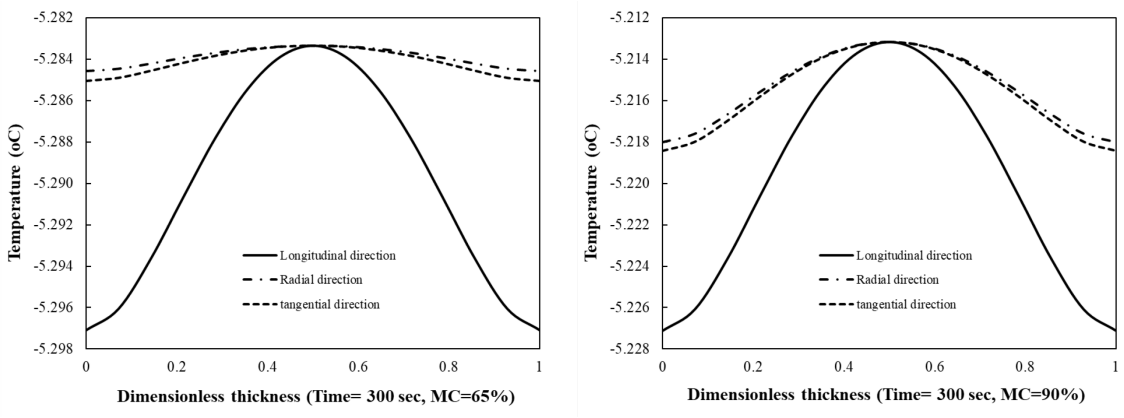

a) MC = 65%

b) MC = 90%

Figure 52: Temperature distribution in the principal directions (L, R, T) at time 300 s for raw White-oak wood samples exposed at RF parameters: I0 =1.0 W/cm2, frequency = 50 MHz: a) MC = 65% and b) MC = 90%.

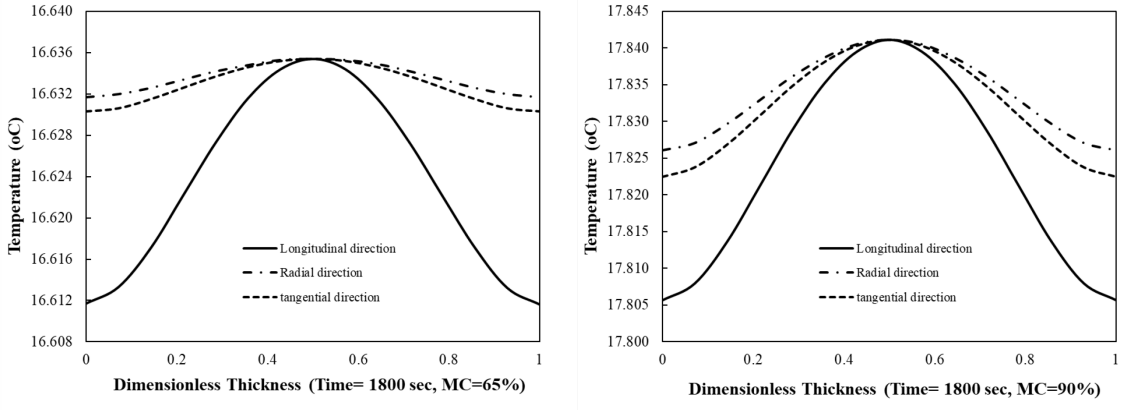

a) MC = 65%

b) MC = 90%

Figure 53: Temperature distribution in the principal directions (L, R, T) at time 1800 s for raw White-oak wood samples exposed at RF parameters: I0 =1.0 W/cm2, frequency = 50 MHz: a) MC = 65% and b) MC = 90%.

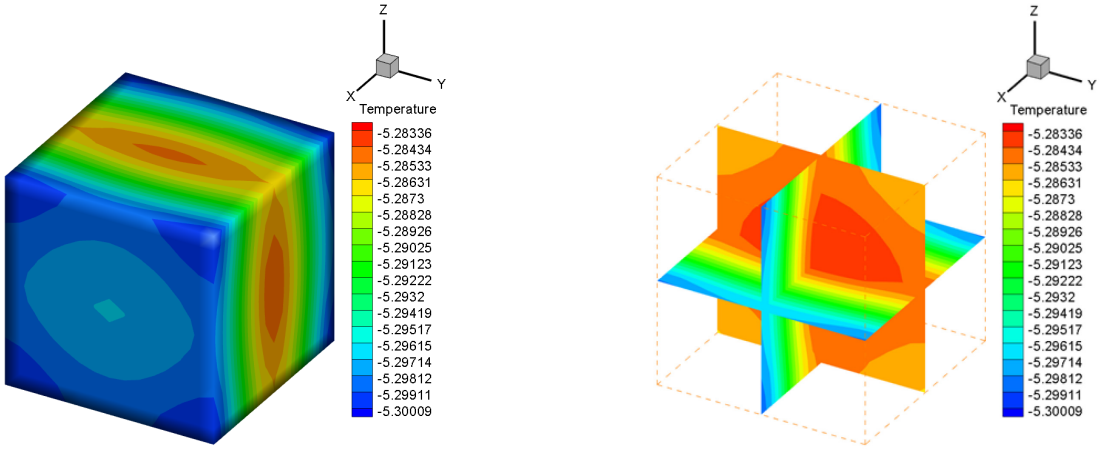

Figure 54: Temperature distribution view at the final heating time (300 s) for raw White oak wood samples exposed at RF parameters: I0 =1.0 W/cm2, frequency = 50 MHz and MC = 65%.

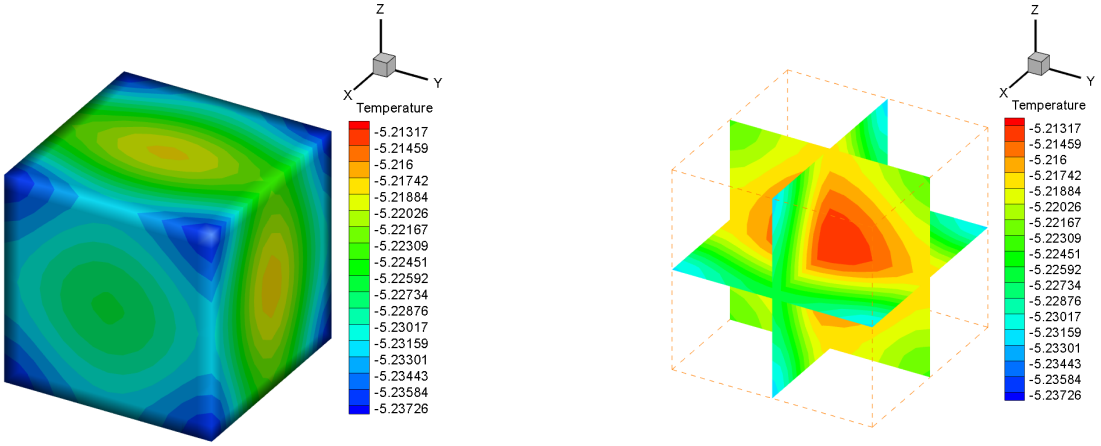

Figure 55: Temperature distribution view at the final heating time (300 s) for raw White oak wood samples exposed at RF parameters: I0 =1.0 W/cm2, frequency = 50 MHz and MC = 90%.

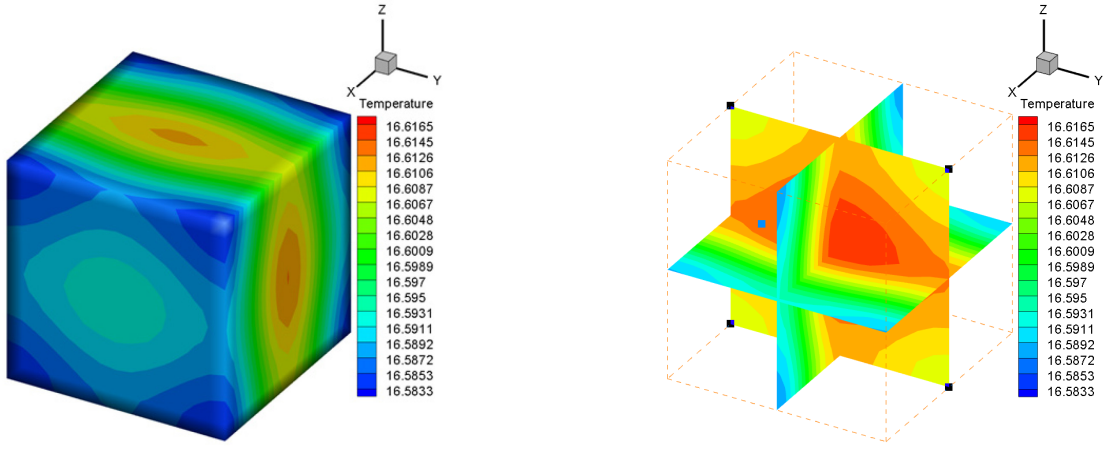

Figure 56: Temperature distribution view at the final heating time (1800 s) for raw White oak wood samples exposed at RF parameters: I0 =1.0 W/cm2, frequency = 50 MHz and MC = 65%.

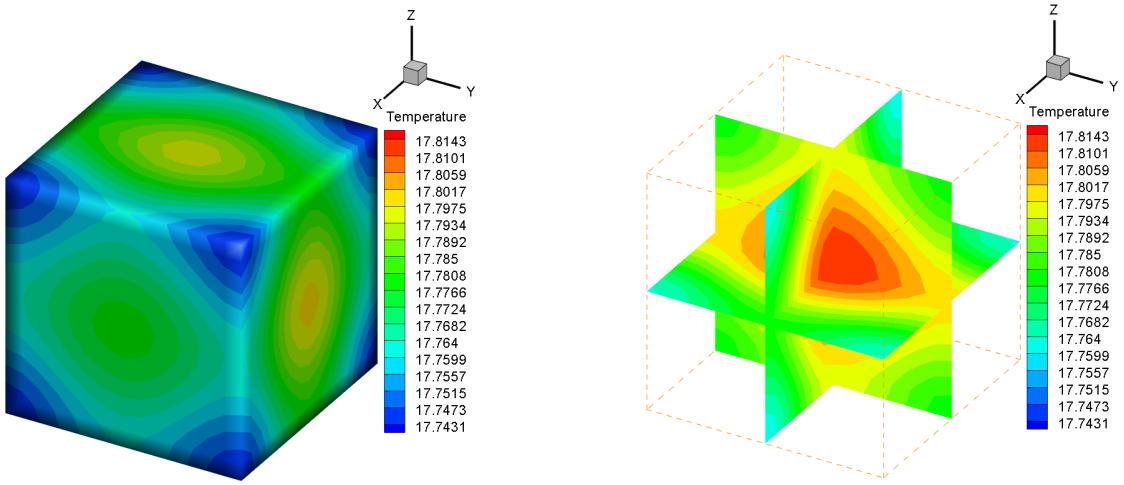

Figure 57: Temperature distribution view at the final heating time (1800 s) for raw White oak wood samples exposed at RF parameters: I0 =1.0 W/cm2, frequency = 50 MHz and MC = 90%.

3.8 Conclusion

This work describes the numerical study of the potential use of plane and normal incident radiofrequencies for the anisotropic dielectric heating of frozen wood with an initial temperature of -20°C. The Douglas-fir (*Pseudotsuga menziesii*), which is a medium-density softwood, and the White oak (*Quercus alba*), which is a moderately high-density ring porous hardwood, were the two North American species investigated. The complex dielectric and the thermo-physical properties were expressed as a function of temperature, moisture content and structural orientations. The study was conducted on two MC (65% and 90%). The results clearly show that the temperature distribution in the wood samples is uniform at the expense of a relatively long time. In addition, the heating time was found to vary not only with the species type through its specific gravity (SG), but also with the latent energy (L) and the moisture content (MC).

CHAPITRE 4

APPLICATION OF THE B-SPLINE METHOD TO SOLVE NONLINEAR PROBLEM OF HEAT CONDUCTION WITH RADIATION BOUNDARY CONDITIONS USING KIRCHHOFF TRANSFORMATION

Annasabi [a] Z., Erchiqui [b,*] F, M. Souli [c1]

Heat Transfer, ASME. Facteur d'impact : 2.01 (Q1) 2022 (en impression)

[a]: Université du Québec en Abitibi-Témiscamingue, école de génie, 455, boulevard de l'Université, Rouyn-Noranda (Québec), Canada J9X 5E4

[b]: Université du Québec en Abitibi-Témiscamingue, école de génie, 455, boulevard de l'Université, Rouyn-Noranda (Québec), Canada J9X 5E4

[c]: Université de Lille Sciences et Technologies, France

Rôle de l'étudiant dans cette publication :

Contribution à l'élaboration de modèles mathématiques, de calcul numérique, de l'interprétation des résultats et de la rédaction de l'article.

Abstract: This paper concerns the joint application of the B-Spline method and the Kirchhoff transformation to solve the nonlinear problem of thermal conduction with radiation type boundary conditions. The proposed method requires few iterations, sometimes none, for solids subjected to prescribed temperature boundary conditions. This method can be deployed by other numerical approaches (Boundary element method, Finite element method, Finite volume method, etc.) for the resolution of the heat conduction equation (linear or nonlinear), in terms of the Kirchhoff transformation θ. For numerical implementation, the steady-state finite element method is considered. The numerical validation was performed for a hollow aluminum cylinder whose outer surface is subjected to radiation. Three types of thermal conductivities are considered: i) constant, ii) linear and iii) nonlinear. As an application, we studied the thermal response of an aluminum reactor, in the form of an annular disc with cooling tubes, exposed to thermal radiation.

Résumé: Cet article concerne l'application de la méthode B-Spline et de la transformation de Kirchhoff pour résoudre le problème non linéaire de la conduction thermique avec des conditions aux limites de type rayonnement. Le nombre des itérations de la méthode proposée est minimisé, voire parfois nul, pour des conditions aux limites de type Dirichlet. Cette méthode peut être utilisée par d'autres approches numériques (méthode des éléments de frontière, méthode des éléments finis, méthode des volumes finis, etc.) pour la résolution de l'équation de conduction thermique (linéaire ou non linéaire), en termes de transformation de Kirchhoff θ. Pour la mise en œuvre numérique, la méthode des éléments finis en régime permanent est considérée. La validation numérique a été réalisée pour un cylindre creux en aluminium dont la surface extérieure est soumise à un rayonnement. Trois types de conductivités thermiques sont considérés : i) constante, ii) linéaire et iii) non linéaire. Comme application, nous avons étudié la réponse thermique d'un réacteur en aluminium, sous forme d'un disque annulaire avec des tubes de refroidissement, exposé au rayonnement thermique.

4.1 Introduction

The mode of heat transmission by radiation is complex and depends on the nature of the body: solid, liquid or gas. This radiation is composed of radiations of different wavelengths, ranging from 0.3μm to 100μm, giving continuous spectra in the case of solids and band spectra for gases. Vacuum and most simple gases (such as H_2, O_2 and N_2) are perfectly transparent media for radiation propagation. However, propagation in some compound gases, considered as semi-transparent media (such as CO_2, H_2O, CO, CH_4), is accompanied by a decrease in the transported energy [[62], [63]].In the case of solids and liquids, the radiation emitted comes from the surface if the medium is opaque and from its entire mass if it is semi-transparent. This phenomenon of emission corresponds to the conversion of material energy (agitation of the electrons constituting the matter whose intensity depends on the temperature) into radiative energy [63]. Received radiation, part of which is absorbed in the form of heat, is a combination of radiation emitted and/or reflected and/or diffused by the bodies surrounding it or by itself (if its surface is curved). The rigorous mathematical treatment of the heat generated by the radiation is very sensitive for real cases if simplifying hypotheses are not used. For closed systems with the presence of gas, the exact solution of radiation coupling and heat conduction (via the Fourier equation) is only possible for simple systems [63]. However, there are methods that allow to obtain approximate solutions to problems and, therefore, they are very interesting alternatives. These methods include: Monte Carlo method [62], Zone method [64], Imaginary plane method [65], Discrete ordinate method [66], Boltzmann method [[67] , [68]] and a discontinuous finite element method [69]. These techniques have been the subject of numerous theoretical and numerical works and experimental verifications. Among the recent theories of interest in radiation, we suggest to readers the theory of transformation multithermotics [70] and the effective-medium theory [71].

However, for cases where a solid is subject to radiation (radiation-type boundary condition), the heat equation can then be formulated either in terms of temperature T or in terms of one of the two following auxiliary variables: i) enthalpy [10], in the transient state and ii) the Kirchhoff transform [44], in the steady state. For incompressible solids, several methods exist in the literature

for the mathematical treatment of this type of problems. Among these methods are the meshless methods for non-linear materials using Laplace transform and its numerical inversion [[72], [73], [74]].

The interest in the last method is its simplicity for the transformation of the nonlinear heat equation into a linear equation by the Kirchhoff transformation (θ) [[44], [75]] which makes the heat equation in terms of θ(T) very attractive for solving problems encountered in physics and engineering. However, for a physical environment where the thermal conductivity and/or boundary conditions are nonlinear, access to the solution becomes very difficult. This thorny problem is basically due to the difficulty of reversing the Kirchhoff transformation, defined as the integral of thermal conductivity with temperature, or of expressing boundary conditions in terms of T(θ). For this reason, several authors discuss the Kirchhoff transform for media where the thermal conductivity is constant or linear with temperature [[10], [18]]. For problems characterized by the non-linearity of θ(T), approximations are used to get around the difficulty of finding T(θ) [[19], [20]]. Recently, a new approach [25], called robust based on the B-Spline method [23], has been proposed by Annasabi and Erchiqui to solve the heat equation for coupled conduction-convection problems. Several validation tests have shown the performance of the approach. For heat conduction in non-linear solids, the proposed method does not require any iteration if the boundary conditions are of the temperature imposed type. As such, let us underline the three-dimensional example treated by the authors on thermal conduction in copper, in the region where its thermal conductivity is strongly nonlinear [25]. It is within this framework that the present work falls and it concerns the combination of the B-Spline method and the Kirchhoff transform for the solution of the heat conduction equation in an incompressible solid subjected to radiation (boundary condition).

For the modeling, in steady state, we considered the finite element method. The numerical validation was performed for a hollow aluminum cylinder whose outer surface is subjected to radiation. Three thermal conductivities are considered: i) constant, ii) linear and iii) nonlinear. As an application, we studied the thermal response of an aluminum reactor, in the form of an annular

disc with cooling tubes (temperature 1 °C), exposed to thermal radiation (1500 °C and 2000 °C). It is worth noting that the proposed method can be deployed by other numerical methods encountered in physics and engineering for the treatment of the inverse of the Kirchhoff T(θ) transformation such as Boundary element method (BEM), Finite element method (FEM), and Finite volume method (FVM).

4.2 The heat conduction equation

The steady state equation of energy, in terms of the Kirchhoff transformation, θ(T), for an anisotropic solid in a region Ω bounded by a surface Γ (=$\Gamma_\theta \cup \Gamma_q$), is defined by equation. (1) in a Euclidean space R^3

$$\nabla^2\,\theta(T) = Q(\theta)\,; \qquad (x,y,z) \in \Omega \tag{1}$$

with:

$$\theta(T) = \int_{T_{ref}}^{T} k\,(T)dT\,; \qquad \forall\, T(x,y,z) \tag{2}$$

Where T [K] is the temperature, Q is the source term [W/m^3], k [W/m/K] is the thermal conductivity and T_{ref} is a reference temperature.

Eq. (1) is subjected to the following boundary condition:

$$\theta(T) = f(x,y,z); \qquad (x,y,z) \in \Gamma_\theta \tag{3}$$

$$\frac{\partial\theta(x,y.z)}{\partial n} = q_c + q_r = g(x,y,z)\,; \qquad (x,y,z) \in \Gamma_q \tag{4}$$

The f and g functions are specified values of the known boundary temperature and heat flux. The vector **n** is the outward normal (n_x, n_y, n_z) to the boundary surface Γ_q and (x,y,z) are coordinates defined on the boundary surface Γ.

The quantity q_c is the convective boundary heat flux given by:

$$q_c = h\,(T - T_\infty) \qquad (x,y,z) \in \Gamma_\theta \tag{5}$$

h [W/m^2/K] is the heat transfer coefficient, T_∞ [K] is the temperature of the surrounding medium. The term h ($T–T_\infty$) represents the convection heat transfer from the material to the surroundings.

The quantity q_r refers to the boundary radiative heat flux. In the case where the surfaces of the source and the receiver are gray and the medium between them is perfectly transparent, the quantity q_r is given by:

$$q_r = \sigma F_{r-s} \bar{\varepsilon} (T^4 - T_s^4) \qquad (x, y, z) \in \Gamma_q \tag{6}$$

F_{r-s}, and T_s, are respectively the view factors between receptor and source [76] and the source temperature (K). The term $\bar{\varepsilon}$ is the effective emissivity of the receptor-source system defined as:

$$\bar{\varepsilon} = \left(\frac{1}{\varepsilon_r} + \frac{1}{\varepsilon_s} - 1\right)^{-1} \tag{7}$$

where ε_r and ε_s are, respectively, the emissivity of receptor and emissivity of source. The parameter σ is the Stefan- Boltzmann constant (=5.67 10^{-8} W/m^{2}K^4).

The merit of expressing the heat equation in terms of Kirchhoff's transformation is its linear form. Nevertheless, the inverse function $T(\theta)$ is difficult to obtain for solids with a strongly temperature-dependent conductivity and for boundary conditions of radiation type (see eq.6). To meet this challenge, we will use the approach based on the B-Spline method [23], which has been successfully used for the heat problem in conduction-convection.

4.3 Numerical Study

The transformation of the limit value problem associated with the differential form of the thermal equation into an equivalent integral form can be achieved by Galerkin's weighted residual approach [34] and the use of the divergence theorem, which leads to:

$$\int_{\Omega} \frac{\partial \mathbf{N}}{\partial x_i}\left(\frac{\partial \mathbf{N}^{\mathbf{T}}}{\partial x_j}\boldsymbol{\theta}\right) d\Omega = \int_{\Omega} \mathbf{N} Q \, d\Omega + \int_{\Gamma} \mathbf{N}\,(q_r + q_c\,)\, d\Gamma \tag{8}$$

N and $\boldsymbol{\theta}$ are respectively the interpolation functions vector and the Kirchhoff transform vector of unknown nodes. According to equation 6, it is clear that the integral solution is strictly linked to the representation of radiation q_r (which depends on T^4) on the one hand and convection losses (which depends on T) on the other hand.

The algebraic form associated with system (8) is then given by the following equation:

$$\mathbf{K} \cdot \boldsymbol{\theta} = \mathbf{F_Q} + \mathbf{F_c} + \mathbf{F_r} \tag{9}$$

where :

$$\mathbf{K} = \int_{\Omega} \frac{\partial \mathbf{N}}{\partial x_i}\left(\frac{\partial \mathbf{N}^{\mathbf{T}}}{\partial x_j}\right) d\Omega \tag{9.1}$$

$$\mathbf{F_Q} = \int_{\Omega} \mathbf{N} Q(\theta)\, d\Omega \tag{9.2}$$

$$\mathbf{F_c} = \int_{\Gamma} \mathbf{N}\ \left(\, h(T_\infty - T\,(\theta))\right) d\Gamma \tag{9.3}$$

$$\mathbf{F_h} = \int_{\boldsymbol{\Gamma}} \mathbf{N}\, F_{m-r}\sigma\, \bar{\varepsilon}\, (T^4(\theta) - T_s^4)\ \mathbf{d\Gamma} \tag{9.4}$$

4.4 Kirchhoff's transformation and its reverse

For the implementation of the B-Spline method, each variable k(T), θ(T) and T(θ) is assumed to be continuous and piecewise defined. Moreover, we assume that each term can be represented by one or more functions of polynomial type defined by piecewise bilinear functions. The strategy on the construction of T(θ) is given in section 5 below. The algebraic expression of equation (9) is then given by the following equation:

$$(\mathbf{K} + \mathbf{C}) \cdot \boldsymbol{\theta} = \mathbf{F} \tag{10}$$

where:

$$\mathbf{C} = \int_{\Omega} \mathrm{h}\,\mathbf{N} \cdot \left(\mathbf{C}_1 \cdot \boldsymbol{\theta}^1 + \mathbf{C}_2 \cdot \boldsymbol{\theta}^2 + \cdots + \mathbf{C}_\mathrm{n} \cdot \boldsymbol{\theta}^\mathrm{n}\right) \cdot \mathbf{N}^\mathrm{T}\, \mathrm{d}\Omega \tag{10.1}$$

$$\mathbf{F} = \int_{\Gamma} \mathbf{N}\ \mathrm{h}\mathrm{T}_\infty\, \mathrm{d}\Gamma + \int_{\Omega} \mathbf{N}\,\mathrm{Q}\,\mathrm{d}\Gamma - \int_{\Gamma} \mathrm{h}\,\mathbf{N} \cdot \mathbf{C}_0 \cdot \mathbf{N}^\mathrm{T}\,\mathrm{d}\Gamma \tag{10.2}$$

$\mathbf{C}_i$ (i=0, n) are coefficient vectors which guarantee the continuity of θ(T) over all the sub-intervals of [T_{min},T_{max}]. The resolution of the algebraic system (7) requires the expression of T in terms of θ.

4.5 Strategy for the determination of T(θ)

The strategy consists, in a first step, in representing the curve θ(T) by a finite set of points (T_i, θ_i) where $0 \leq i \leq n$. Then, an optimal interpolation, using B-splines functions and a least square algorithm, is performed on each interval forming the curve. The optimized interpolation permits, for a desired accuracy, to determine the minimum number of intervals that adequately represents the curve T(θ).

The construction of the B-spline curve by pieces, over the (n +1) intervals (sub-domains), is carried out using the vector $\overrightarrow{OM}$ defined by:

$$\overrightarrow{\mathrm{OM}} = \sum_{\mathrm{i}=0}^{\mathrm{n}} \mathrm{B}_{(\mathrm{i},\mathrm{k})} \overrightarrow{\mathrm{OP_i}} \tag{11}$$

$\mathrm{B}_{(\mathrm{i},\mathrm{k})}$ are polynomial functions of degree k, defined on the interval i, whose influence is localized on a certain number of elementary sub-domains of the curve θ(T). The vector $\overrightarrow{\mathrm{OP_i}}$ represents the point control vector defined in the interval i. Consequently, the appropriate polynomial degree can be selected for each interval of the curve θ(T). However, if the number of intervals n is small, the expression of the temperature (T) as a function of the Kirchhoff transform (θ) cannot be representative of the physical phenomenon (fewer polynomial segments). To improve the quality of the representation of T(θ), there are several optimization approaches in the literature

to solve this problem. Concerning this present work, we have considered the approach proposed in [23]. For this purpose, the following steps are used:

1. Choice of the optimization algorithm (least square);
2. Definition of the desired precision for the construction of the B-spline curve;
3. Initialization of the control points in the interval T_{min}, T_{max} for which the Kirchhoff transforms are defined;
4. For each iteration, determination of the position of the control points which minimize the curve determination coefficient T(θ);
5. The loop stops when the desired accuracy is reached.

The interest of the B-splines method is that it allows a local control of the curve θ(T) (or T(θ)), while preserving the continuity of the function θ(T) (or T(θ)) and its derivative.

4.6 Validation

For numerical validation, we considered mathematical regressions on experimental data of thermal conductivity of aluminum, extracted from reference [21]. As shown in **Figure 58**, the three regression functions used for thermal conductivity are presented.

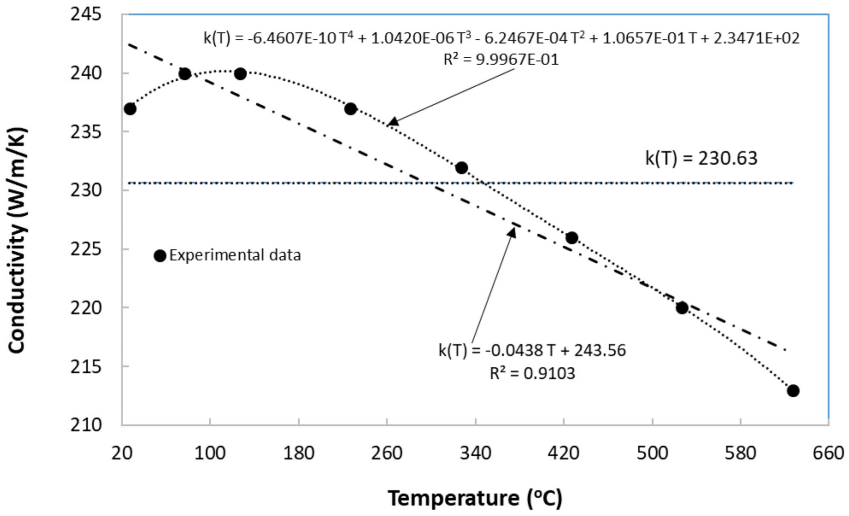

Figure 58: Comparative aluminum thermal conductivity regression versus experimental data

For validation, three situations are considered:

- A material subjected to radiation and prescribed temperature (case a with k(T)=C^{te}; see **Table 4**)
- A material subjected to radiation and prescribed temperature (case a with k(T)=Linear; see **Table 4**)
- A material subjected to radiation and imposed temperature (case a with k(T)=Nonlinear; see **Table 4**)

The study is based on a circular ring (2D) with outer and inner radii of 0.125 m and 0.5 m respectively. The outer region of the ring is subjected to thermal radiation at a temperature of 500°C, while the inner region is subjected to a constant temperature of 1 °C. The analytical expressions of thermal conductivity and emissivity are given in **Table 4**. For modeling, the physical domain is meshed using quadrilateral elements (1520 elements).

Tableau 6 : Thermal conductivity of aluminum and emissivity

Thermal conductivity (W/m/K) as function of T(°C)
$k(T) = 230$
$k(T) = -0.0438\,T + 243.56$
$k(T) = -6.4607\,10^{-10}\,T^4 + 1.0420\,10^{-6}\,T^3 - 6.2467\,10^{-4}\,T^2 + 1.065710^{-1}\,T + 2.3471\,10^2$

Figure 59-a illustrates, for the three studied cases of thermal conductivities for aluminum (constant, linear and non-linear), the excellent quality of the results obtained by using the B-Spline method for the resolution of the heat conduction equation in terms of θ and those obtained by ANSYS software. **Figure 59-b** illustrates the relative errors between the results obtained by ANSYS and the present method. **Figure 59-c**, **Figure 59-d** and **Figure 59-e** illustrate, respectively, for the three studied cases of thermal conductivities for aluminum, a fringe of the temperature distributions induced in the annular disc.

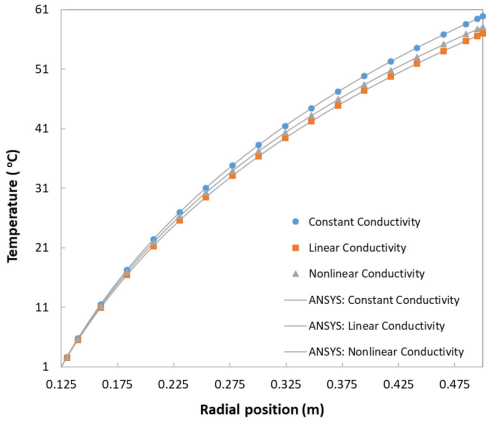

a. Comparison of temperature distribution: present method vs ANSYS

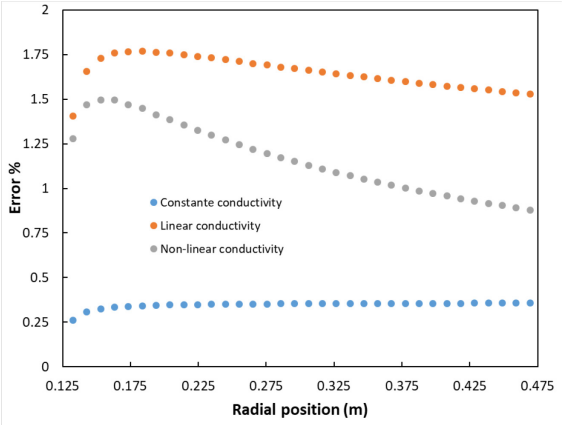

b. Relative results error between ANSYS and present method

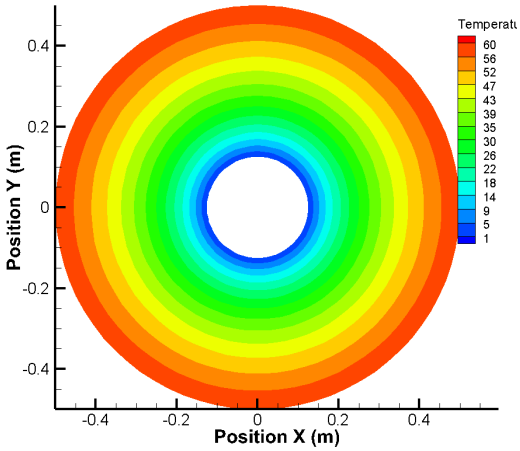

c. View of temperature distribution (k=Constant)

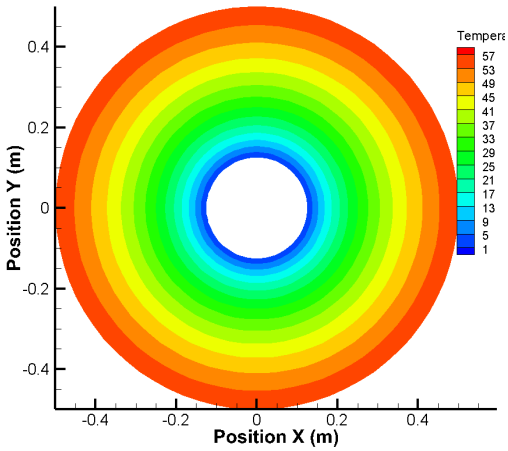

d. View of temperature distribution (k=Linear)

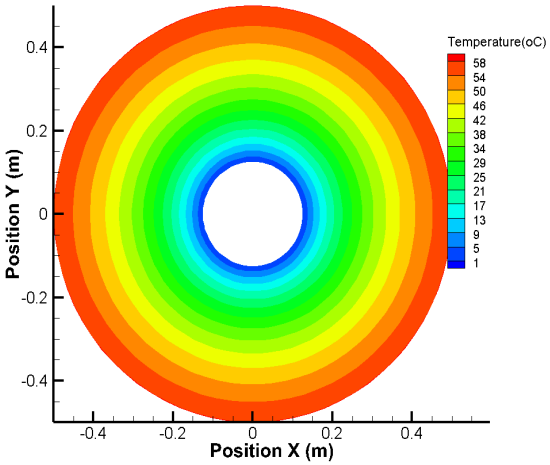

e. View of temperature distribution (k=Nonlinear)

Figure 59: Comparative numerical results of the temperature distributions obtained by ANSYS and the proposed method

Tableau 7 : Comparison, in term of iterations, between ANSYS and present method

	ANSYS (*Full Newton Raphson*)	**ThermoForm**
Case 1-2-3	2 iterations	2 iterations

Remark: *ThermoForm* is house software developed by Pr Erchiqui for numerical analysis of heat conduction in materials.

4.7 Application

As an application, we study the thermal response of an aluminum reactor in the form of an annular disc with tabular cooling and whose outer surface is exposed to radiation. For this, we consider, on the one hand, two types of reactors (reactor A with 17 cooling pipes and reactor B with 9 cooling pipes) and, on the other hand, two-radiation temperatures (2000 °C and 1500 °C). The rays of reactor and tabular are 50 mm and 2.5 mm respectively. For the modelling, the physical system is meshed with hexahedrons; for reactor A we have 2233 elements and 2429 nodes and for reactor B, we have 1797 elements and 1921 nodes(**Figure 60**). The non-linear thermal conductivity of aluminum is given in **Table 4.**

Figure 61-a and **Figure 61-b** illustrate the view temperature distribution in the reactors A and B respectively. According to these figures, we notice different temperature distributions can be observed in each of the reactors. In the first cases, where the temperature of the radiation is 2000 °C, the temperature generated in Reactor B is much hotter than in Reactor A. The maximum temperatures in each of the two reactors B and A are 196.9 °C and 131.1°C respectively, with a variation of 33.4%. In the second case, see **Figure 62-a** and **Figure 62-b**, the maximum temperatures generated in each of the two reactors B and A are 78.8 and 49.2 °C respectively, with a variation of 37.5%.

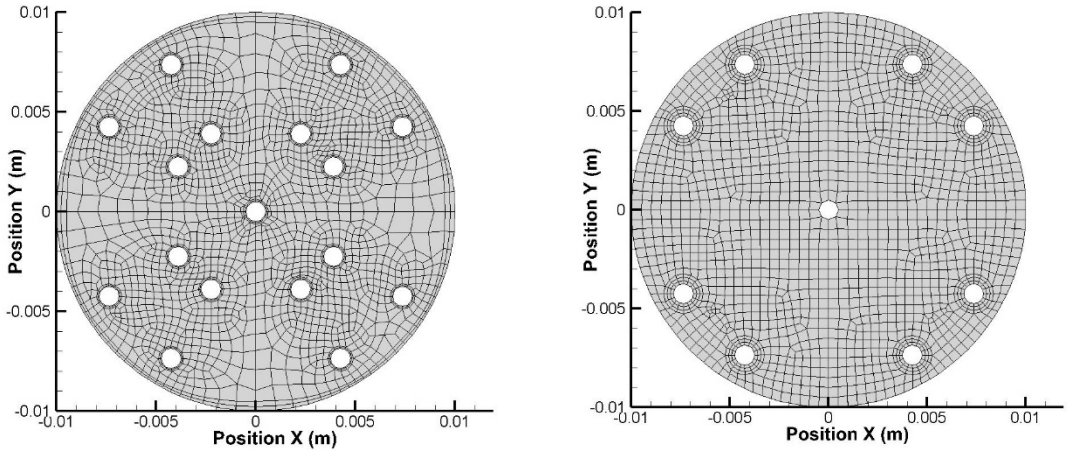

a. Aluminum reactor with 17 cooling tubes

b. Aluminum reactor with 9 cooling tubes

Figure 60: Meshed geometry with hexahedrons mesh elements

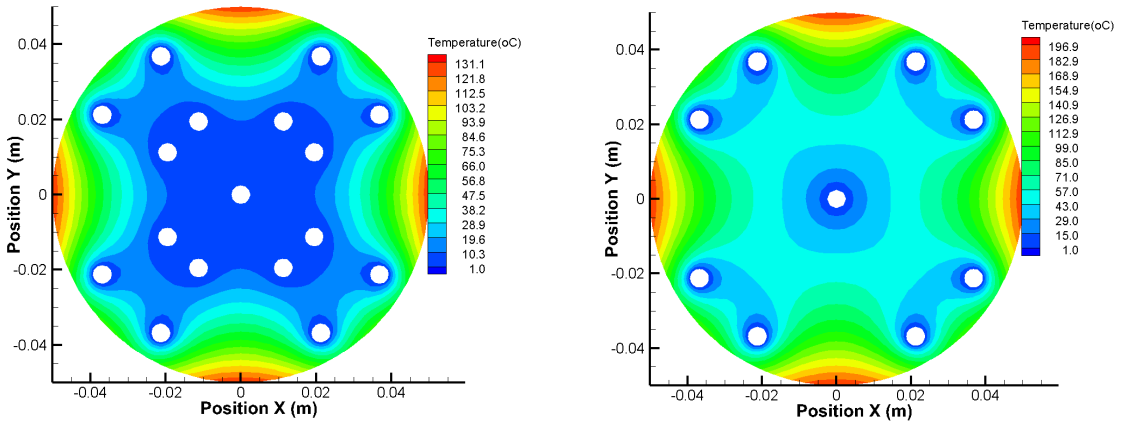

a. Reactor A *b. Reactor B*

Figure 61: Fringe distribution of the temperature distribution for case where the radiation temperature is 2000 °C

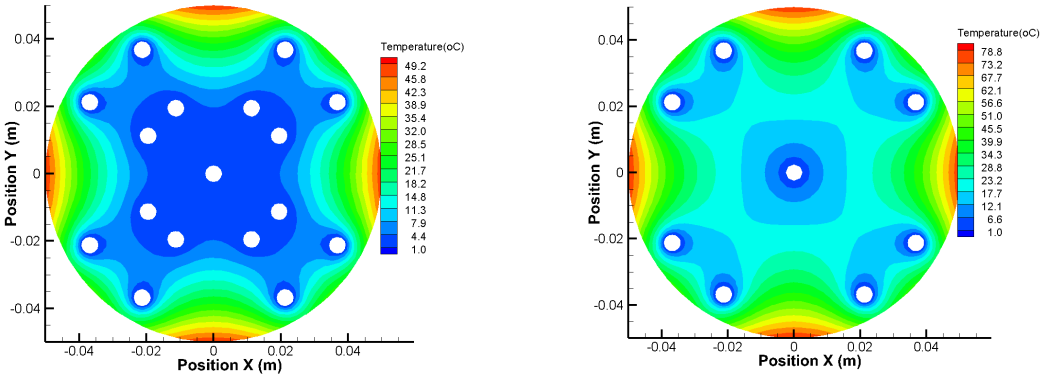

a. Reactor A *b. Reactor B*

Figure 62: View of the temperature distribution for case where the radiation temperature is 1500 °C

Figure 63 shows the temperature distribution, on the symmetry axes as shown in **Figure 63-a** and **Figure 63-b**, for Reactors A and B subjected to radiative temperatures of 2000°C and 1500 °C. It can be seen, on the one hand, that the shapes of the temperature curves are different for each of the reactors and, on the other hand, that the number and position of the coolers have an impact on the temperature distribution. In comparison with reactor B, the heat dissipation by Reactor A is greater. Indeed, in the case where the radiative temperature is 1500 °C, the maximum temperature induced in reactor A is 42.9 °C while it is 78.8 °C for reactor B; with a

difference of 35.9 °C. For the case where the radiation temperature is 2000 °C, the maximum induced temperature in reactor A is 131.1 °C while it is 196.9 °C for reactor B; with a difference of 65.8 °C. Consequently, the efficiency of heat dissipation by a given reactor is closely related to the number of coolers, their temperature and their positioning.

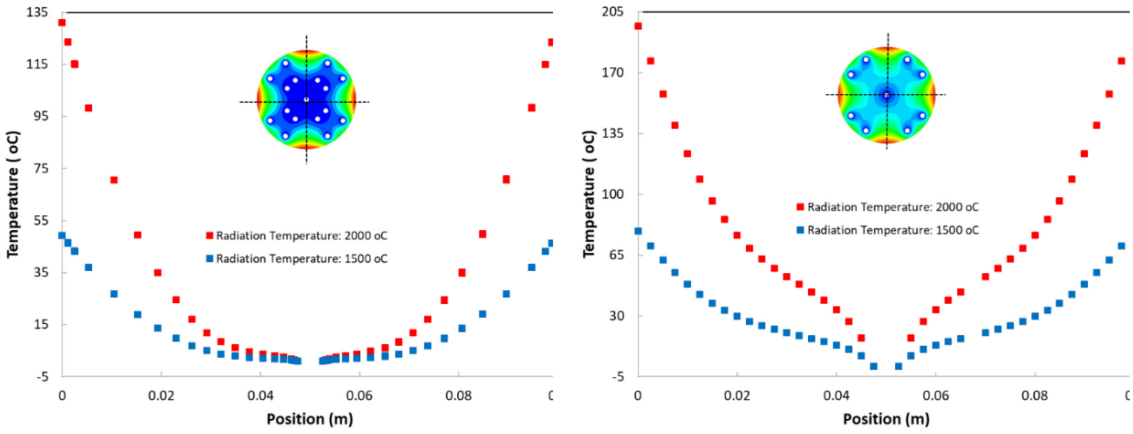

a. Reactor A *b. Reactor B*

Figure 63: Effect of the coolers of reactors A and B on radiation-induced temperatures

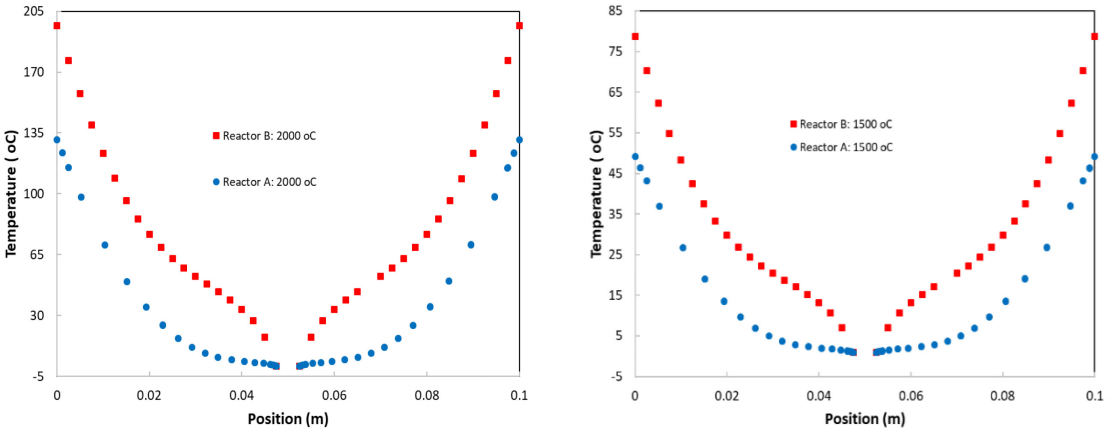

a. Radiation temperature 2000 °C *b. Radiation temperature 1500 °C*

Figure 64: Effect of Radiation Temperatures on the Performance of Reactors A and B

Finally, in order to compare the performance of each of the two reactors A and B, the temperature distributions on the axes of symmetry for the radiation temperatures 2000 °C and 1500 °C are shown in **Figure 64-a** and **Figure 64-b**. It can be seen that Reactor A is more efficient both in terms of cooling and the state of the temperature distribution.

On the basis of the results obtained, using the proposed approach to solve the problem of conduction-radiation coupling in steady state and in terms of the Kirchhoff transform, the following observations can be made:

- The method proposed for the determination of the Kirchhoff transform and its inverse is very robust, regardless of the mathematical representation of $\theta(T)$.
- The approach proposed for the analysis of thermal conduction by radiation, through the Kirchhoff transform, can be, without difficulty, combined with other numerical methods (MEF, BEM, MDF, etc.).
- The proposed method requires few iterations for solids subjected to radiation and imposed temperatures.
- For imposed temperatures (boundary conditions), the proposed method requires no iteration.
- The proposed approach is robust and can be combined with numerical and analytical methods to solve the problems of heat transfer for physical environments with high non-linearity of materials (radiative and electromagnetic heating, heating by convection; etc.).
-

4.8 Conclusion

This article proposes a new approach to solve nonlinear steady-state heat conduction-radiation using Kirchhoff transformation and B-Spline in solids. For this, a recent method is used. The method requires few iterations, sometimes none, for solids subjected to imposed temperatures. This new method can be deployed by other numerical approaches (BEM, FEM, FDM, etc.) for the resolution of the heat conduction equation (linear or not), in terms of the θ. For numerical implementation, the finite element method is considered. The numerical validation was performed for a hollow aluminum cylinder whose outer surface is subjected to radiation. Three thermal conductivities are considered: i) constant, ii) linear and iii) nonlinear. As an application, we studied the thermal response of an aluminum reactor, in the form of an annular disc with cooling tubes, exposed to thermal radiation.

CONCLUSION

Ce projet de recherche est orienté vers la modélisation de transfert de chaleur dans les multi-matériaux anisotropes et non linéaires. À cet effet, l'équation de la conduction de la chaleur classique pour les solides en termes de l'enthalpie volumique et de la transformée de Kirchhoff, a été redéfinie par une nouvelle formulation utilisant l'enthalpie hybride anisotrope et la transformée de Kirchhoff anisotrope. L'approche proposée a été validée autant au niveau mathématique (analytique et numérique) qu'expérimentale. Cette approche, contrairement aux méthodes numériques existantes, permet le traitement numérique, par la méthode des éléments finis, le transfert de chaleur, avec ou sans changement de phase, dans les milieux formés de plusieurs solides dont les tenseurs de conductivités thermiques sont de natures différentes (sphériques et/ou cylindriques et/ou cartésiens). De surcroit, on a adapté la nouvelle formulation hybride pour la résolution de la conduction de la chaleur en fonction de la température (au lieu de l'enthalpie et de la transformée de Kirchhoff) pour les solides multi-matériaux et multi-anisotropies. Aussi, nous avons couplé l'approche hybride avec l'énergie diélectrique (radiofréquence) pour estimer le temps de chauffage de bois gelé (anisotrope et non linéaire). Finalement, le problème de la non linéarité de la conduction de la chaleur, en régime stationnaire, est contourné par le déploiement d'une nouvelle approche, que nous avons initiée, utilisant la méthode de Spline, pour traiter les problèmes thermiques assujettis à des conditions aux limites de type température et/ou convection et/ou radiation.

RÉFÉRENCES

[1] S. J. Drake, D. A. Wetz, J. K. Ostanek, S. P. Miller, J. M. Heinzel, and A. Jain, "Measurement of anisotropic thermophysical properties of cylindrical Li-ion cells," *Journal of Power Sources,* vol. 252, pp. 298-304, 2014, doi: 10.1016/j.jpowsour.2013.11.107.

[2] F. Erchiqui, Z. Annasabi, M. Souli, and F. Slaoui-Hasnaoui, "3D numerical analysis of the thermal effect and dielectric anisotropy on thawing frozen wood using microwave energy," *International Journal of Thermal Sciences,* vol. 89, pp. 58-78, 2015, doi: 10.1016/j.ijthermalsci.2014.09.012.

[3] X. Li, S. Raith, and M. Itskov, "Numerical simulation of anisotropy directions in soft tissues and particular in skin," *PAMM _Proc. Appl. Math. Mech.,* vol. 13, pp. 57-58, 2013.

[4] V. B. L. Boppana, Z. T. Xie, and I. P. Castro, "Thermal Stratification Effects on Flow Over a Generic Urban Canopy," *Boundary-Layer Meteorology,* vol. 153, no. 1, pp. 141-162, 2014, doi: 10.1007/s10546-014-9935-1.

[5] J. M. C. Duhamel, "Sur les Équations Générales de la Propagation de la Chaleur dans les Corps Solides dont la Conductibilité n'est pas la Même dans Tous les Sens"," *J. Ec. Polytech.,* vol. 13, no. 21, pp. 356-399, 1832.

[6] L. Onsager, "Reciprocal relations in irreversible processes. I," *Physical Review,* vol. 37, no. 4, pp. 405-426, 1931, doi: 10.1103/PhysRev.37.405.

[7] D. Sarkar, K. Shah, A. Haji-Sheikh, and A. Jain, "Analytical modeling of temperature distribution in an anisotropic cylinder with circumferentially-varying convective heat transfer," *International Journal of Heat and Mass Transfer,* vol. 79, pp. 1027-1033, 2014, doi: 10.1016/j.ijheatmasstransfer.2014.08.060.

[8] D. Sarkar, A. Haji-Sheikh, and A. Jain, "Thermal conduction in an orthotropic sphere with circumferentially varying convection heat transfer," *International Journal of Heat and Mass Transfer,* vol. 96, pp. 406-412, 2016, doi: 10.1016/j.ijheatmasstransfer.2016.01.027.

[9] M. H. Hsieh and C. C. Ma, "Analytical investigations for heat conduction problems in anisotropic thin-layer media with embedded heat sources," *International Journal of Heat and Mass Transfer,* vol. 45, no. 20, pp. 4117-4132, 2002, doi: 10.1016/S0017-9310(02)00136-9.

[10] F. Erchiqui and Z. Annasabi, "3D hybrid finite element enthalpy for anisotropic thermal conduction analysis," *International Journal of Heat and Mass Transfer,* vol. 136, pp. 1250-1264, 2019, doi: 10.1016/j.ijheatmasstransfer.2019.02.096.

[11] P. N. Peralta and A. P. Bangi, "Finite element model for the heating of frozen wood," *Wood and Fiber Science,* vol. 38, no. 2, pp. 359-364, 2006.

[12] Y. C. Shiah and C. L. Tan, "BEM treatment of two-dimensional anisotropic field problems by direct domain mapping," *Engineering Analysis with Boundary Elements,* vol. 20, no. 4, pp. 347-351, 1997, doi: 10.1016/s0955-7997(97)00103-3.

[13] Y. C. Shiah and C. L. Tan, "BEM treatment of three-dimensional anisotropic field problems by direct domain mapping," *Engineering Analysis with Boundary Elements,* vol. 28, no. 1, pp. 43-52, 2004, doi: 10.1016/S0955-7997(03)00114-0.

[14] D. Prestini, G. Filippini, P. Zdanski, and M. Vaz Jr, "Fundamental approach to anisotropic heat conduction using the element-based finite volume method," *Numerical Heat Transfer, Part B: Fundamentals,* vol. 71, no. 4, pp. 327-345, 2017.

[15] M. Darwish and F. Moukalled, "A compact procedure for discretization of the anisotropic diffusion operator," *Numerical Heat Transfer, Part B: Fundamentals,* vol. 55, no. 5, pp. 339-360, 2009.

[16] M. Sameti, F. R. Astaraie, F. Pourfayaz, and A. Kasaeian, "Analytical and FDM solutions for anisotropic heat conduction in an orthotropic rectangular," *Am. J. Numer. Anal.,* vol. 2, no. 2, pp. 65-68, 2014.

[17] U. Projahn, "Heat conduction in anisotropic composites of arbitrary shape (a numerical analysis)," 1981.

[18] S. Kim, "A simple direct estimation of temperature-dependent thermal conductivity with Kirchhoff transformation," *International Communications in Heat and Mass Transfer,* vol. 28, no. 4, pp. 537-544, 2001, doi: 10.1016/S0735-1933(01)00257-3.

[19] P. Vadasz, "Analytical solution to nonlinear thermal diffusion: Kirchhoff versus Cole-Hopf transformations," *Journal of Heat Transfer,* vol. 132, no. 12, 2010, Art no. 121302, doi: 10.1115/1.4002325.
[20] E. Hopf, "The partial differential equation ut + uux = μxx," *Communications on Pure and Applied Mathematics,* vol. 3, no. 3, pp. 201-230, 1950, doi: 10.1002/cpa.3160030302.
[21] R. W. Powell, C. Y. Ho, and P. E. Liley, "Thermal conductivity of selected materials," *Thermal Conductivity of Selected Materials,* 1966.
[22] B. Al-Khamaiseh, Y. S. Muzychka, and S. Kocabiyik, "Effect of temperature-dependent thermal conductivity on spreading resistance in flux channels," *J. Thermophys. Heat Transf.,* vol. 32, no. 5, pp. 1-9, 2018.
[23] W. Wang, F. Shi, G. Zhao, and D. Xiaoxiao, "A new method for knot placement of B-Spline curve approximation and interpolation," *3Rd International Conference on Materials Engineering, Manufacturing Technology and Control,* pp. 1527-1532, 2016.
[24] V. T. Dung and T. Tjahjowidodo, "A direct method to solve optimal knots of Bspline curves: An application for non-uniform B-spline curves fitting," *PLoS ONE,* vol. 12, no. 3, 2017, Art no. e0173857, doi: 10.1371/journal.pone.0173857.
[25] Z. Annasabi and F. Erchiqui, "Robust Kirchhoff transformation using B-spline for finite element analysis of the non-linear heat conduction," (in English), *International Communications in Heat and Mass Transfer,* Article vol. 120, 2021, Art no. 104985, doi: 10.1016/j.icheatmasstransfer.2020.104985.
[26] G. I. Torgovnikov, "Dielectric properties of wood and wood-based materials," *Dielectric Properties of Wood and Wood-Based Materials,* 1993.
[27] M. Norimoto and T. Yamada, "The Dielectric Properties of Wood V, On the Dielectric Anisotropy of Wood," *Wood research: bulletin of the Wood Research Institute Kyoto University,* vol. 51, pp. 12-32, 1971.
[28] F. Erchiqui, Z. Annasabi, A. Koubaa, F. Slaoui-Hasnaoui, and H. Kaddami, "Numerical modelling of microwave heating of frozen wood," *Canadian Journal of Chemical Engineering,* vol. 91, no. 9, pp. 1582-1589, 2013, doi: 10.1002/cjce.21826.
[29] F. Erchiqui, "3d numerical simulation of thawing frozen wood using microwave energy: frequency effect on the applicability of the beer–lambert law," *Drying Technology,* vol. 31, no. 11, pp. 1219-1233, 2013.
[30] T. Ohlsson and N. Bengtsson, "Microwave heating profiles in foods.: A comparison between heating experiments and computer simulation. A research note," *Microwave Energy Applications Newsletter,* vol. 4, no. 6, pp. 3-8, 1971.
[31] P. Rattanadecho, "The simulation of microwave heating of wood using a rectangular wave guide: Influence of frequency and sample size," *Chemical Engineering Science,* vol. 61, no. 14, pp. 4798-4811, 2006, doi: 10.1016/j.ces.2006.03.001.
[32] S. Swami, *Microwave heating characteristics of simulated high moisture foods*. University of Massachusetts, 1982.
[33] A. Buffa and R. Hiptmair, "Galerkin boundary element methods for electromagnetic scattering," in *Topics in computational wave propagation*: Springer, 2003, pp. 83-124.
[34] B. Finlayson, "The method of weighted residuals and variational principles, volume 87 of Mathematics in Science and Engineering," ed: Academic Press, New York, NY, 1972.
[35] D. Li, C. Zhang, W. Wang, and Y. Zhang, "Implicit–explicit predictor–corrector schemes for nonlinear parabolic differential equations," *Applied mathematical modelling,* vol. 35, no. 6, pp. 2711-2722, 2011.
[36] C. C. Ma and S. W. Chang, "Analytical exact solutions of heat conduction problems for anisotropic multi-layered media," *International Journal of Heat and Mass Transfer,* vol. 47, no. 8-9, pp. 1643-1655, 2004, doi: 10.1016/j.ijheatmasstransfer.2003.10.022.
[37] M. Norouzi, A. Amiri Delouei, and M. Seilsepour, "A general exact solution for heat conduction in multilayer spherical composite laminates," *Composite Structures,* vol. 106, pp. 288-295, 2013, doi: 10.1016/j.compstruct.2013.06.005.
[38] B. J. Pangrle, K. G. Ayappa, H. T. Davis, E. A. Davis, and J. Gordon, "Microwave thawing of cylinders," *AIChE Journal,* vol. 37, no. 12, pp. 1789-1800, 1991, doi: 10.1002/aic.690371204.

[39] J. M. Powers, "On the necessity of positive semi-definite conductivity and onsager reciprocity in modeling heat conduction in anisotropic media," *Journal of Heat Transfer,* vol. 126, no. 5, pp. 670-675, 2004, doi: 10.1115/1.1798913.
[40] Q. Liu, Y. L. He, and Q. Li, "Enthalpy-based multiple-relaxation-time lattice Boltzmann method for solid-liquid phase-change heat transfer in metal foams," *Physical Review E,* vol. 96, no. 2, 2017, Art no. 023303, doi: 10.1103/PhysRevE.96.023303.
[41] H. Hu and S. A. Argyropoulos, "Modelling of Stefan problems in complex configurations involving two different metals using the enthalpy method," *Modelling and Simulation in Materials Science and Engineering,* vol. 3, no. 1, pp. 53-64, 1995, Art no. 005, doi: 10.1088/0965-0393/3/1/005.
[42] M. A. Dokainish and K. Subbaraj, "A survey of direct time-integration methods in computational structural dynamics-I. Explicit methods," *Computers and Structures,* vol. 32, no. 6, pp. 1371-1386, 1989, doi: 10.1016/0045-7949(89)90314-3.
[43] H. P. Steinhagen and H. W. Lee, "Enthalpy method to compute radial heating and thawing of logs," *Wood Fiber Sci.,* vol. 20, no. 4, pp. 415-421, 1988.
[44] G. Kirchhoff, "Vorlesungen über die Theorie der Wärme," *Vorlesungen über die Theorie der Wärme,* 1894.
[45] R. Morales-Rodriguez, *Thermodynamics Fundamentals and its Application in Science,* 2012.
[46] C. M. Elliott and J. R. Ockendon, *Weak and Variational Methods for Moving Boundary Problems,* 1982.
[47] B. A. Finlayson, *The Method of Weighted Residuals and Variational Principles,* 1972.
[48] F. Erchiqui, H. Kaddami, F. Slaoui-Hasnaoui, and A. Koubaa, "3D finite element enthalpy method for analysis of phytosanitary treatment of wood by microwave," *European Journal of Wood and Wood Products,* vol. 78, no. 3, pp. 577-591, 2020, doi: 10.1007/s00107-020-01534-9.
[49] I. Bunget and M. Popescu, *Physics of Solid Dielectrics,* 1984.
[50] S. Chandrasekaran, S. Ramanathan, and T. Basak, "Microwave material processing-a review," *AIChE Journal,* vol. 58, no. 2, pp. 330-363, 2012, doi: 10.1002/aic.12766.
[51] J. B. Burch *et al.*, "Radio frequency nonionizing radiation in a community exposed to radio and television broadcasting," *Environmental Health Perspectives,* vol. 114, no. 2, pp. 248-253, 2006, doi: 10.1289/ehp.8237.
[52] D. M. Pozar, *Microwave Engineering,* 1998.
[53] P. Rattanadecho, N. Suwannapum, and W. Cha-um, "Interactions between electromagnetic and thermal fields in microwave heating of hardened type I-Cement paste using a rectangular waveguide (influence of frequency and sample size)," *Journal of Heat Transfer,* vol. 131, no. 8, pp. 1-12, 2009, doi: 10.1115/1.2993134.
[54] F. Erchiqui, H. Kaddami, G. Dituba-Ngoma, and F. Slaoui-Hasnaoui, "Comparative study of the use of infrared and microwave heating modes for the thermoforming of wood-plastic composite sheets," *International Journal of Heat and Mass Transfer,* vol. 158, 2020, Art no. 119996, doi: 10.1016/j.ijheatmasstransfer.2020.119996.
[55] M. Bhattacharya, T. Basak, and K. G. Ayappa, "A fixed-grid finite element based enthalpy formulation for generalized phase change problems: Role of superficial mushy region," *International Journal of Heat and Mass Transfer,* vol. 45, no. 24, pp. 4881-4898, 2002, doi: 10.1016/S0017-9310(02)00178-3.
[56] C. J. Coleman, "The microwave heating of frozen substances," *Applied Mathematical Modelling,* vol. 14, no. 8, pp. 439-443, 1990, doi: 10.1016/0307-904X(90)90100-J.
[57] F. J. Asencor and M. Panizo, "Finite-difference operators in anisotropic inhomogeneous dielectrics: General case," *Journal of Computational Physics,* vol. 95, no. 2, pp. 387-399, 1991, doi: 10.1016/0021-9991(91)90282-P.
[58] D. Soares Jr and M. P. Vinagre, "Numerical computation of electromagnetic fields by the time-domain boundary element method and the complex variable method," *CMES - Computer Modeling in Engineering and Sciences,* vol. 25, no. 1, pp. 1-8, 2008.
[59] C. A. Bunge, T. Gries, and M. Beckers, *Polymer Optical Fibres,* 2017.
[60] A. P. Kaestner and L. B. Bååth, "Microwave polarimetry tomography of wood," *IEEE Sensors Journal,* vol. 5, no. 2, pp. 209-215, 2005, doi: 10.1109/JSEN.2004.841343.

[61] W. L. James, "Dielectric properties of wood and hardboard: variation with temperature, frequency, moisture content, and grain orientation," *Dielectric Properties of Wood and Hardboard: Variation with Temperature, Frequency, Moisture Content, and Grain Orientation,* 1975.
[62] M. F. Modest, *Radiative Heat Transfer* (Radiative Heat Transfer). Elsevier Inc. (in English), 2013.
[63] J. R. Howell, M. P. Mengüç, and R. Siegel, *Thermal radiation heat transfer, sixth edition* (Thermal Radiation Heat Transfer, Sixth Edition). CRC Press (in English), 2015, pp. 1-971.
[64] H. C. Hottel and E. S. Cohen, "Radiant heat exchange in a gas-filled enclosure: Allowance for nonuniformity of gas temperature," (in English), *AIChE Journal,* Article vol. 4, no. 1, pp. 3-14, 1958, doi: 10.1002/aic.690040103.
[65] A. Charette, F. Erchiqui, and Y. S. Kocaefe, "The imaginary planes method for the calculation of radiative heat transfer in industrial furnaces," (in English), *Can. J. Chem. Eng.,* Article vol. 67, no. 3, pp. 378-384, 1989, doi: 10.1002/cjce.5450670305.
[66] W. A. Fiveland, "Three-dimensional radiative heat-transfer solutions by the discrete-ordinates method," (in English), *J Thermophys Heat Transfer,* Article vol. 2, no. 4, pp. 309-316, 1988, doi: 10.2514/3.105.
[67] S. C. Mishra, H. Poonia, A. K. Das, P. Asinari, and R. Borchiellini, "Analysis of conduction-radiation heat transfer in a 2D enclosure using the lattice boltzmann method," (in English), *Numer Heat Transfer Part A Appl,* Article vol. 66, no. 6, pp. 669-688, 2014, doi: 10.1080/10407782.2014.894376.
[68] Y. Sun and X. Zhang, "Analysis of transient conduction and radiation problems using the lattice boltzmann and discrete ordinates methods," (in English), *Numer Heat Transfer Part A Appl,* Article vol. 68, no. 6, pp. 619-637, 2015, doi: 10.1080/10407782.2014.994406.
[69] C. H. Wang, Y. Y. Feng, K. Yue, and X. X. Zhang, "Discontinuous finite element method for combined radiation-conduction heat transfer in participating media," (in English), *International Communications in Heat and Mass Transfer,* Article vol. 108, 2019, Art no. 104287, doi: 10.1016/j.icheatmasstransfer.2019.104287.
[70] L. Xu, G. Dai, and J. Huang, "Transformation Multithermotics: Controlling Radiation and Conduction Simultaneously," (in English), *Phys. Rev. Appl.,* Article vol. 13, no. 2, 2020, Art no. 024063, doi: 10.1103/PhysRevApplied.13.024063.
[71] L. Xu and J. Huang, "Metamaterials for Manipulating Thermal Radiation: Transparency, Cloak, and Expander," (in English), *Phys. Rev. Appl.,* Article vol. 12, no. 4, 2019, Art no. 044048, doi: 10.1103/PhysRevApplied.12.044048.
[72] Z. J. Fu, W. Chen, and Q. H. Qin, "Three boundary meshless methods for heat conduction analysis in nonlinear FGMs with Kirchhoff and Laplace transformation," (in English), *Adv. Appl. Mat. Mech.,* Article vol. 4, no. 5, pp. 519-542, 2012, doi: 10.4208/aamm.10-m1170.
[73] Q. Xi, Z. J. Fu, and T. Rabczuk, "An efficient boundary collocation scheme for transient thermal analysis in large-size-ratio functionally graded materials under heat source load," (in English), *Comput Mech,* Article vol. 64, no. 5, pp. 1221-1235, 2019, doi: 10.1007/s00466-019-01701-7.
[74] M. Mierzwiczak, W. Chen, and Z. J. Fu, "The singular boundary method for steady-state nonlinear heat conduction problem with temperature-dependent thermal conductivity," (in English), *International Journal of Heat and Mass Transfer,* Review vol. 91, pp. 205-217, 2015, Art no. 12266, doi: 10.1016/j.ijheatmasstransfer.2015.07.051.
[75] R. Morales-Rodriguez, *Thermodynamics: fundamentals and its application in science*. BoD–Books on Demand, 2012.
[76] F. Erchiqui and G. D. Ngoma, "Analyse comparative des méthodes de calcul des facteurs de formes pour des surfaces à contours rectilignes," (in French), *International Journal of Thermal Sciences,* Article vol. 46, no. 3, pp. 284-293, 2007, doi: 10.1016/j.ijthermalsci.2006.06.001.